BIOCATALYTIC CONVERSION OF RENEWABLE FEEDSTOCKS FOR PRODUCTION OF VALUE-ADDED CHEMICALS

Luis Erick Mota Pacheco

A thesis submitted for the degree of

Doctor of Philosophy

To

University College London

The Advanced Centre for Biochemical Engineering

Department of Biochemical Engineering

University College London

London

WC1E 7JE

2020

I, Luis Erick Mota Pacheco, confirm that the work presented in this thesis is my own. Where information has been derived from other sources, I confirm that this has been indicated.

Signature: _____ Date: _____

To my Mom Noemí Pacheco, my most beautiful and important motivation.

To my Dad José Luis Mota, my personal hero and my wise Master in life.

To my Sister Alma, for all her support during all my academic adventures.

To my dear Itzel, the woman that came out of my dreams for joining me in life.

To my unconditional brother Icken Hernández, for all the learning together, the music, the plans, and the laughter.

To all my dear family, that always believed in me.

To Music, my eternal love, always waiting for me...

Finally, to Abril, for all the things she taught me without even got to know each other.

“There are men who fight one day and are good. There are men who fight one year and are better. There are some who fight many years and they are better still. But there are some that fight their whole lives; these are the ones that are indispensable”. – Bertolt Brecht.

ABSTRACT

Biocatalytic processes using transketolase have previously been developed in order to produce polyalcohols; an important class of chiral molecule, often used for the synthesis of active pharmaceutical ingredients. Transketolase catalyses asymmetric carbon-carbon bond formation by transferring a two-carbon moiety between a ketose and an aldose sugar. Nowadays, there is a focus on sustainable processes, based on the use of renewable feedstocks, in order to reduce energy consumption and waste production.

The aim of this study was to establish novel methods for the evaluation and optimisation of the transketolase-catalysed upgrading of L-arabinose and D-galacturonic acid, the major pectin components of sugar beet pulp, a by-product obtained from sugar beet bio-refineries, and to explore their subsequent amination.

The first objective involved transketolase production, activity evaluation and the development of a detailed kinetic model for the bioconversion of L-arabinose to L-glucoheptulose using cell lysates. Optimising cell growth and protein expression for the H461Y transketolase mutant and using clarified lysate as biocatalyst, an initial reaction rate of 51 μmol L^{-1} min^{-1} was reached. This is the highest initial reaction rate for the production of L-glucoheptulose reported to date. It was found that the high Michaelis constant of L-arabinose determines the rate of the overall reaction, and that Lithium hydroxypyruvate is inhibitory at concentrations > 1 mM. Screening of a library of transaminase enzymes identified a transaminase that could convert L-glucoheptulose to (2*S*,3*S,*4*S*,5*R*)-6-aminoheptane-1,2,3,4,5,7-hexaol. A kinetic model for the L-arabinose

bioconversion using pure H461Y transketolase as biocatalyst was also generated. Comparison of the kinetic parameters of the purified and lysate forms of the enzyme indicated that there is no significant difference between the two enzyme preparations. A second objective was to assess the utilisation of transketolase for the upgrading of D-galacturonic acid. Mutant H461Y was identified as also being able to achieve the bioconversion of D-galacturonic acid into 2,3,4,5,6,8-hexahydroxy-7-oxooctanoic acid. A detailed kinetic model of this bioconversion was also established. This showed that H461Y transketolase presents higher affinity for D-galacturonic acid than for L-arabinose since D-galacturonic acid bioconversions reached completion in less than 12 hours. The model showed that Lithium hydroxypyruvate exhibits inhibition to the reaction at concentrations > 1 mM. This is consistent with the L-arabinose bioconversion study. Optimum conditions for 2,3,4,5,6,8-hexahydroxy-7-oxooctanoic acid synthesis would involve the use of high D-galacturonic acid and low Lithium hydroxypyruvate concentrations. Based on the insights of the kinetic model for the lysate TK, options to improve the productivity of the bioconversion process were finally explored. The most productive conditions for the synthesis of L-glucoheptulose in a fed-batch process at preparative scale involved using high L-arabinose (111 mM) and low Lithium hydroxypyruvate (>10 mM) concentrations. Under the optimised conditions the maximum L-glucoheptulose productivity achieved was 56.8 mg $L^{-1}h^{-1}$.

Overall, this work has established the foundations for the biocatalytic upgrading of L-arabinose and D-galacturonic acid from SBP as a sustainable feedstock. The products formed have potential applications in hypoglycaemia and cancer treatment.

IMPACT STATEMENT

This research has established the foundations for the transketolase (TK) mediated upgrading of L-arabinose and D-galacturonic acid, two of the major components of the pectin fraction of Sugar Beet Pulp (SBP), a by-product obtained from sugar beet biorefineries. The results of this work can be put to beneficial use in different areas including public health, industry and academia, having also an important impact on the environment.

The principal benefit of this work could be reflected in the public health as the polyalcohols obtained from the TK bioconversion of L-arabinose and D-galacturonic acid have potential applications in hypoglycaemia and cancer treatment. This benefit is undoubtedly related with the industry field, in which the application of the results of this research could lead to the establishment of sustainable processes for the production of chiral building blocks for the synthesis of active pharmaceutical ingredients. Moreover, this work can open an important opportunity for the search of other renewable feedstocks with similar characteristics as SBP, not only in the UK but in different countries. For example, in Mexico, sugar industries process sugar cane for the obtaining of sucrose, producing sugar cane bagasse as a by-product. This could be further hydrolysed for obtaining different substrates for biocatalysis.

From the academic perspective, this work can be a basis for future research students working in the TK bioconversion optimisation of other monosaccharides obtained from SBP or other starchy sources. Moreover, the methodologies and results of this work can be written up for publication in order to facilitate science divulgation across the world and serving as teaching materials in courses related to biochemical engineering, biocatalysis, and organic chemistry.

Finally, from the environmental perspective, the application of the results of this work in the industry would contribute to decrease the use of non-renewable resources, as well as reducing pollutant wastes production, leading to a greener environment, away from a fossil-based economy.

ACKNOWLEDGEMENTS

I am grateful with every single person that I met during this wonderful journey and helped me with their knowledge, motivation and advice.

My most sincere gratitude goes to my supervisor, Professor Gary Lye, for giving me the extraordinary opportunity to be under his guidance. I also would like to thank him for his confidence, invaluable advice, ideas and support for improving the quality of my research. I am also grateful to my second supervisor, Professor Helen Hailes, for her support, interesting analysis and key advice.

Special thanks also to Dr. Fabiana Subrizi (UCL Department of Chemistry) for performing the transaminase screen described in Section 3.3.3. Also, my sincere thanks to Dr. Maria Bawn, as her support and advice were so important during my work in the Lab.

Thanks to the Sugar Beet Pulp Team, for the help given: Max, Ashikin, Roberto, and David. I am sincerely thankful to my department mates Haoran Yu, Gerardo Santiago, Ribia, Reema, Rana, Cheng, Baolong, Fiona, Jose, and especially to my dear friend Patrick Mugisha for all his wise advice, the interesting talks, and his support in every single day at the Department.

All my gratitude goes to my Aztec brother Icken Hernández, for all the learning, the support, the advice, the motivation, travels, and all the projects that we created during this journey full of learning.

My sincere acknowledgements to my support team from the Universidad Tecnológica de la Mixteca in Huajuapan de León, Oaxaca, México. Especially to my friends Ana, Claudia, Francisco, Karla, Magda, Moni, Nancy and Tenoch for always believing in me and supporting me during all these years. Also, I

would like to thank my dear professors Dr. Norma, Dr. Raúl, Dr. Rogelio, Dr. Paula and Dr. Alma for all their motivation for pursuing this scientific adventure in the UK.

Words are not enough to thank my family for always helping me to achieve my life goals. Thanks to my Mom and Dad, for all their love, support, motivation, and for giving me the most beautiful family in the universe. Thanks to my sister and my brother in law Cuauhtémoc for bringing joy to the family. Special thanks to my cousin Mario Alvarado for believing in me, and all his unconditional support.

My deepest thanks go to my fiancé Itzel, for all her love and support during all the stages of this journey.

A special mention with all my gratitude to my uncle Juan Pacheco and my aunt Teresita Mendez for all their help during my writing process, all their support and motivation for helping me reach the conclusion of my PhD.

I would like to thank also to my beloved friends Carlitos and Ana “Kikis” for always being there for me, all their love, support, and motivation.

I would like to extend my deepest gratitude to The Mexican National Council for Science and Technology (CONACyT), and the UK Engineering and Physical Science Research Council (EPSRC) for their financial support. Without their support, it would not be possible for me to pursue my PhD, and I am truly grateful for this opportunity.

Finally, to Bichito, Jerry, Nena, and Chester, for making me smile even when life gets tough…

CONTENTS

LIST OF FIGURES

LIST OF TABLES

NOMENCLATURE AND ABBREVIATIONS

%Y	Total conversion yield (mol/mol)
ε	Extinction coefficient
μ	Specific growth rate (h^{-1})
Spr_0	Specific initial conversion rate (μmol $g^{-1}min^{-1}$)
ABT	2-amino-1,3,4-butanetriol
AHH	(2*S*,3*S*,4*S*,5*R*)-6-aminoheptane-1,2,3,4,5,7-hexaol
AP	Acetophenone
BSA	Bovine serum albumin
dcw	Dry cell weight
DMSO	Dimethyl sulfoxide
dt	Doubling time
Ei	Enzyme concentration
HPIC	High performance ion chromatography
HPLC	High performance liquid chromatography
IPTG	Isopropyl β-D-1-thiogalactopyranoside
k_{cat}	Reaction rate constant

Ki	Inhibition constant
K	Michaelis constant
ARA	L-Arabinose
LB	Luria Bertani
GLU	L-Glucoheptulose
Li-HPA	Lithium hydroxypyruvate
MBA	Methylbenzylamine
OOA	2,3,4,5,6,8-hexahydroxy-7-oxooctanoic acid
PLP	Pyridoxal 5’ phosphate
PMP	Pyridoxamine 5’ phosphate
RO	Reverse osmosis
SDS-PAGE	Sodium dodecyl sulfate polyacrylamide gel electrophoresis
TAm	Transaminase
TK	Transketolase
ThDP	Thiamine diphosphate
Tris	Tris(hydroxymethyl)aminomethane

1. INTRODUCTION

1.1. Introduction to biocatalysis

Biocatalysis is the application of enzymes as catalysts to perform chemical synthesis or transformations on organic molecules. These reactions are referred to as biotransformations or bioconversions. Its importance rests in the exploitation of the properties of the enzymes, in particular their chemoselectivity, regioselectivity (positional selectivity) and stereoselectivity (chiral selectivity) to specifically modify or create a chiral centre on an organic molecule (Schulze & Wubbolts, 1999; Schmid et al., 2001; Clark et al., 2002; Adams et al., 2010; Wang & Lu, 2011; Wu & Tao, 2012; Bawn et al., 2018).

Enzymes can be used as purified enzymes, lysates or whole cells, and the reaction medium can consist of an aqueous phase, organic phase, or a two liquid phase aqueous-organic system that can be optimised to dissolve substrates and products while maintaining enzymatic activity (Schmid et al., 2001; Wang & Lu, 2011). The biocatalytic processes can be engineered at the level of the enzyme, the host cell, or the process to achieve the best performance for the bioconversion (Schmid et al., 2001).

1.1.2. Classification of biocatalytic reactions

Biocatalytic processes can be classified as *in vivo* and *ex vivo*. In the *in vivo* process the biocatalytic reaction is carried out inside a living cell (Findrik, 2009; Santacoloma, 2011). *Ex vivo* reactions take place outside the cell (in the form of a cell lysate or as a purified enzyme) and can make use of catalysts in different forms, such as the trapping of enzymes in polymeric microcapsules (artificial cells), immobilized enzymes or cellular extracts and purified enzymes (Li et al.,

1993; Chang, 1988; Woodley, 2006; Sheldon, 2007; Chi et al., 2008; Matosevic et al., 2011).

1.2. Fields of application of biocatalysis

Although the world market for industrial enzymes covers diverse segments (Figure 1.1), it is gaining increasing importance in the fine chemicals industry for the production of building blocks for active pharmaceutical ingredients (APIs), such as polyalcohols, aminoacids, amino alcohols, amines, and epoxides in high yield and purity. These molecules are characterized as having specific functional groups and chiral centres (Patel, 2018; Jemli et al., 2016; DiCosimo et al., 2013; Straathof et al., 2002; Panke et al., 2004).

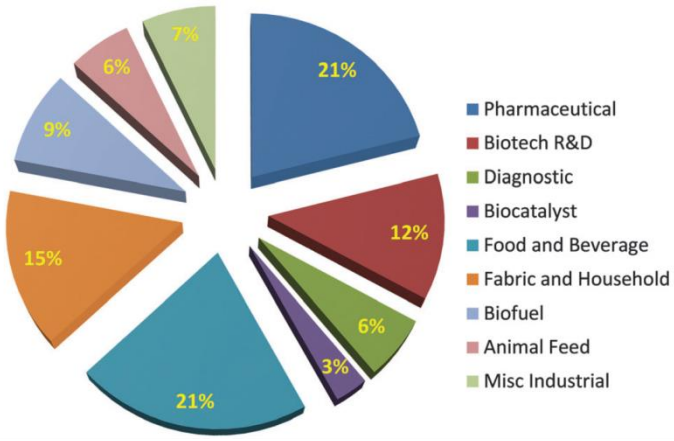

Figure 1.1. Breakdown of the world enzyme market by sector (DiCosimo et al., 2013).

The increasing development of biocatalysis in the pharmaceutical industry is due to the exponential growth in the gene sequence database for accessing diverse enzyme libraries, efficient molecular cloning and protein expression platforms. By the optimal utilisation of these tools it is now possible to produce biocatalysts more robust, selective and economically viable than in previous years (Tao et al., 2007; Wang & Lu, 2011).

1.2.1. Pharmaceutical manufacture

The pharmacological activity of a small molecule medicine depends mainly on its interaction with biological matrices or drug targets such as proteins, nucleic acids or biomembranes. This interaction is unique among the many possible arrangements in the three-dimensional space, and for this reason chirality is a fundamental factor for efficacy of new medicines. Therefore, the production of single enantiomers of chiral intermediates has become increasingly important (Patel, 2001; Lin et al., 2011).

Chiral building blocks for APIs production can be obtained by chemical synthesis and by different approaches such as chiral resolution of a racemate or through manipulation of chiral starting materials (Schulze & Wubbolts, 1999; Patel, 2001; Lin et al., 2011). These processes use petrochemical resources such as coal, petroleum, and natural gas. This situation leads to depletion of non-renewable resources, production of pollutant wastes and an increase in the price of the final products (Franssen et al., 2010; Soetaert & Vandamme, 2010).

Nowadays, one of the principal objectives of researchers is the development of sustainable processes. A sustainable process is based on the use of renewable materials, and the reduction of energy consumption, dangerous substances and waste production. Moreover, the products of a sustainable process are able to improve the quality of life, and are competitive in the marketplace, opening the way for a future away from a fossil based economy (Soetaert & Vandamme, 2010; Bawn et al., 2018).

For all the above, biocatalysis could emerge as a sustainable process for the production of building blocks for the pharmaceutical industry.

1.2.2. Biocatalysis versus chemical synthesis

One of the principal advantages of biocatalysis over chemical synthesis is that due to the specificity of enzymes, and their capability to achieve the reaction at ambient temperature and atmospheric pressure, the production of specific chiral molecules can be achieved with high enantiomeric excess and low energy costs. Moreover, biocatalytic syntheses reduce the number of process steps, avoiding the need for protection and deprotection steps that are common in chemical synthesis. Thanks to these characteristics, associated problems as such as isomerisation, racemisation, epimerisation, and rearrangement can be prevented (Schmid et al., 2001; Patel, 2001; Pollard & Woodley, 2007; Woodley, 2008; Bawn et al., 2018).

Another major advantage of biocatalysis over chemical catalysis is avoiding the need to use organic solvents in pharmaceutical and fine chemical synthetic processes as most enzymatic reactions take place in water. The chemical and pharmaceutical industries currently use organic solvents in around 80% of their processes; this is a concern given the fact that many organic solvents are toxic and therefore dangerous for personnel. In addition, at industrial scale, many of these solvents are difficult to recover, which can lead to environment pollution (Woodley, 2008).

Biocatalysis exhibits some other advantages over chemical synthesis, as the properties of the biocatalyst can be modified to suit the process. Also biocatalytic processes are rarely endo- or exothermic, which helps in reducing the costs for energy requirements (Woodley, 2008).

Although biocatalysis has emerged as an important tool for novel industrial pharmaceutical synthesis, not all the biocatalytic processes will be better than

the chemical alternative. It is important to analyse each conversion objectively on a case-by-case basis. Designing sustainable processes involves (Adams et al., 2010):

• Designing efficient processes that minimize the use of resources.

• Considering the environmental, health and safety effects of the materials used.

• Considering the economic viability of the process.

• Considering the waste generated in the process; both in nature and quantity.

From the process-engineering perspective, there are two economic factors that also have to be taken into account:

• As many enzymes are cofactor dependent, and these molecules tend to be expensive, recycling methods must be established in order to maintain the economic advantage of the process (Schmid et al., 2001).

• The pharmaceutical industry requires productivities of around 10 – 35 kg of product per kg of dry cell weight, 100 – 250 kg of product per kg of free enzyme, or 50 – 100 kg of product per kg of immobilised enzyme (Tufvesson et al., 2011). This means that in biocatalysis, enzymes will always be operating away from their natural conditions, so process development and protein engineering have to be optimised (Pollard & Woodley, 2007).

Nevertheless, the tremendous potential of biocatalysis for the design and implementation of multistep biocatalytic pathways is still in development for overcoming the drawbacks outlined in this section.

1.2.3. Chiral polyalcohols

A number of recent works have indicated the potential of biocatalysis using transketolase and transaminase (whether using lysates or a whole cell biocatalyst) for the production of amino polyalcohols (Ingram et al., 2006; Smithies et al., 2009; Smith et al., 2010; Rios-Solis et al., 2011; Rios-Solis, 2012; Halim et al., 2014; Gruber et al., 2018; Bawn et al. 2018). Chiral polyalcohols are an important class of compounds due to their biological activities; they are used as building blocks for the production of complex molecules and optically pure pharmaceuticals as well as ligands and auxiliaries for asymmetric synthesis (Kwon & Ko, 2002; Panke et al., 2004; Rios-Solis, 2012; Birrel and Jacobsen, 2013; Gruber et al., 2018). One example of these key industrial chiral molecules is myriocin, a chiral amino-triol with antifungal and immunosuppressant activity that is a precursor of fingolimod (2-amino-2-[2-(4-octylphenyl)ethyl]-1,3-propanediol), an oral agent in the treatment of multiple sclerosis (Miyake et al., 1995; Gasperini and Ruggieri, 2012; Gruber et al., 2018). Another example is the (2*S*, 3*R*)-2-amino-1,3,4-butanetriol (ABT), a polyaminoalcohol that has been demonstrated to be a key industrial synthon for the synthesis of protease inhibitors and detoxifying agents (Rios-Solis et al., 2015; Gruber et al., 2018). The chemical synthesis of these compounds is complex, requiring many steps and obtaining low productivities (Hailes et al., 2009; Rios-Solis et al., 2015; Gruber et al., 2018), and for this reason biocatalysis is considered competitive.

The production of polyalcohols by biocatalysis rather than chemical synthesis avoids the use of hazardous hydride reagents and provides an environmentally friendly process that can be implemented at large-scale without the concern of

using corrosive and hazardous materials (Woodley, 2008; Rios-Solis et al., 2015; Sehl et al., 2015; Bawn et al., 2018).

Given the importance of these chiral polyalcohols, and the extensive previous study at UCL, their synthesis provides a logical focus for the work described in this thesis.

1.3. Multi-step bioconversions

Multiple step enzymatic bioconversions can be linked together in *de novo* synthetic pathways. These processes can be designed without any natural precedent, offering incredible opportunities to synthetize a wide range of compounds (Ferrer et al., 2005; Tyo et al., 2007; McArthur IV & Fong, 2010). They often involve linking unrelated enzymes towards the synthesis of a specific high value unnatural compound (Ferrer et al., 2005). The *de novo* approach is useful for obtaining molecules with more than one chiral centre, because these molecules are difficult to synthesize with conventional organic chemistry.

De novo pathways include bioconversions that can be divided into two categories depending on the specific functionality of each enzyme: functionalization, where a functional group is created or modified; and conjugation, where another molecule is transferred to the substrate (Krämer & Testa, 2008).

In this project the key first step in two *de novo* pathways will be optimised using transketolase (TK) for conjugation; the products obtained could be then further upgraded via the utilisation of transaminase (TAm) for functionalisation. Information about transketolase and transaminase is described in Section 1.4

and Section 1.5 respectively, and further information about coupled transketolase and transaminase bioconversions is presented in Section 1.6.

1.4. Transketolase

Transketolase is an enzyme that catalyses carbon-carbon bond formation by transferring a two carbon moiety (1, 2-dihydroxyethyl group) between a ketose sugar and an aldose sugar (Sprenger & Pohl, 1999), as showed in Figure 1.2. The enzyme requires thiamine diphosphate (ThDP) and Mg^{+2} as cofactors to perform the conversion (Morris et al., 1996).

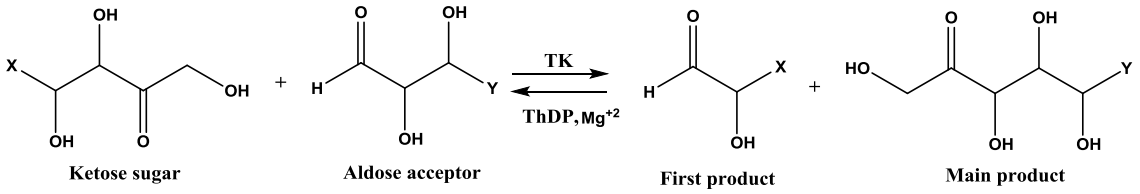

Figure 1.2. General reaction scheme of the carbon-carbon bond formation catalysed by transketolase. A 1,2-dihydroxyethyl group is transferred between a ketose and an aldose. X and Y are variable groups (Adapted from Morris et al., 1996).

In vivo, transketolases catalyse the conversion of D-xylulose-5-phosphate and D-ribose-5-phosphate to D-sedoheptulose-7-phosphate and D-glyceraldehyde-3-phosphate; and the conversion of D-xylulose-5-phosphate and D-erythrose-4-phosphate to D-fructose-6-phosphate and D-glyceraldehyde-3-phosphate (Sprenger & Pohl, 1999). *Ex vivo*, several transketolases have been found to accept a wide range of substrates, making them ideal to integrate into *de novo* pathways. Of particular interest is the use of β-hydroxypyruvate (HPA) as a keto donor so that CO_2 is released as a side product, making the reaction irreversible (Mitra & Woodley, 1996).

The most widely used transketolase is that obtained from *E. coli*; its activity has been found to be 6 and 30 times higher than the yeast or spinach enzyme (Sprenger & Pohl, 1999). In addition it can enable carbon-carbon bond formation between a broader spectrum of substrates including hydroxylated and unphosphorylated compounds (Pohl et al. 2004; Bawn et al., 2018).

E. coli TK is a homodimer with a subunit molecular weight of 72 kDA (Figure 1.3). The active site of each subunit is located at the interface between the two identical subunits. The thiamine diphosphate cofactor is also situated at the interface between the subunits (Sprenger & Pohl, 1999).

Figure 1.3. Ribbon structure of the *E. coli* transketolase homodimer. One monomer is coloured blue and the other is coloured grey. Figure created from the PDB structure file 1QGD using PyMOL Molecular Graphics System World Wide Web http://www.pymol.org (Rios-Solis, 2012).

Each subunit of transketolase is composed by three domains (Figure 1.4). The amino-terminal, or PP-domain, consists of a five-stranded parallel β-sheet with

α-helices on both sides. The second domain, the Pyr-domain is a six-stranded parallel β-sheet, sandwiched between α-helices. Both domains are involved in binding ThDP and therefore have an important role in catalysis. The carboxy-terminal domain or C-domain contains a mixed β-sheet with four parallel and one antiparallel strand, it does not contribute any amino acids to the active site and its function remains unclear (Muller et al., 1993; König et al., 1994).

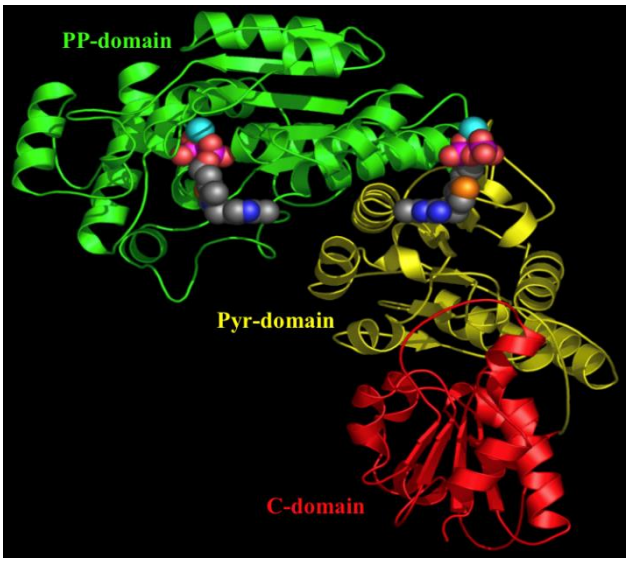

Figure 1.4. Ribbon structure of a single subunit of *E. coli* transketolase. Two ThDP molecules, which bind to the PP- and Pyr-domains are shown as spherical space-filling models. The divalent metal ion Mg^{+2} binding to ThDP required for catalytic activity is highlighted in cyan. Figure created from the PDB structure file 1QGD using PyMOL Molecular Graphics System on World Wide Web http://www.pymol.org (Rios-Solis, 2012).

In the transketolation mechanism, ThDP plays a fundamental role. This molecule can lose a proton forming a carbanion, which can be stabilised by the adjacent nitrogen in the molecule (Figure 1.5).

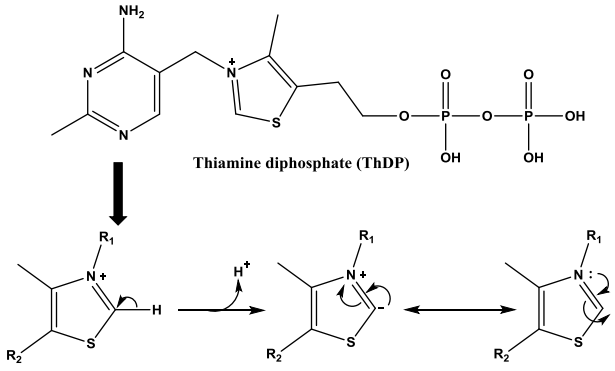

Figure 1.5. Forming a carbanion of thiamine diphosphate.

The kinetic mechanism of transketolase follows a ping-pong bi-bi ordered mechanism, which can be described as two half reactions. Following the general reaction displayed in Figure 1.2, in the first half of the reaction the ketose sugar binds to the enzyme via the cofactor ThDP, yielding the first product and another carbanion that can be stabilised by resonance (Figure 1.6).

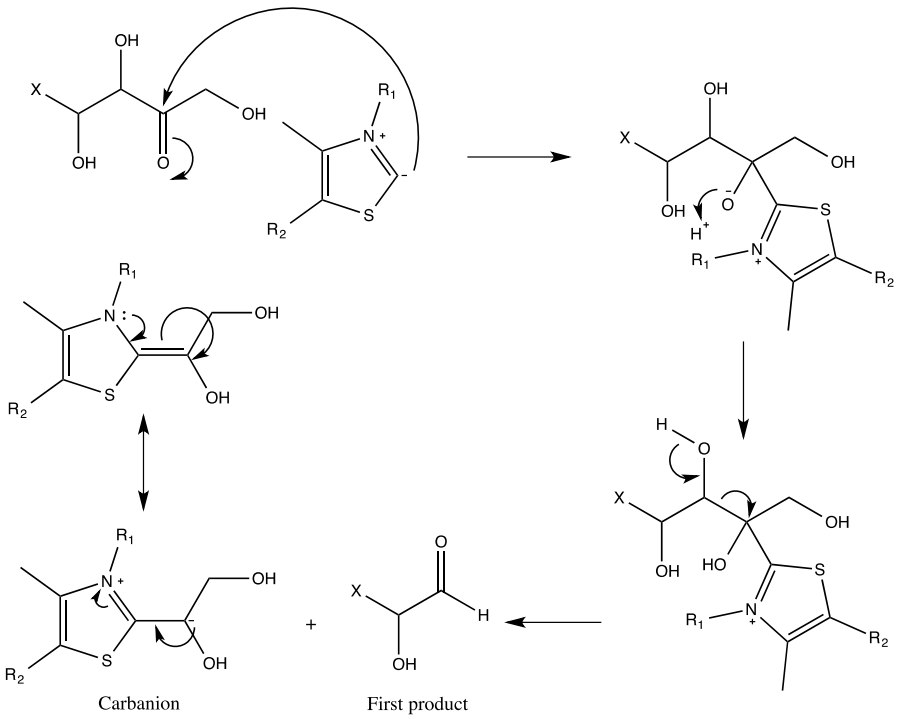

Figure 1.6. First step of the transketolation between a ketose and an aldose sugars: transfer of the 1, 2-dihydroxyethyl group from the ketose sugar to the ThDP. Figure adapted from Wikner et al. (1997).

In the second half of the reaction, the aldose sugar suffers a nucleophilic attack by the carbanion, forming a ketose with an extended two-carbon skeleton while releasing the ThDP (Figure 1.7).

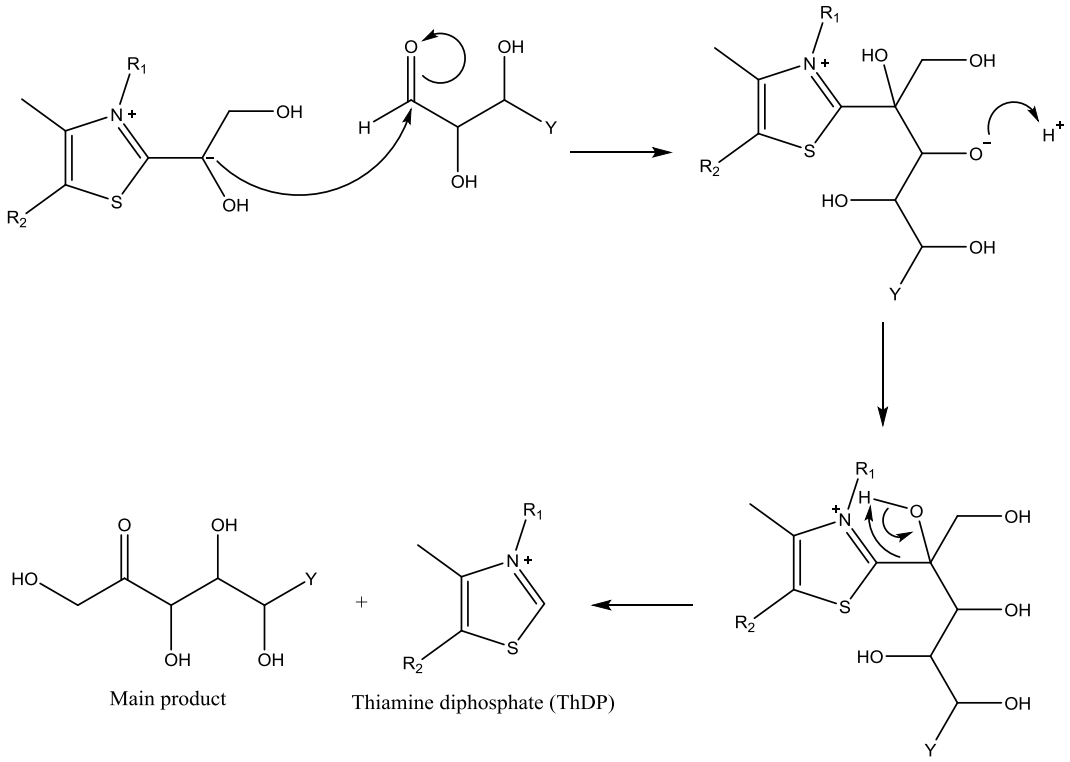

Figure 1.7. Second step of the transketolation between a ketose and an aldose sugars: transfer of the 1, 2-dihydroxyethyl group from the ThDP to the aldose sugar. Figure adapted from Wikner et al. (1997)

1.4.1. Kinetic modelling of transketolase bioconversions

For the effective design of bioconversion processes the use of kinetic models is fundamental; such models are tools that contain information about a particular process in order to describe the enzymatic behaviour over a limited set of physical conditions (Jiménez-González & Woodley, 2010). Kinetic modelling and simulation can help to explore alternative routes and hypothetical changes to an existing or new process before experimentation in order to speed up its

development. These models are also useful to develop and evaluate process control strategies to ensure stability and efficiency (Sin et al., 2009).

Kinetic models usually consist of differential and non-linear algebraic equations that describe the mass balance of substrates, intermediates and products, and the different reaction rates (Meyer et al., 2007). These models can predict the outcomes under different scenarios (e.g. substrate and enzyme concentrations), enabling substantial time saving for the identification of the optimum reaction conditions. Moreover, kinetic parameters are useful to identify the bottlenecks of the reaction, which are helpful for the setting up of reactor configurations (Chou & Voit, 2009; Santacoloma, 2011; Rios-Solís, 2011). The specific model used in this work to quantify TK bioconversion kinetics is described later in Chapter 3.

1.5. Transaminase

Transaminase (or an aminotransferase) is an enzyme included in the class of acid dehydrogenases (Brunhuber & Blanchard, 1994) or amine dehydrogenases (Hyun & Davidson, 1995) that convert a carbonyl group to an amino group. The enzyme needs the cofactor pyridoxal 5' phosphate (PLP) to catalyse the reaction (Richard et al., 2011) as shown in Figure 1.8.

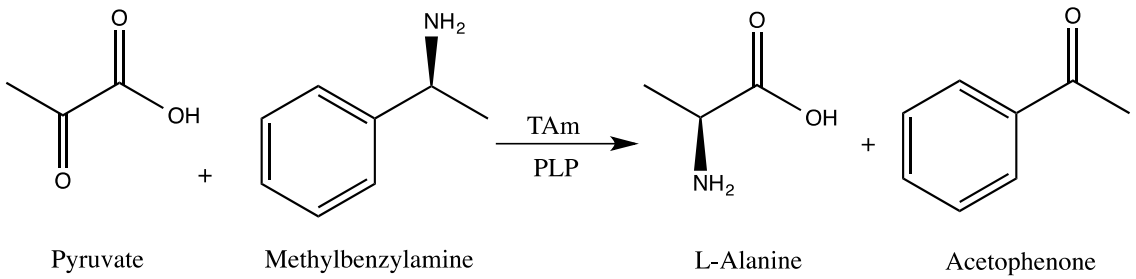

Figure 1.8. Example of a TAm reaction scheme, where an amino group is transferred from methylbenzylamine to a pyruvate molecule.

In vivo, TAms are one of the key enzymes for the biosynthesis of amino acids. The main aim of a transaminase reaction within amino acid metabolism is to collect the amino groups from several different amino acids in the form of mainly L-glutamate (or L-alanine to a lesser degree) (Lombardo et al., 1989). This L-glutamate then functions as an amino group donor for biosynthetic anabolism or for the nitrogen excretion pathway (urea cycle) (Stitt et al., 2002). *Ex vivo*, several transaminases with a broad range of substrate specificity have been identified (Taylor et al., 1998). This has led to the increasing industrial synthesis of either natural or unnatural D- or L- amino acids (Stewart, 2001).

TAms have been divided in four groups. Groups I, III and IV are comprised of α-TAm whilst the ω-TAms make up Group II (Mehta et al., 1993; Mehta & Christen, 1994). The ω-TAm enzymes have the potential to access a range of substrates not accepted by α-TAm, as the need for a α-amino acid or α-keto acid is not necessary (Shin & Kim, 1999; Koszelewski & Tauber et al., 2010). Several ω-TAms have been reported to show catalytic activity towards primary and secondary amines, which do not need to have a carboxylic group (Shin & Kim, 2001; Koszelewski & Göritzer et al., 2010). The α-TAms have been studied more extensively due to their potential in the industrial synthesis of amino acids (Stewart, 2001).

The ω-TAm from *Vibrio fluvialis* has shown the best performance to date for kinetic resolution and asymmetric synthesis of chiral amines (Shin & Kim, 2001). This enzyme showed high selectivity towards (*S*)-enantiomers and was capable of converting a broad range of ketones, making it ideal for asymmetric synthesis (Shin & Kim, 2002).

Each subunit of ω-TAm from *V. fluvialis* has a molecular weight of 50 kDa (Figure 1.9). The active site of the TAm results in a two-binding site model, which contain two pockets, one large and one smaller (Figure 1.10). The latter presents a strong repulsion for a carboxylate, playing an important role in the substrate specificity and stereoselectivity. The large pocket shows a dual recognition mode for both hydrophobic and carboxyl groups, and corresponds to a carboxylate trap, while the small pocket plays the role of a side chain recognition site (Shin & Kim, 2002).

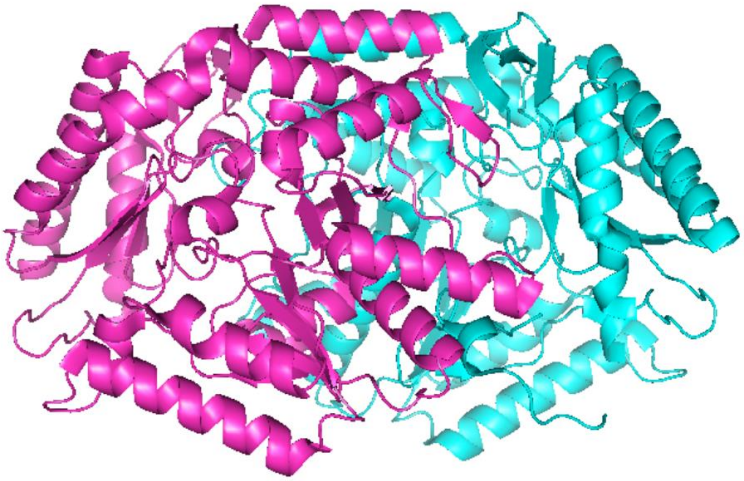

Figure 1.9. Ribbon structure of homodimeric TAm from *V. fluvialis* JS17. Figure created from the PDB structure file 1qgd using PyMOL Molecular Graphics System on World Wide Web http://www.pymol.org (Rios-Solis, 2012).

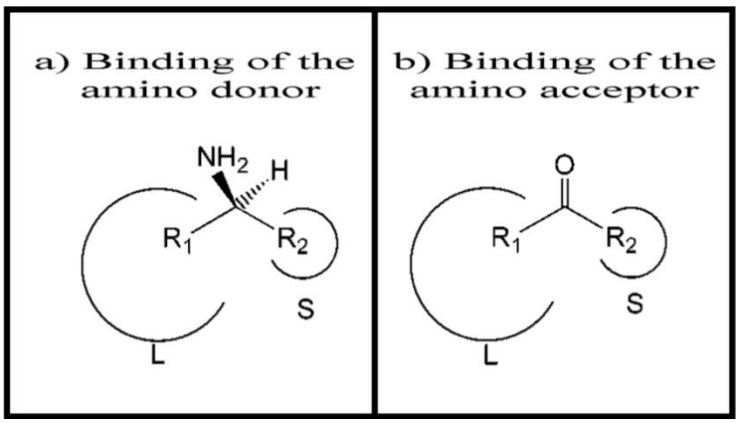

Figure 1.10. Two-binding site model of TAm of *V. fluvialis* showing (a) the binding of the amino donor and (b) the binding of the amino acceptor. L and S denote large and small binding pockets respectively (Adapted from Shin & Kim, 2002).

In order to find homologues of ω-TAm from *V. fluvialis*, Kaulmann et al. (2007) and Smith et al. (2010) carried out a detailed search and found that a transaminase from *C. violaceum* DSM330191 (TAm CV2025) was the best transaminase for ketodiol conversion. This enzyme has a molecular weight of 51 KDa and exhibited 38% sequence identity to the TAm from *V. fluvialis*.

TAm CV2025 has been coupled with transketolase for the multi-step synthesis of polyaminoalcohols using glycolaldehyde, propionaldehyde, hydroxypyruvate and methylbenzylamine as substrates (Smith et al., 2010; Rios-Solis et al., 2011; Rios-Solis, 2012; Rios-Solis et al., 2013; Halim et al., 2014; Rios-Solis et al., 2015). In this project polyaminoalcohols will be synthesized using the transketolation products of L-arabinose and D-galacturonic acid.

1.5.1. Kinetic mechanism of transaminase

TAm catalyses the enzymatic amino transfer by a ping-pong bi-bi ordered mechanism (Bulos & Handler, 1965; Smith et al., 1998). Following the general reaction displayed in Figure 1.8, on the first half of the reaction, the

methylbenzylamine (MBA) binds to the enzyme and the amino group is transferred to the pyridoxal 5' phosphate (PLP), yielding acetophenone (AP) and pyridoxamine 5' phosphate (PMP) (Figure 1.11).

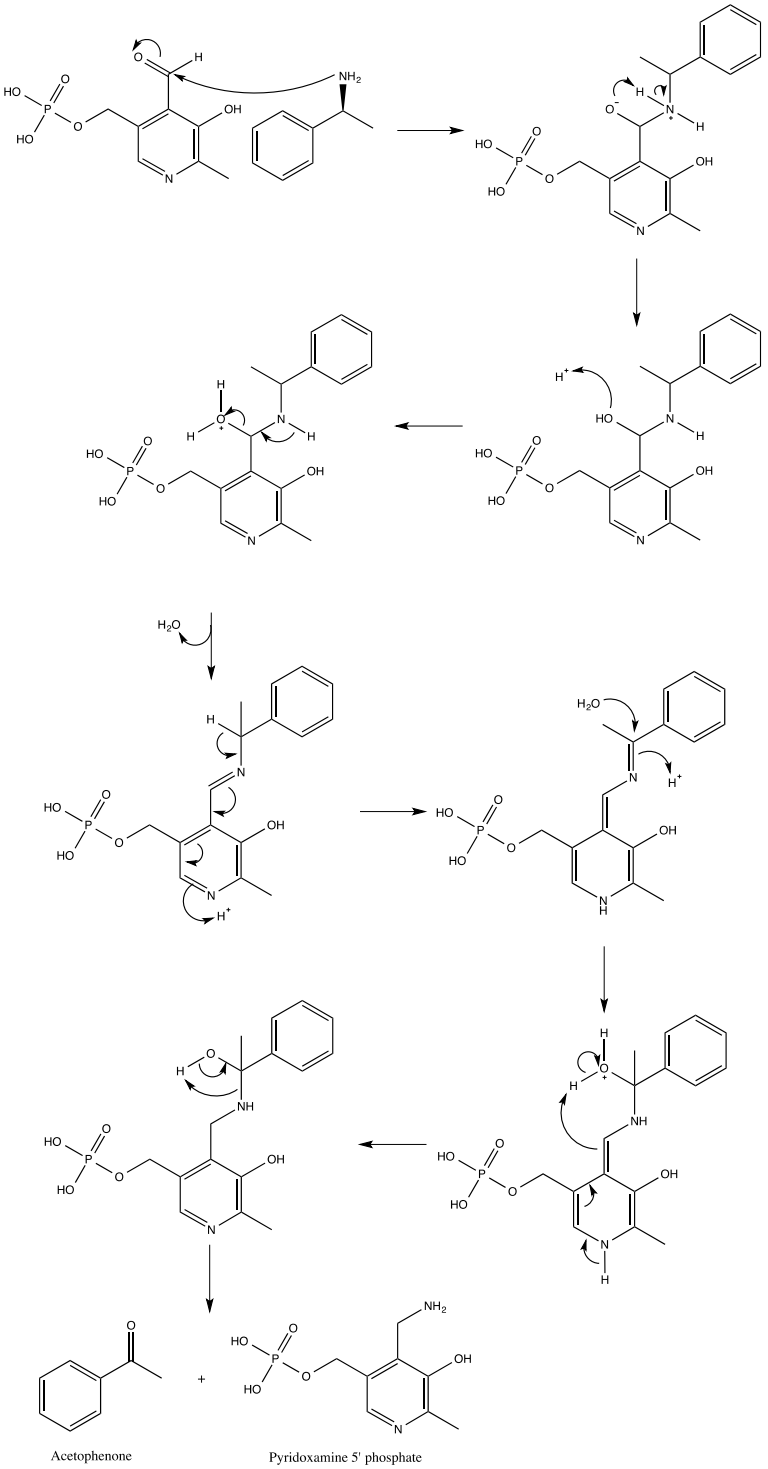

Figure 1.11. First step of the transamination between pyruvate and methylbenzylamine: transfer of the amino group from the methylbenzylamine to the PLP, and the releasing of acetophenone and PMP. Figure adapted from Bulos & Handler (1965) and Smith et al. (1998).

In the second half of the reaction, the pyridoxamine 5' phosphate transfers the amino group to the pyruvate, PLP is regenerated while L-alanine is released (Figure 1.12).

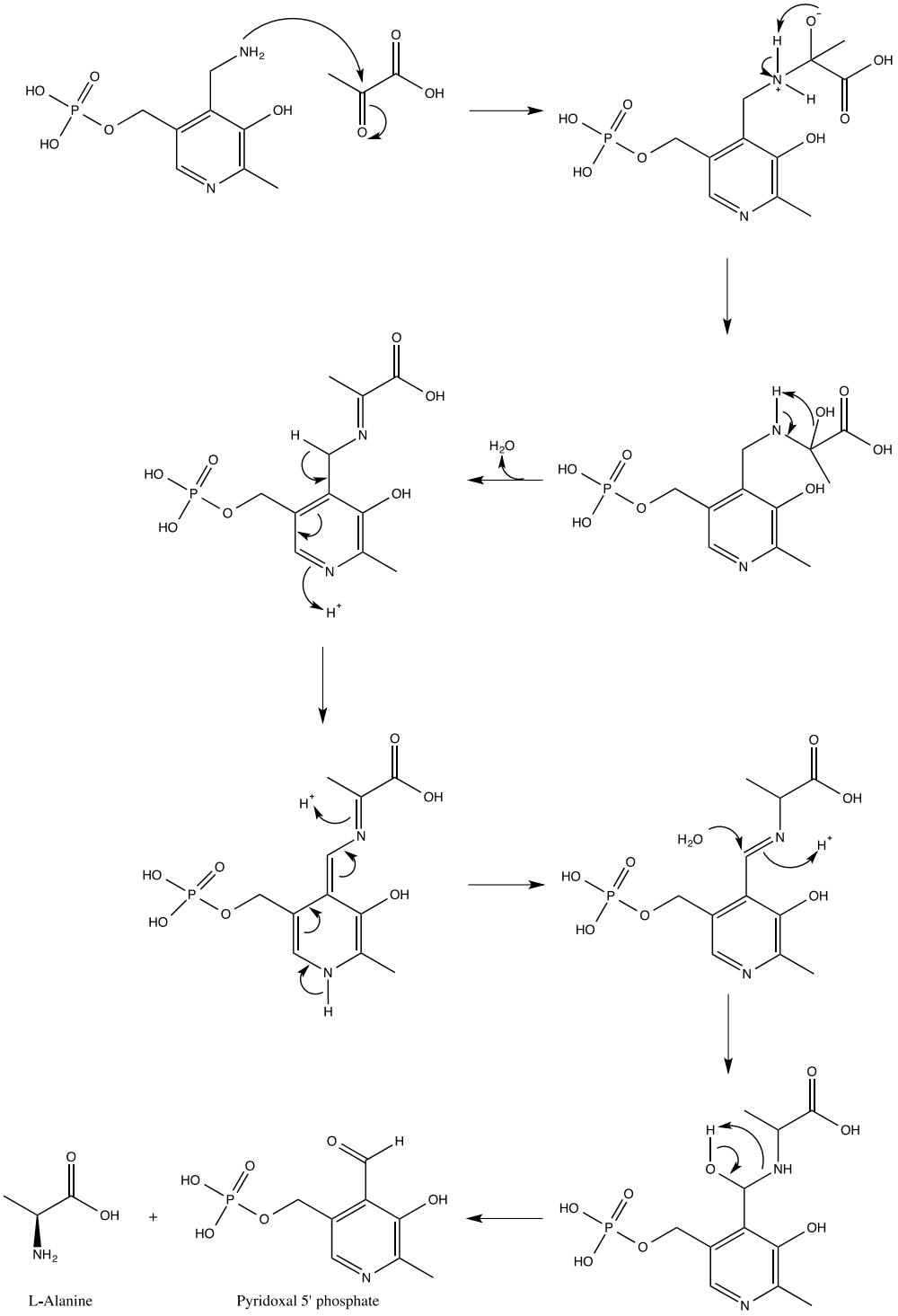

Figure 1.12. Second step of the transamination between pyruvate and methylbenzylamine: transfer of the amino group from the PMP to the pyruvate, and the releasing of PLP and L-alanine. Figure adapted from Bulos & Handler (1965) and Smith et al. (1998).

Transaminase is an important enzyme for this project as the final products obtained in this work can be further upgraded via transamination for obtaining the corresponding polyaminoalcohols, another important group of chiral molecules for the pharmaceutical industry.

1.6. Bioconversions coupling transketolase and transaminase

The most studied multistep pathway for amino polyalcohols production is the transketolation-transamination of glycolaldehyde to produce 2-amino-1,3,4-butanetriol (Rios-Solis et al., 2013). The reaction scheme of this pathway is shown in Figure 1.13.

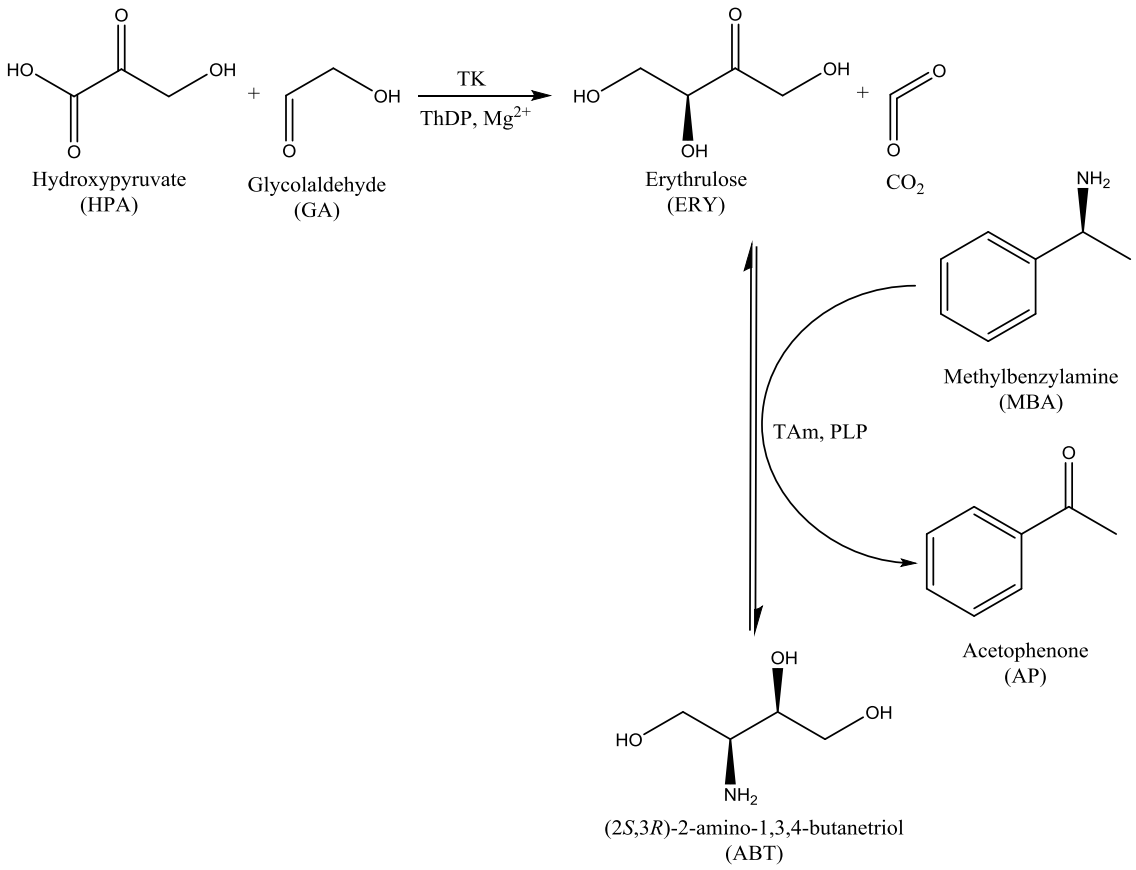

Figure 1.13. Reaction scheme for the TK-catalysed production of L-erythrulose followed by the TAm-catalysed production of ABT (Adapted from Abdul Halim et al., 2013).

In 2006 Ingram et al. achieved multistep ABT production in a one-pot process using cell lysates and whole cells, while Chen et al. (2006) assessed the integrated use of transketolase and transaminase with reaction modelling and simulation of this reaction scheme. Smith et al. (2010) evaluated the scale up of the TK-TAm pathway to a preparative scale in batch stirred reactors. Rios-Solis et al. (2011) developed a toolbox approach for the evaluation of the multi-step synthesis on previously engineered and cloned TK and TAm libraries. Abdul Halim et al. (2013) characterised an immobilized enzyme microreactor for the multistep transketolase-transaminase catalysed production of ABT. Finally, Rios-Solis et al. (2015) established an optimised method for kinetic parameter determination of this multistep pathway.

The results of this project will establish the basis for designing TK-TAm coupled bioconversions that could lead to polyaminoalcohols of special importance for the pharmaceutical industry. For example, the multistep TK-TAm biocatalysis of L-arabinose to (2*S*,3*S,*4*S*,5*R*)-6-aminoheptane-1,2,3,4,5,7-hexaol (AHH) could be studied in future works. The reaction scheme of this biosynthesis is shown in Figure 1.14.

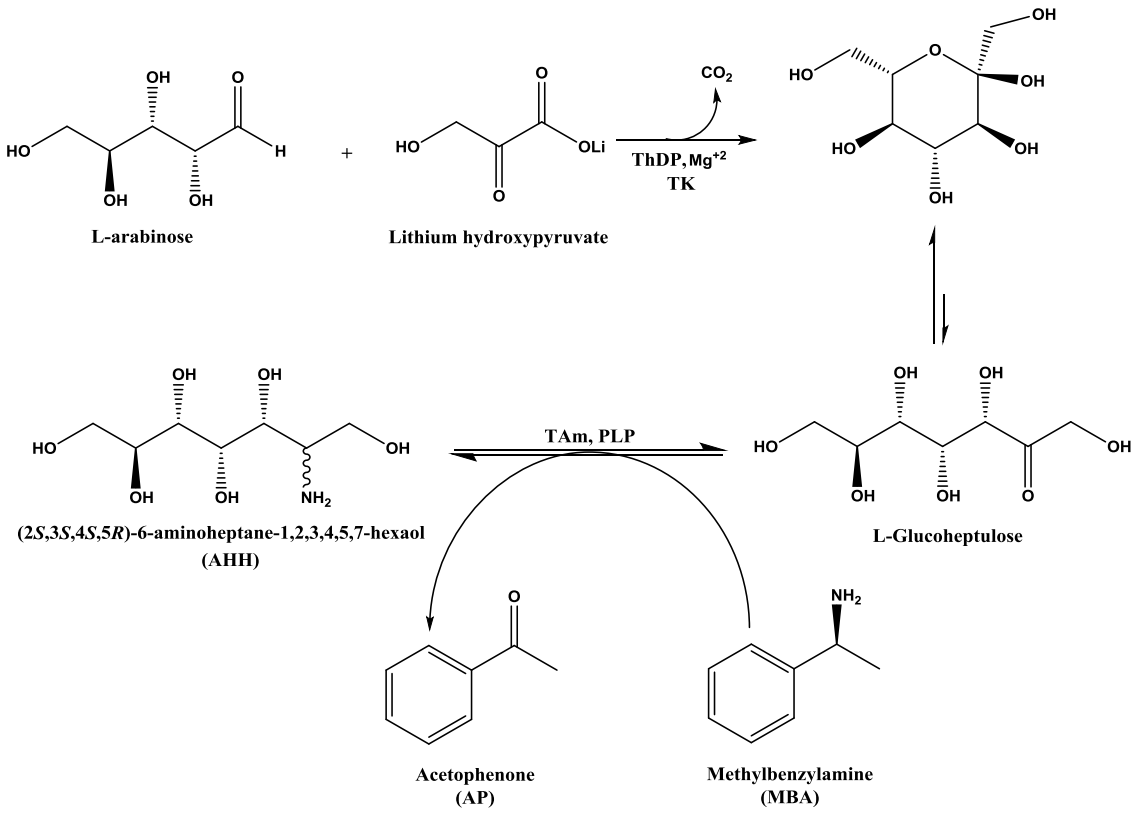

Figure 1.14. Reaction scheme for the TK-catalysed production of L-glucoheptulose followed by the TAm-catalysed production of AHH.

1.7. Biocatalysis as a sustainable process

Many millions of tonnes of bulk chemicals are produced every year and it is not an easy task to replace these existing chemical processes with more environmentally friendly bioprocesses. There have been many examples of processes in which biotechnology is applied but where the feedstock is still fossil-derived (Franssen et al., 2010).

Pharmaceutical companies have been interested to develop processes that are also environmentally friendly; that is, that can be sustainable from raw material to final product (Woodley, 2008). One factor of importance for achieving this is the selection of substrate. For large-scale biocatalysis implementation, a

strategic screening of medium and substrate has to be carried out besides the reaction engineering, enzymology and biocatalysts discovery (Tao et al., 2007).

In order to help establish sustainable processes, it is possible to consider several industrial sectors that already make use of renewable raw materials as described below (Soetaert & Vandamme, 2010):

• Sugar and starch sector: produces carbohydrates such as sugar, glucose, starch, and molasses from plant raw materials such as sugar beet, sugar cane, wheat, corn, potatoes, rice, etc.

• Oil and fat-processing sector: produces numerous oleo-chemical intermediates such as triglycerides, fatty acids, fatty alcohols, and glycerol from plant raw materials like seeds, soybeans, palm oil, coconuts, and animal fats.

• The wood-processing sector, particularly the cellulose and paper industry: produces mainly cellulose, paper and lignins from wood.

These industries make use of two technological pillars:

• Fractionation technology: this is primarily based on physical and chemical separation methods to separate agricultural raw materials into their separate components.

• Enzymatic technology: this can be applied during the transformation of agricultural raw materials. In practice, mainly hydrolytic enzymes are used, for example amylases, which hydrolyse starch to glucose.

Process sustainability can be assessed using semi-quantitative tools as the “EcoScale” designed by Van Aken et al. (2006), which is an algorithm that evaluates sustainability of processes in terms of safety and ecological

friendliness. This approach analyses six general parameters that influence the quality of a process such as yield, price of reaction components, safety, technical setup, temperature/time of reaction, and workup/purification. The “EcoScale” is a parameter that could be applied in industry processes for sustainability validation.

1.7.1. Sugar beet pulp (SBP) as a renewable feedstock

Nowadays, sugar industry by-products are receiving considerable attention for their suitability for the production of value-added goods (Berlowska et al., 2015). In 2016, more than 112 million tonnes of sugar beet were grown in the European union (Cardenas-Fernandez, et al., 2018), and UK factories process around 7.5 million tons of beet annually, producing 2.3 million tonnes of products including co-products as tomatoes, electricity, bioethanol, lime, topsoil and animal feed (British Sugar, 2011), and some processes have been applied for obtaining several co-products as shown in Figure 1.15.

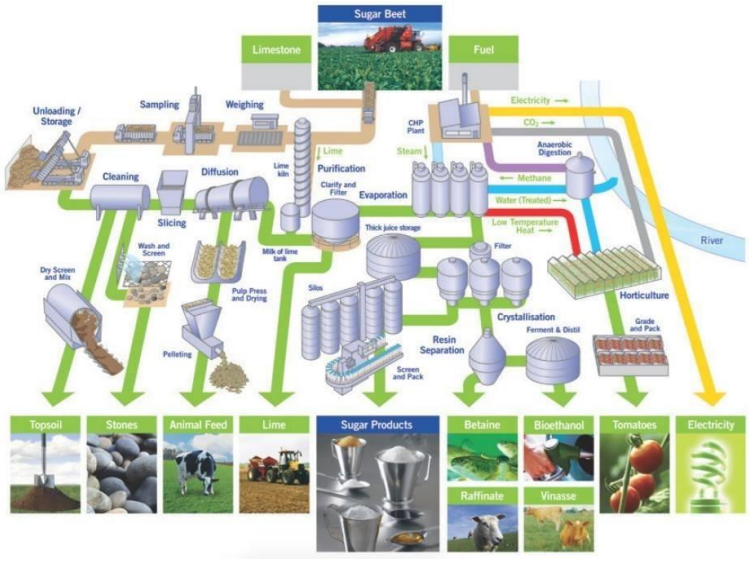

Figure 1.15. Schematic illustration of a biorefinery (Wissington, UK) for sugar beet processing to yield table sugar and a wide range of value-added co-products (British Sugar, 2011).

One of the by-products from these biorefineries is sugar beet pulp (SBP). This is obtained after the diffusive extraction of sucrose and pressing of the residual solid material. Currently, SBP is mainly used as a low value animal feed formulation and has few other commercial uses. The drying process requires a considerable input of energy, enhancing the carbon footprint of the overall biorefinery (Chen et al., 2015).

SBP contains 22-30% cellulose, 22-30% hemicellulose (mainly arabinans), 24-32% pectin and 1-3% lignin on a dry weight basis (Zheng et al., 2013). Due to the value of its components, there have been several studies to utilise this waste for production of biosorbents, pectins, dietary fibres, biofuels, emulsification materials, biogas, propylene glycol, xantham gum, soil fertilizers, soil additives, and paper (Gigac et al., 2008; Zhang et al., 2014; Suhartini et al., 2014; Ziemiński et al., 2014; Yilmaz, 2014; Chen et al., 2015; Berlowska et al., 2015).

Another process for SBP utilisation is saccharification, which is the enzymatic or chemical breakdown of its components to hexose and pentose feedtocks as D-glucose, L-arabinose and D-galacturonic acid, with minor percentages of xylose and other monosaccharides (Coughlan et al., 1986; Chamy et al., 1994; Micard et al., 1996; Spagnuolo et al., 1997; Leijdekkers et al., 2013; Zheng et al., 2013; Berlowska et al., 2015). D-glucose is mainly used for ethanol production, while the other saccharides can be used as substrates for bioconversions to obtain building blocks for biobased chemicals products as polyesters, polyamides, plasticizers or amino poly alcohols for APIs production (Werpy & Petersen, 2004).

The integration of bioconversion methodologies in the biorefinery industry could lead to the establishment of processes in which bio-waste is reduced as more value-added products are generated, in order to increase the sustainability of biorefineries.

1.8. Aim and objectives

To date, biocatalysis has been gaining increasing importance in the fine chemical industry due to its various advantages over chemical synthesis, low energy costs and the avoidance of racemisation as described in Section 1.2. However, most industrial applications of biocatalysis have been utilising fossil-derived feedstocks. On the other hand, the pharmaceutical industry is currently interested in the development of environmental friendly processes utilising renewable raw materials as described in Section 1.7. SBP is an excellent candidate as a renewable feedstock for obtaining chiral polyalcohols and aminoalcohols using transketolases (Section 1.4) and transaminases (Section 1.5), due to its availability and abundance and the composition of pentose and hexose sugars released after saccharification (Section 1.7). Nevertheless, bioconversions of the main SBP-derived monosaccharides, L-arabinose and D-galacturonic acid have been poorly explored.

Kinetic modelling of these conversions, as described in Section 1.4., offers the potential to better characterise and optimise processes in which the conversion of such renewable substrates is being explored for obtaining chiral molecules of relevance to the pharmaceutical industry.

The **aim** of this project is therefore to characterise and model the bioconversion of L-arabinose and D-galacturonic acid using a range of mutant transketolases cloned and produced at UCL. The TK-catalysed conversion of these SBP-

derived substrates represents an important first step in the design of *de novo* pathways (Section 1.2) toward the synthesis of chiral aminopolyols (Section 1.2) In particular, a kinetic model will be developed and kinetic parameters obtained for each TK mutant – substrate combination in order to simulate and optimise the performance of larger scale industrial processes. Mutant transketolase enzymes (Section 1.4), which do not naturally catalyse the bioconversion of either L-arabinose or D-galacturonic acid, will be selected from an existing TK mutant library, with the purpose of obtaining the highest possible conversion yield of the corresponding chiral polyalcohols. In order to achieve this aim, the principal **objectives** of the project are summarized below.

- The initial objective is to select a transketolase mutant with the highest conversion yield of L-arabinose as the most abundant monosaccharide present in SBP. The TK mutant will be selected from a TK library cloned and previously screened for their ability to accept non-phosphorylated sugars. Different fermentation and harvesting conditions for optimising biomass and enzyme expression of the selected TK mutant will be explored. The kinetic model of the reaction of lithium hydroxypyruvate and L-arabinose using cell lysate as biocatalyst for producing L-glucoheptulose will then be obtained based on a novel numerical approach. Moreover, the TAm catalysed upgrade of L-glucoheptulose will be explored via the utilisation of a selection of transaminases cloned from various sources. The results of this work are presented and discussed in Chapter 3.

- The next objective will be to establish a comparison of the kinetic model obtained when cell lysate is used as biocatalyst (Chapter 3) with the

kinetic model obtained when the TK mutant enzyme is used in purified form. This is important for establishing the more suitable system for industry applications. To achieve this, purification of TK will be performed prior to obtaining of the kinetic parameters that regulate its reaction with L-arabinose and lithium hydroxypyruvate. These results are shown in Chapter 4.

- The next objective will be to explore the ability of the same TK mutant for accepting D-galacturonic acid as substrate since this is the second most abundant monosaccharide in SBP. Reactions of D-galacturonic acid and lithium hydroxypyruvate with pure TK as biocatalyst will be performed for demonstrating the capacity of the enzyme for accepting the two major breakdown products of SBP as substrates. The results of this work and the corresponding kinetic model are presented and discussed in Chapter 5.

- The final objective will be to explore the improvement of the L-glucoheptulose productivity at preparative scale using L-arabinose, lithium hydroxypyruvate and cell lysate based on the kinetic parameters determined in Chapter 3. Larger and small scale biocatalyst reactions will be compared. These results are presented in Chapter 6.

Chapter 2 outlines the experimental and modelling approaches used in this work, while Chapter 7 presents a discussion of the main conclusions of this study and provides suggestions for future work.

2. MATERIALS AND METHODS

2.1. Materials

2.1.1. Reagents and suppliers

Yeast extract and casein peptone were obtained from Oxoid Ltd (Hampshire, UK). All other reagents were obtained from Sigma-Aldrich (Gillingham, UK) unless noted otherwise and were of the highest purity available. Reverse osmosis (RO) water or MiliQ water was used for all experimental work.

2.1.2. Microorganisms

E. coli XL-10 Gold was used to express two *E. coli* transketolase mutants, namely R520Y and H461Y from the plasmid pQR791. These mutants were selected for their ability to accept L-arabinose based on initial screening results from a library of TK mutants performed by Dr. Fabiana Subrizi (UCL Department of Chemistry). The pQR791 plasmid was generated at the Department of Biochemical Engineering to be used as a backbone for the production of transketolase mutants (Martinez-Torres, 2008). Competent *E. coli* BL21-Gold (DE3) cells were obtained from Stratagene (Amsterdam, NL).

A selection of transaminases cloned from various sources, namely *Chromobacterium violaceum* (Cv-TAm), *Rhodobacter sphaeroides* (Rh-TAm), *Mycobacterium vanbaalenii* (Mv-TAM) and three additional transaminases cloned into the plasmids pQR2189, pQR2191 and pQR2208, previously screened by Dr. Fabiana Subrizi et al. (2018) were also used in this study. The identity of the transaminases expressed on the pQR2189, pQR2191 and

pQR2208 plasmids cannot be disclosed at this stage for reasons of commercial confidentiality.

2.1.3. Media preparation

All batch *E. coli* fermentations for TK production were performed using LB medium, with the components outlined in Table 2.1.

Table 2.1. Composition of LB broth

Component	Concentration (g L^{-1})
Yeast extract	5
Casein peptone	10
NaCl	10

For TAm production, complex media (CM) was used and its composition is shown in Tables 2.2 and 2.3.

Table 2.2. Composition of CM broth used in transaminase fermentations

Component	Concentration
Glycerol	30 g L^{-1}
Yeast Extract	5 g L^{-1}
$MgSO_4 \cdot 7H_2O$	1 g L^{-1}
NH_4Cl_2	0.2 g L^{-1}
NaCl	5 g L^{-1}
KH_2PO_4	13 g L^{-1}
K_2HPO_4	10 g L^{-1}
Trace Solution	150 µL L^{-1}

Table 2.3. Trace solution used in CM media formulation (see Table 2.2)

Component	Concentration (g L^{-1})
$FeCl_3 \cdot 6H_2O$	10
$MnSO_4 \cdot H_2O$	10
$CaCl_2 \cdot 2H_2O$	2
$CoCl_2$	0.2
$ZnSO_4 \cdot 7H_2O$	2
$Na_2MoO_2 \cdot 2H_2O$	5
$CuCl_2 \cdot 2H_2O$	30
H_3BO_3	30

The components of the media were weighed out and dissolved in RO water and the pH was adjusted to pH 7 using 1M NaOH whenever required. After sterilisation at 121°C for 20 minutes and cooling to 40-50°C, ampicillin at 150 µg mL^{-1} was aseptically added.

2.1.4. Agar plates

Plate cultivations were prepared by adding 15 g of agar to 1 L of LB medium as described in Table 2.1. The LB agar was then sterilised at 121°C for 20 min. Once cooled to 40-50 °C, antibiotic was added at 150 µg mL^{-1} and 30 mL of media was poured into each standard size Petri dish (Fisher Scientific, UK).

2.1.5. Antibiotic solutions

The antibiotic ampicillin sodium salt (for TK production) or kanamycin sulphate (for TAm production) was dissolved in MiliQ water to a concentration of 150 mg mL^{-1}. The solution was then sterilised by passing it slowly through a 0.2 µm

sterile filter (Fisher Scientific, UK), and aseptically transferred into previously sterilised 1.5 mL Eppendorf tubes and stored at -20 °C.

2.2. Enzyme production

In order to reduce variability in the enzyme activity of biocatalyst batches used in this work, all biocatalysts were prepared using the standardised methods described in the following sections and were immediately used for the experiments needed. Moreover, remaining lysates were discarded and not re-utilised in further experiments. The initial activity of each batch was also checked before use.

2.2.1. Glycerol stocks

To prepare glycerol stock cultures, a single *E. coli* colony of each TK or TAm mutant culture was picked from agar plates incubated for 12 hours at 37 °C from the Master stock cultures. This was then inoculated into sterile 50 mL Falcon tubes containing 20 mL of LB broth using sterile sponge stoppers to allow better oxygenation. When the culture reached an OD_{600} ≈ 0.5, 400 µL aliquots of cell broth were mixed aseptically in 1.5 mL Eppendorf tubes with 200 µL of a 50% (v/v) sterilised glycerol solution. The aliquots were then frozen and stored at -80 °C until required.

2.2.2. Shake flask fermentations

All fermentations started from an inoculum culture prepared from a frozen glycerol stock (Section 2.2.1). After thawing in a water bath at 37 °C for 2 minutes, 150 µL of glycerol stock culture was inoculated into sterile 50 mL Falcon tubes containing 15 mL of either LB or CM broth (Table 2.1 and Table 2.2) using sterile sponge stoppers. The remaining glycerol stock was discarded

and the cultures were incubated on an Innova 4330 orbital shaker (New Brunswick Scientific, Germany) at 37 °C and 450 rpm. Samples were taken every hour for OD_{600} measurement (Section 2.7.1).

E. coli fermentations were carried out in 1 L baffled shake flasks with a working volume of 150 mL of either LB or CM media. The inoculum concentration was standardized at 0.1 $g_{dcw}\,L^{-1}$ and the cultures were incubated on a Kühner ISF-1-W orbital shaker (Kühner Technology, Switzerland) at 37 °C and 450 rpm for 24 hours. Cell growth was monitored during the fermentation by taking samples at periodic time intervals for OD_{600} measurement. For transaminase fermentations Isopropyl β-D-1-thiogalactopyranoside (IPTG) at 0.1 mM was used as inducer and was added to the fermentation at an $OD_{600} \approx 3$ (9 h post inoculation). Samples were subsequently taken every hour after induction to measure TAm activity as described in Section 2.7.6. The harvesting time was set as the time in which the end of the logarithmic phase is reached ($OD_{600} \approx 6$), typically 24 h for TAm and 6 – 9 h for TK production.

After fermentation, cells were harvested by centrifugation using a Hettich Universal 320R Centrifuge (Buckinghamshire, UK) at 4000 x g for 30 minutes. The cell pellets were either used for lysate preparation or stored at -20 °C until required.

2.2.3. Biocatalyst preparation

Cell pellets were re-suspended using 50 mM Tris-HCL buffer for transketolase production or 2 mM PLP in 50 mM HEPES buffer for transaminase production at a ratio of 1 mL per 10 mL of cell broth and sonicated with a MSE Soniprep 150 sonicator (Sanyo, Japan) with 10 cycles consisting of 10 seconds ON and 15 seconds OFF at 10 µm amplitude. The tube was placed on ice during

sonication to avoid overheating. The sonicated product was centrifuged at 4000 x g and 4°C for 30 minutes to remove cell debris, and the clarified lysate was aliquoted into 2 mL Eppendorf tubes for immediate protein quantification (Section 2.7.2), TK purification (when needed), and bioconversion (Section 2.4). When required, fresh lysates were stored at -20 °C and used within 1 month. Before use, lysates were thawed in a water bath at 37 °C for 2 minutes.

2.2.4. Enzyme purification (Ammonium sulphate precipitation)

Salt precipitation was used for the purification of *E. coli* TK mutants that were expressed without the N-terminal His_6-tag necessary for rapid purification using Ni-NTA spin columns. The purification process was performed following the method by Sprenger et al. (1995).

Cell pellet was re-suspended using 50 mM Tris-HCl, 6 mM $MgCl_2$, 1.67 mM ThDP and sonicated with 10 cycles consisting of 10 seconds ON and 15 seconds OFF at 10 µm amplitude. The tube was placed on ice during sonication to avoid overheating. The sonicated product was centrifuged at 4000 x g and 4°C for 30 minutes to remove cell debris. The protein lysate volume was measured and crystalline ammonium sulphate was added slowly under constant stirring until a 40% salt saturation was reached. The mixture was stirred for 1 hour, centrifuged at 4000 x g for 45 minutes and the precipitate was discarded. The volume of the supernatant was measured and ammonium sulphate was added under constant stirring until 80% salt saturation was reached. After stirring and centrifugation, the precipitate was dissolved in 50 mM Tris-HCL, 6 mM $MgCl_2$, 1.67 mM ThDP to reach the initial volume. In a second round of experiments, ammonium sulphate precipitations were carried out in steps of

55% and 75% salt saturation. In both cases, the precipitate from the last step was dissolved in 50 mM Tris-HCL and stored at 4 °C for later use.

2.2.5. Enzyme purification (His_6-Tag purification)

The *E. coli* TK mutants used in this project that were expressed with an N-terminal His_6-tag, were purified using Nickel – Nitrilotriacetic acid (Ni-NTA) spin columns, or 1 mL cartridges (QUIAGEN, UK). The composition of all buffers used for enzyme purification is shown in Table 2.4. The pH of all buffers was standardized to 7.

Table 2.4. His_6-tag enzyme purification buffers

Buffer	Components
Binding	50 mM Tris-HCl, 6 mM $MgCl_2$, 1.67 mM ThDP
Wash	50 mM Tris-HCl, 300 mM NaCl, 50 mM Imidazole, 6 mM $MgCl_2$, 1.67 mM ThDP
Elution	50 mM Tris-HCl, 300 mM NaCl, 500 mM Imidazole, 6 mM $MgCl_2$, 1.67 mM ThDP

2.2.5.1. Spin column purification

After equilibration of the column with 600 µL of binding buffer and following centrifugation in an AccuSpin Micro Centrifuge (Fisher Scientific, USA) at 890 x g for 2 minutes, 600 µL of lysate were loaded into the column and centrifuged at 270 x g for 5 minutes. The column was washed twice with 600 µL of wash buffer and then centrifuged at 890 x g for 2 minutes. Finally, the pure enzyme was

eluted twice with 300 µL of elution buffer and centrifugation at 890 x g for 2 minutes.

2.2.5.2. Cartridge purification

After equilibration of the cartridge with 4 mL of binding buffer, 12 mL of lysate were passed twice through the cartridge at a rate of 1 mL min^{-1}. The cartridge was then washed with 20 mL of wash buffer. Finally, the pure enzyme was eluted with 12 mL of elution buffer.

2.2.5.3. Pure enzyme buffer exchange

Following elution, in order to remove imidazole from the purified enzyme, a buffer exchange was performed using PD-10 Desalting columns (GE Healthcare, Sweden). PD-10 desalting columns contain *Sephadex G-25 medium*, this material allows rapid separation of high molecular weight substances from low molecular weight components. Preparation of the column was performed by opening the top cap, removing the storage buffer and cutting the seal at the end of the column. The column was equilibrated by filling it with binding buffer and discarding the flow-through. This step was repeated 4 times before use. A maximum of 2.5 mL of pure enzyme solution was loaded per PD-10 desalting column and the flow-through was discarded. The pure enzyme was eluted by loading 3.5 mL of binding buffer to the column and recovering the flow-though. The purity and the concentration of the pure enzyme were determined by SDS-PAGE and Bradford assay as described in Section 2.7.2. The pure enzyme was stored in the fridge at 4 °C for a period of up to 2 weeks before use.

2.3. Synthesis of substrates

2.3.1. Synthesis of lithium hydroxypyruvate

For the synthesis of Li-HPA, 5 g of bromopyruvic acid (Alfa Aesar, UK) was dissolved in 100 mL of distilled water; afterwards 1 M LiOH solution was added until a pH of 9.5 was reached. The reaction mixture was transferred into a round bottomed flask and glacial acetic acid was then added until the pH reached 5. The water was removed under reduced pressure (at 40-45 °C) to a final volume of approximately 20 mL, and the solution was left for 24 hours at 4 °C for product crystallisation. The product was washed with 50 mL of ethanol and stirred at 40 °C for 30 minutes before being collected by vacuum filtration and washed again with ethanol to finally obtain the lithium hydroxypyruvate as a white powder. The powder was left to dry in a desiccator before being collected and stored at - 20 °C. Synthesis of Li-HPA was performed under the supervision of Dr. Fabiana Subrizi following the method by Morris et al. (1996).

2.4. Bioconversion kinetics

2.4.1. Bioconversion of L-arabinose to L-glucoheptulose

Standard bioconversions were performed in triplicate in 1.5 mL Eppendorf tubes at the following reaction conditions: 33 mM Li-HPA, 33 mM L-arabinose, 1.7 mM ThDP, 6 mM $MgCl_2$, transketolase either as lysate (33% v/v) or purified enzyme (0.5 mg mL^{-1}) and 50 mM Tris-HCl buffer at pH 7. The reaction protocol was implemented as follows: the enzyme solution or lysate was mixed with the cofactors into a 1.5 mL Eppendorf tube; the mix was left at 25 °C and shaken at 450 rpm on a Thermomixer Comfort shaker (shaking diameter of 6 mm, Eppendorf, Cambridge, UK) for 20 minutes before adding the substrates. The

reactions (final volume of 600 µL) were then incubated at 25 °C and 450 rpm orbital rotation on a Thermomixer Comfort shaker. 50 µL samples were taken at constant time intervals and mixed immediately with 50 µL of 0.5% (v/v) H_2SO_4 to quench the reaction. The tubes were centrifuged at 12000 x g for 30 minutes in an Eppendorf 5424 R Centrifuge (Eppendorf AG, UK) and 5 µL of the supernatant was mixed with 1000 µL of MiliQ water into a HPLC vial for subsequent analysis (Section 2.7.5).

The specific activities were determined as the amount of product formed per unit of time, normalized by the amount of biocatalyst used in the reaction.

2.4.2. Bioconversion of D-galacturonic acid to 2,3,4,5,6,8-hexahydroxy-7-oxooctanoic acid

Standard bioconversions were performed in triplicate in 1.5 mL Eppendorf tubes at the following reaction conditions: 20 mM Li-HPA, 33 mM D-galacturonic acid (DGA), 1.7 mM ThDP, 6 mM $MgCl_2$, transketolase either as lysate (33% v/v) or purified enzyme (0.5 mg mL^{-1}) and 50 mM Tris-HCl buffer at pH 7. The reaction protocol was implemented as in Section 2.4.1.

2.5. Bioconversion kinetic modelling

The determination of the full kinetic model of a bioconversion has several advantages in the development of industrial processes as described in Section 1.4. Kinetic parameters are helpful to enable the simulation of reactions at large scale for providing guidance for process improvement, and to identify the bottlenecks of the reaction which allow the establishment of ideal reactor design and operating conditions.

These models can predict the outcomes under different scenarios (as substrate and enzyme concentrations), enabling substantial time saving for the identification of the optimum reaction conditions. Moreover, kinetic parameters are useful to identify the bottlenecks of the reaction, which are helpful for the setting up of reactor configurations (Chou & Voit, 2009; Santacoloma, 2011; Rios-Solís, 2011)

There are two major methods for kinetic parameters identification: linear plotting and non-linear regression (Chen et al., 2008). Linear methods are time consuming as the amount of experiments required for obtaining the full kinetic model is considerable. On the other hand, non-linear regression methods are less time and resource intensive as they use algorithms to help determine the kinetic parameters. However the principal drawback of both methods is that they can lead to local optimisation because the final values rely fundamentally on the given initial values.

In this project, a hybrid method was followed in order to utilise the advantages of the linear and non-linear methods while avoiding their disadvantages. This novel approach was first introduced by Chen et al. (2008) for the transketolase catalysed synthesis of 1,3-dihydroxypentan-2-one from propionaldehyde and β-hydroxypyruvate. The hybrid approach is schematically presented in Figure 2.1, and consists of five procedures that require only three experimental steps.

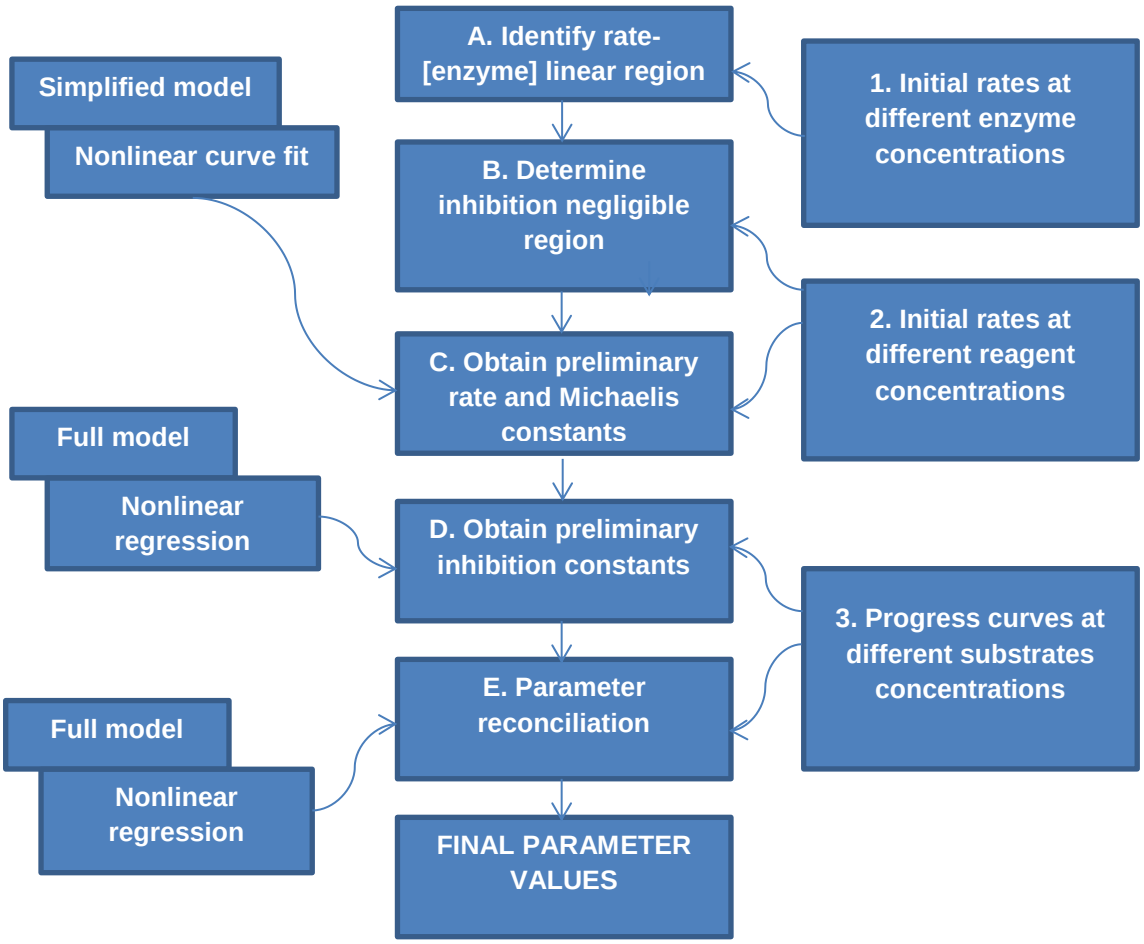

Figure 2.1. Schematic representation of the systematic procedure for rapid apparent kinetic parameter identification.

This hybrid approach was followed for obtaining of the kinetic model for both L-arabinose (Section 2.5.1) and D-galacturonic acid (Section 2.5.2) reaction systems. The methods for the three experimental steps in the procedure are described in the following sections.

2.5.1. Kinetic experiments for L-arabinose to L-glucoheptulose TK reaction

2.5.1.1. Proportionality between reaction rate and enzyme concentration

For the reaction to be kinetically controlled by the enzyme, the reaction velocity must be directly proportional to enzyme concentration (Maragoni, A.G., 2003), for this reason, the first step to obtain the kinetic parameters of the reaction is to determine the region of linear proportionality between the TK concentration and the initial reaction rate. This is necessary to ensure that any change in enzyme concentration would contribute to the measured kinetics.

The substrate concentrations were 33 mM Li-HPA and 33 mM L-arabinose for all reactions. When TK lysate was used, the concentration was varied between 0.33 and 3.6 mg mL^{-1}; and when pure TK was used, the concentrations varied from 1.3 to 3.6 mg mL^{-1}. The range of biocatalyst concentrations used was based on the maximum amount of protein/enzyme that was obtained from the enzyme production methods described in Section 2.2. The reactions were performed as described in Section 2.4.1.

2.5.1.2. Kinetic model of TK and initial rate experiments

For the second step described in Figure 2.1., two sets of kinetic data were obtained using one single concentration of either lysate or pure TK. When lysate was used, the first set of data was obtained by varying Li-HPA from 0.1 to 10 mM at a fixed concentration of 30 mM of L-arabinose, and the second set of data was obtained by varying L-arabinose from 5 to 1000 mM at a fixed concentration of 30 mM Li-HPA. These substrate ranges were established based on the experiments reported by Chet et al. (2008).

When pure TK was used, the first set of data was obtained by varying Li-HPA from 0.2 to 10 mM at a fixed concentration of 30 mM of L-arabinose, and the second set was obtained by varying L-arabinose from 10 to 150 mM at a fixed concentration of 30 mM Li-HPA. These substrate concentration ranges were established based on previous lysate experiments.

2.5.1.3. Progress curves for kinetic parameter identification

The fourth step in the proposed methodology consisted of obtaining complete reaction progress curves at different substrates concentrations and varying enzyme concentrations. A set of five and nine progress curves, each with 13 sample points at different time intervals were obtained for both lysate and pure TK systems respectively. The substrate concentrations used are shown in Tables 2.5 and 2.6 for lysate and pure enzyme systems respectively.

Table 2.5. Initial substrate and protein concentrations used for the 5 progress curves for obtaining the kinetic parameters of the TK lysate catalysed reaction of L-arabinose and Li-HPA to L-glucoheptulose

Progress Curve	1	2	3	4	5
[HPA] (mM)	86	30	30	52	89
[ARA] (mM)	32	86	65	107	280
Ei (mg/mL)		0.8		1.2	1.9

Table 2.6. Initial substrate and protein concentrations for the 9 progress curves used to obtain the kinetic parameters of the purified H461Y-HT TK catalysed reaction of L-arabinose and Li-HPA to L-glucoheptulose

Progress Curve	1	2	3	4	5	6	7	8	9
[HPA] (mM)	93	145	124	97	97	52	33	90	33
[ARA] (mM)	224	131	92	130	167	93	85	34	60
Ei (mg mL^{-1})		3.67			2.4			1.5	

2.5.2. Kinetic experiments for D-galacturonic acid to 2,3,4,5,6,8-hexahydroxy-7-oxooctanoic acid TK reaction

2.5.2.1. Proportionality between reaction rate and enzyme concentration

The substrate concentrations used were 30 mM Li-HPA and 30 mM D-galacturonic acid for all reactions and 3, 2.5, 2, 1.5, 1, and 0.5 mg mL^{-1} of pure TK. The reactions were performed as described in Section 2.4.1.

2.5.2.2. Kinetic model of TK and initial rate experiments

Two data sets were generated using one single concentration of pure TK of 2 mg mL^{-1}. The first set of data was obtained by varying Li-HPA from 0.2 to 10 mM at a fixed concentration of 30 mM of D-galacturonic acid, and the second set of data was obtained by varying D-galacturonic acid from 5 to 50 mM at a fixed concentration of 30 mM Li-HPA. No higher D-galacturonic acid concentrations were used as the substrate solubility limit under the reaction conditions used is approximately 50 mM.

2.5.2.3. Progress curves for kinetic parameter identification

A set of nine progress curves, each with 12 sample points at different time intervals were obtained. The substrate concentrations used are shown in Table 2.7.

Table 2.7. Initial substrate and protein concentrations for the 9 progress curves used to obtain the kinetic parameters of the purified H561Y-HT TK catalysed reaction of D-galacturonic acid and Li-HPA to OOA

Progress Curve	1	2	3	4	5	6	7	8	9
[HPA] (mM)	90	47	40	80	50	70	60	90	40
[DGA] (mM)	33	47	50	36	25	30	30	33	40
Ei (mg mL^{-1})		3			1.5			0.5	

2.6. Preparative scale L-arabinose to L-glucoheptulose bioconversion

L-arabinose to L-glucoheptulose bioconversions at preparative scale (50 mL) were performed in a 902 Tritando System (Metrohm Ion Analysis, Switzerland) using a 100 mL titration vessel with thermostated jacket. Temperature was maintained at 25 °C using a circulating RO water bath system (Grant Instruments, Cambridge, UK), a magnetic stirrer was used at 350 rpm and the pH was maintained at 7.0 by the addition of 0.1 M NaOH. For fed-batch reactions, a high initial L-arabinose concentration was used (50 mM, unless noted otherwise), and Li-HPA (300 mM) aliquots (1.67 mL) were added to the reaction at regular time intervals. Aliquots of 100 µL were taken at various time

intervals and mixed with 100 µL of 0.5% (v/v) H_2SO_4 to quench the reaction. The sample tubes were centrifuged at 12000 x g for 30 minutes on an Eppendorf 5424 R Centrifuge (Eppendorf AG, UK) and 5 µL of the supernatant was mixed with 1000 µL of MiliQ water into a HPLC vial for subsequent analysis (Section 2.7.5).

2.7. Analytical techniques

2.7.1. Biomass quantification

Optical density measurements were performed at a wavelength of 600 nm (OD_{600}) using a NanoDrop 2000c spectrophotometer (Thermo Scientific, UK). 1 mL of *E. coli* culture medium was taken from the shake flask culture and diluted with RO water so that the optical density measurement was between 0.1-0.8 absorbance units.

In order to convert OD_{600} values to grams of dry cell weight per litre of culture (g_{dcw} L^{-1}), a calibration curve was constructed as shown in Appendix I. After thawing in a water bath at 37 °C for 2 minutes, 500 µL of the *E. coli* glycerol stock was inoculated in duplicate into sterile 500 mL baffled flasks containing 100 mL of LB media and incubated at 37 °C and 250 rpm for 24 hours on a Kühner ISF-1-W orbital shaker. After fermentation, dilutions of the culture broth were prepared in triplicate using MiliQ water, and their OD_{600} values were obtained on a NanoDrop 2000c. Afterwards, 2 mL of the dilutions were added to pre-dried (24 hours at 100 °C) and pre-weighed 2 mL Eppendorf tubes and centrifuged at 12000 x g, 4 °C for 30 min in an Eppendorf 5424 R Centrifuge. After discarding the supernatant, the tubes were left to dry at 100 °C until a constant weight was reached. A calibration curve relating the OD_{600}

measurement from the serial dilutions to the corresponding g_{dcw} L^{-1} measurement was constructed. The calibration relationship determined was that 1 unit of OD_{600} was equal to 0.5 g_{dcw} L^{-1}.

2.7.2. Protein concentration quantification (Bradford Assay)

Total protein concentration was measured using a bovine serum albumin (BSA) standard curve that relates concentration to absorbance at 600 nm as shown in Appendix II. Solutions at 0.2, 0.4, 0.6, 0.8, and 1 mg mL^{-1} of BSA were prepared from a 2 mg mL^{-1} BSA stock solution (Sigma-Aldrich, USA). The protein samples were diluted 8 times either with water or 50 mM Tris-HCl buffer. 5 µL aliquots of the protein standard and sample solutions were added by triplicate on a 96 well microtiter plate (Radleys Discovery Technologies, Essex, UK); MiliQ water was used as blank. Afterwards, 250 µL of Bradford reagent (Sigma-Aldrich, USA) was added to each well and the plate was mixed on a Thermomixer Comfort shaker for 30 seconds, and incubated at 25 °C for 5 minutes before reading in a FLUOstar Optima microplate reader (BMG Labtech, Germany) at 600 nm. The protein concentration of the samples was calculated using the plot of the average absorbance versus the concentration of the standard solutions.

2.7.3. SDS-PAGE electrophoresis

SDS-PAGE electrophoresis was carried out on a Mini-Protean II system (Bio-Rad Laboratories Inc., Hemel Hempstead, UK) using Mini-Protean Precast Gels (12% Tris/Glycin, 10 wells). Protein solutions were prepared using 10 µL of 4x Laemmli loading buffer with 50 mM dithiothreitol and the necessary amount of lysate or purified enzyme and MiliQ water to achieve a final concentration of 0.5 µg $µL^{-1}$ of protein in a 40 µL final volume. The samples were heated at 100 °C

on a Stuart SB200D/3 block heater (Stuart equipment, Staffordshire, UK) before loading 20 µL into the gel wells, 5 µL of protein ladder (Thermo Fisher Scientific, UK) were also loaded in the first well. The electrophoresis chamber was operated at 200 volts for 45 minutes using Bio Rad running buffer at 25 mM Tris, 192 mM glycine, 0.1% SDS (w/v), and pH 8.3. After opening the cassette, the gel was stained with 20 mL of InstantBlue staining solution (Expedeon, Cambridge, UK) for 15 minutes, and then washed three times with MiliQ water before being distained in MiliQ water for 24 hours. The protein bands were visualized on a Gel–Doc–It bioimaging system with Labworks 4.5 software (Bioimaging systems, Cambridge).

2.7.4. Densitometry analysis

In order to assess the purity of transketolase in the lysates or in the purified solutions, a densitometry analysis was performed. BSA standard (0.1, 0.2, 0.3, 0.4 and 0.5 mg mL^{-1}) and lysate (1 mg mL^{-1}) solutions were prepared as described in Section 2.5.4. After heating at 100 °C on a Stuart SB200D/3 block heater for 5 minutes, 10 µL of each standard solution, samples and 5 µL of protein ladder were loaded to each gel well. After SDS-PAGE and analysis on the Labworks 4.5 software, the transketolase concentration of the sample was calculated using a calibration curve that related the integrated optical density of the bands near to 72 KDa of the BSA dilution series with the concentration of protein loaded as shown in Appendix III.

2.7.5. HPLC quantification of substrates and product concentrations

2.7.5.1. Quantification of L-arabinose, L-glucoheptulose, and Li-HPA

Quantitative analysis of L-arabinose, L-glucoheptulose and Li-HPA was performed by high performance anion-exchange chromatography with pulsed amperometric detection (HPIC-PAD) using a Reagent-Free Ion Chromatography System (ICS 5000+, Dionex, Sunnyvale, CA, USA). A 4 x 250 mm Dionex CarbopacTM PA1 anion exchange column fitted with a 4 x 50 mm Dionex CarbopacTM PA1 guard column was used with an injection volume of 10 µL. The system had an electrochemical detector, and an eluent generator fitted with a KOH 500 cartridge. Analysis was carried out under isocratic flow conditions using 7.5 mM KOH as the mobile phase with a flow rate of 1.5 mL min^{-1} for 18 min at 30 °C. Retention times for L-arabinose, L-glucoheptulose and Li-HPA were 6.9, 9.8 and 14.5 minutes respectively. A sample chromatogram is shown in Appendix IV. Quantitative analyses were performed measuring peak height or area using the external standard method. Calibration curves for each of the solutes are shown in Appendix V.

2.7.5.2. Quantification of D-galacturonic acid

Quantitative analysis of D-galacturonic acid was performed using the ion chromatography system described in Section 2.7.5.1. D-galacturonic acid was analysed with a mobile phase of 5% (v/v) 0.5 M aqueous sodium acetate at 1 mL min^{-1} for 5 min at 30°C giving a retention time of 3.0 min. Quantitative analyses were performed measuring peak height or area using the external standard method. Sample chromatograms and calibration curves are shown in Appendix VI.

2.7.6. Measurement of transaminase activity

The activity of transaminase was determined by investigating the model bioconversion between methylbenzylamine (MBA) and pyruvate for the TAm-catalysed synthesis of L-alanine and acetophenone (AP). Samples of 20 µL of lysate were mixed with 180 µL substrate buffer (50 mM phosphate buffer at pH 7.4 containing 0.785 M MBA, 11 mM pyruvate, 1.25% (v/v) DMSO and 1 mM PLP) in a 96-well flat bottomed microtiter plate (Radleys Discovery Technologies, Essex, UK). During the reaction, the increasing absorbance of the reaction mixture was measured at 280 nm and 30 ºC every 10 seconds. The enzymatic activity was calculated according to Equation 2.1.

Eq. 2.1

$$\frac{U}{mL} = \frac{\Delta Abs}{min} \times \frac{V_{total}}{V_{sample}} \times \frac{1}{\varepsilon_{AP}} \times \frac{1}{d}$$

Where ΔAbs min-1 is the slope of the linear equation for each activity test, d is the path of light and ε_{AP} is the extinction coefficient of acetophenone (0.8477 mM^{-1} cm^{-1}). One unit of activity (U) is defined as the amount of enzyme that catalyses conversion of 1 µ mole of acetophenone per minute.

2.7.7. Colorimetric and MBA screening assays for transaminase bioconversions

As shown in Section 1.3, the products obtained from the transketolase mediated reaction of L-arabinose and D-galacturonic acid can be further upgraded via the utilisation of transaminase. In order to evaluate the successful amination of different sugars including, L-arabinose, L-glucoheptulose and D-galacturonic

acid, colorimetric and MBA assays were performed as described by Subrizi et al. (2019).

2.7.7.1. Colorimetric assay

The assay is based on the use of commercially available 2-(4-nitrophenyl)ethan-1-amine as amine donor which once converted into the corresponding aldehyde with subsequent basic work-up and deprotonation would give a red precipitate (Figure 2.2).

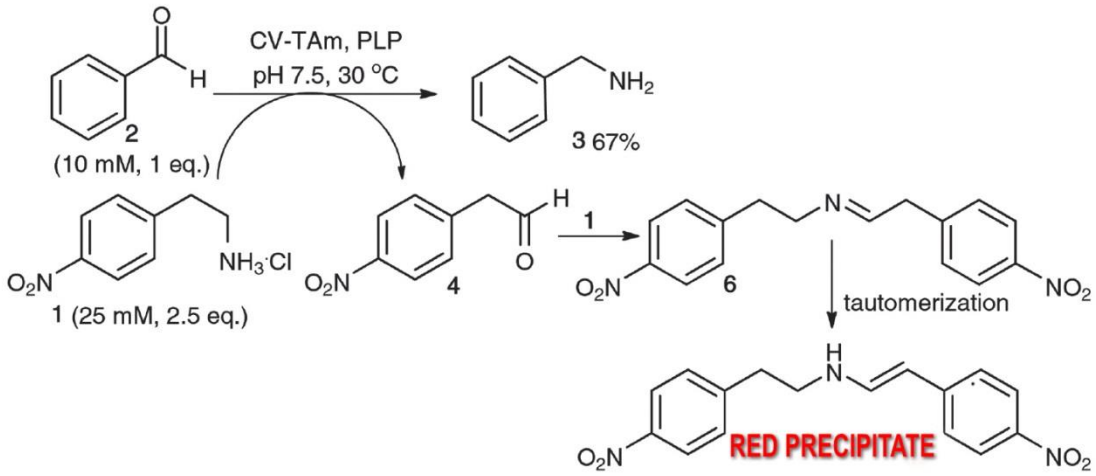

Figure 2.2. Use of 2-(4-nitrophenyl)ethan-1-amine as amine donor in a transamination reaction with Cv-TAm (Baud et al., 2015)

The assay was performed in 96 well-plates with a total volume of 200 µL containing 25 mM 2-(4-nitrophenyl)ethan-1-amine hydrochloride as amine donor, 10 mM of the selected amine acceptor (D-galacturonic acid, L-arabinose, D-Ribose, D-xilose, L-rhamnose, D-ribulose, D-fructose, L-sorbose, D-tagatose, and L-glucoheptulose), 0.5 mM PLP and 100 mM potassium phosphate buffer (pH 8.0). The reaction was started by the addition of 20 µL TAm clarified lysate and the reaction was incubated at 30 °C with shaking at 500 rpm for 24 h. Pyruvate and buffer were used as positive and negative controls respectively.

An orange/red coloration provided a visual indication that the TAms could accept the selected aldehydes.

2.7.7.2. MBA screening

The assay was performed in an Eppendorf tube with a total volume of 500 µL containing 20 mM of *(R)*- or *(S)*-MBA, 2 mM PLP, 100 mM potassium phosphate buffer (pH 8.0), 5 mM of the amine acceptor (D-galacturonic acid, L-arabinose, D-Ribose, D-xilose, L-rhamnose, D-ribulose, D-fructose, L-sorbose, D-tagatose, and L-glucoheptulose) and 30 µL of crude cell lysate. After 24 h of incubation at 30 °C with orbital shaking at 350 rpm, 100 µL of 0.1% trifluoroacetic acid (TFA) in water was added to stop the reaction. After centrifugation at 12000 x g and 4°C for 10 minutes in an Eppendorf 5424 R Centrifuge, the supernatant was diluted with water and analysed by analytical HPLC using an ACE 5-C18 300 column (150 × 4.6 mm) with UV detection at 250 nm. The concentration of acetophenone produced was determined using a linear gradient from 15–72% B over 10 minutes at a flow rate of 1 mL min^{-1} (A = water with 0.1% of TFA and B = acetonitrile). Negative controls without amine acceptor were also prepared for all substrates. The acetophenone (ACP) produced eluted at a retention time of 8.8 min.

3. TK MUTANT SELECTION, AND KINETIC PARAMETER DETERMINATION FOR THE BIOCONVERSION OF L-ARABINOSE TO L-GLUCOHEPTULOSE USING TK LYSATE

3.1. Introduction

As described in Section 1.7.1, sugar beet pulp could be used as a sustainable source of substrates for obtaining chiral polyalcohols via TK bioconversion for the production of active pharmaceutical ingredients. L-arabinose is one of the major components of sugar beet pulp after saccharification, accounting for 20.9% of the total dry mass (Micard et al., 1996). The TK catalysed reaction of L-arabinose and Li-HPA yields CO_2 which makes the reaction irreversible, and L-glucoheptulose; a ketoheptose not found in nature with potential for hypoglycaemia and cancer applications (Board et al.,1995; Waschke et al., 2012; Bawn et al., 2018) (Figure 3.1).

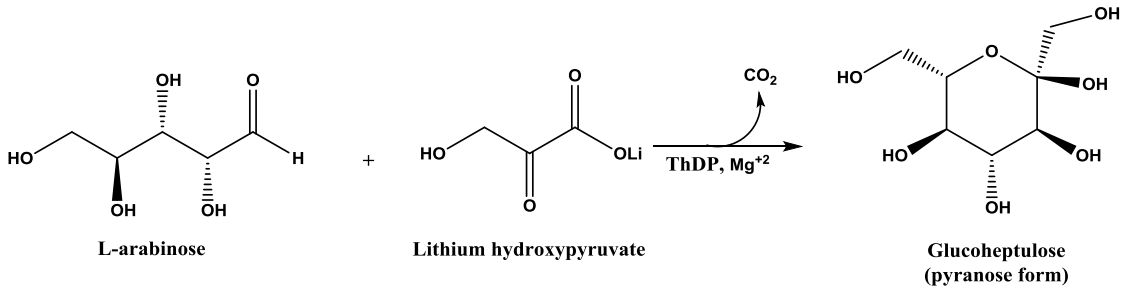

Figure 3.1. Reaction scheme of the TK catalysed reaction of L-arabinose and Li-HPA to CO_2 and L-glucoheptulose.

Initial studies on the bioconversion of L-arabinose and Li-HPA to L-glucoheptulose have been carried out by Subrizi et al. (2016), using a colorimetric screening method on a TK mutant library. This work identified a small group of mutants that can accept L-arabinose as substrate. However, for optimisation and scale up of the production of L-glucoheptulose, it is necessary to establish a methodology for selecting the best of these TK mutants and to optimise its production. Obtaining the kinetic parameters for the overall reaction will provide fundamental insights into the reaction kinetics that will establish a basis for bioconversion optimisation.

3.2. Aim and objectives

The aim of this chapter is to obtain the kinetic parameters of the reaction of L-arabinose and Li-HPA to L-glucoheptulose, using TK lysate as biocatalyst. The lysate form of the biocatalyst was investigated since this provides high activity but overcomes the need for expensive purification steps, making it more suited to biorefinery applications. Initial work involved the selection of the best TK mutant from the previous selection by Subrizi et al. (2016), the optimisation of growth and TK expression on the selected mutant, as well as obtaining the kinetic parameters of the reaction based on the approach developed by Chen et al. (2006). The key objectives of this chapter are thus:

- Determination of the best TK mutant candidate for the synthesis of L-glucoheptulose based on overall cell growth, protein content, TK expression, and total bioconversion yield.
- Evaluation of cell growth kinetics and TK expression in shake flasks for the selected TK mutant in order to maximize TK production.

- Determination of the kinetic parameters for the TK lysate mediated bioconversion of L-arabinose and Li-HPA to L-glucoheptulose, in order to guide subsequent bioconversion process design.
- Evaluation of the subsequent TAm-catalysed conversion of L-glucoheptulose to (2*S*,3*S*,4*S*,5*R*)-6-aminoheptane-1,2,3,4,5,7-hexaol (AHH) production.

3.3. Results

3.3.1. Biocatalyst selection

According to initial studies by Subrizi et al. (2016) on UCL-TK mutant libraries selected for their ability to accept polyhydroxylated substrates, the *E. coli* TK mutants with the highest conversion yield of L-arabinose to L-glucoheptulose after 24 h were R520Y and H461Y. Therefore, these two TK mutants were further investigated in this work.

Growth profiles of *E. coli* XL-10 Gold constitutively expressing either the R520Y or H461Y TK mutants are shown in Figure 3.2. The calculated maximum specific growth rate (μ_{max}) was 0.2 and 0.22 h^{-1} for R520Y and H461Y respectively, with a doubling time (dt) of 3.5 and 3.2 h respectively. H461Y biomass production was slightly higher than R520Y with peak biomass concentration of 2.54 ± 0.02 and 2.1 ± 0.02 g_{dcw} L^{-1} respectively. It was established that the mid log phase for both R520Y and H461Y mutants is around 4 hours.

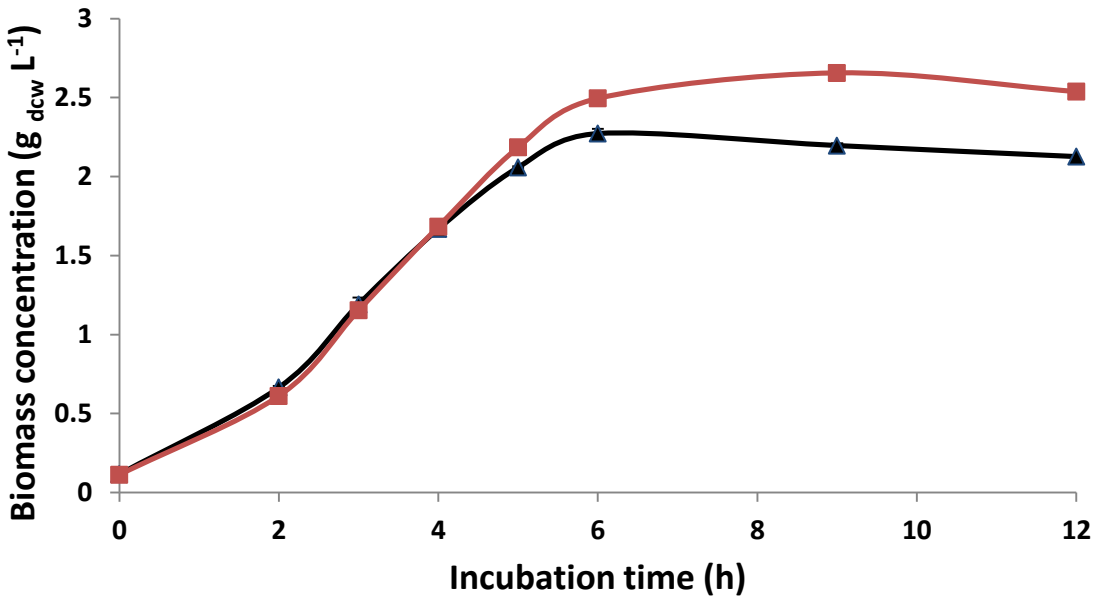

Figure 3.2. *E. coli* growth kinetics, expressing (■) H461Y and (▲) R520Y TK mutants grown in LB media. Fermentation was performed in 100 mL shake flasks with a total volume of 150 mL of LB broth at 450 rpm and 37 °C as described in Section 2.2.2. Samples were taken at regular time intervals for OD measurement as described in Section 2.7.1. Error bars represent one standard deviation of the mean (n=3).

In terms of protein content, as Figure 3.3 shows, the R520Y mutant was found to produce the highest amount of total protein in comparison with the H461Y mutant. However, a densitometry analysis was also required in order to verify that high protein expression in the R520Y mutant also corresponded to the highest TK production.

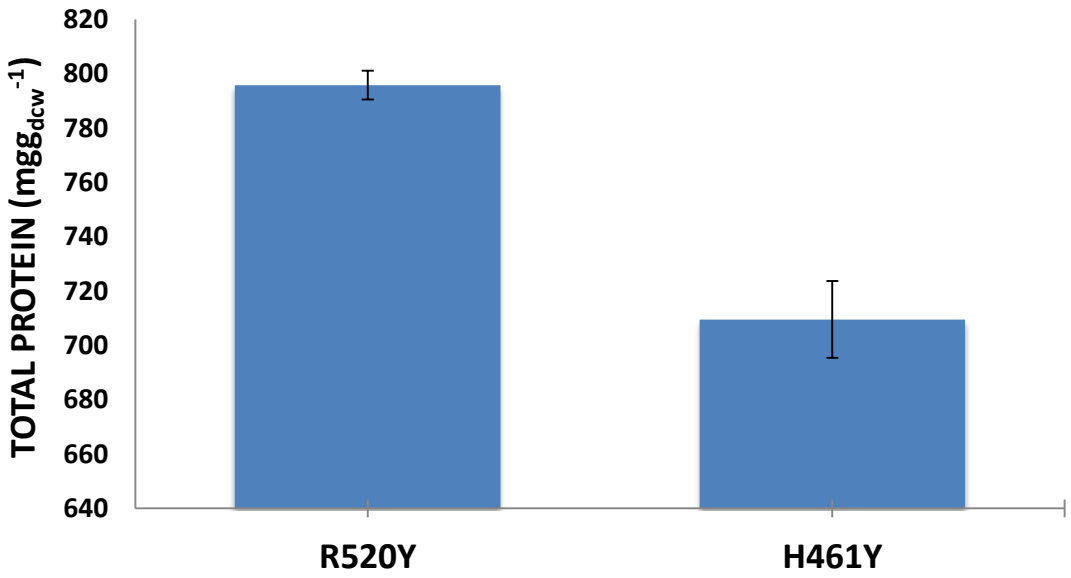

Figure 3.3. Total protein content of the different *E. coli* TK mutant strains using the Bradford Assay. Experiment was performed as described in Section 2.7.2. Error bars represent one standard deviation of the mean (n=3)

According to Klumpp et al (2009), bacterial gene expression depends not only on regulatory mechanisms, but also on bacterial growth as important parameters as RNA polymerase and ribosome abundance are growth-dependant, and will change when the cell state changes. For this reason, densitometry analysis was performed with both R520Y and H461Y mutant strains as described in Section 2.7.4 in order to quantify the concentration of TK at different times during fermentation. As Figure 3.4 shows, the H461Y mutant strain produced a considerably higher amount of TK than the R520Y mutant strain, reaching its highest after twelve hours of incubation with 0.36 mg of TK per mg of total protein. In contrast, the R520Y mutant only produces a maximum of 0.27 mg of TK per mg of total protein.

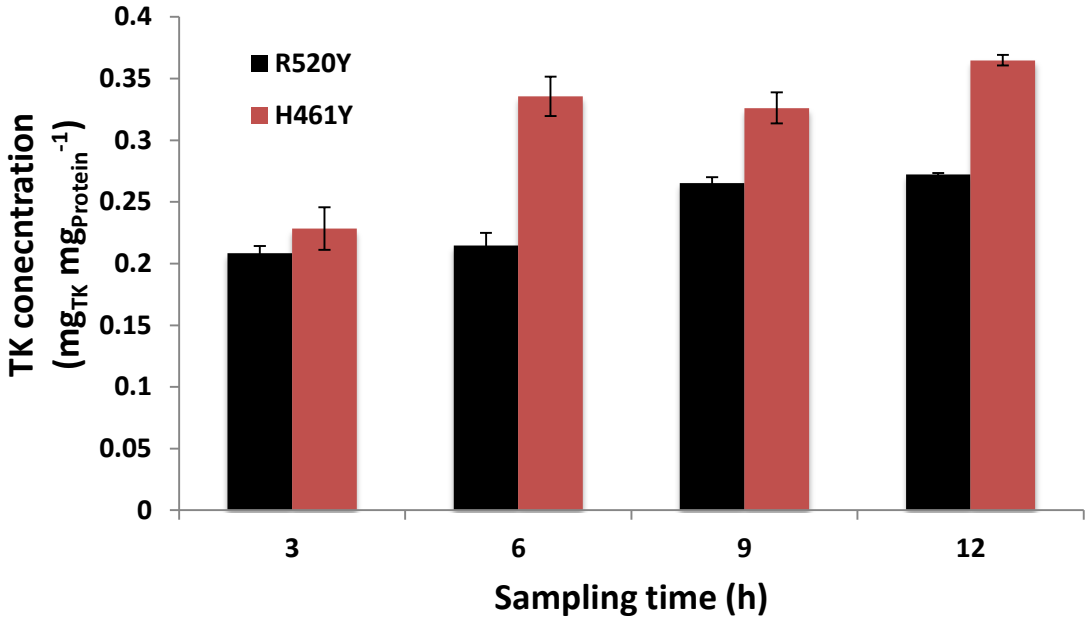

Figure 3.4. Specific concentration of R520Y and H461Y TK mutants by densitometry analysis at different harvesting times during fermentation. Fermentation was performed in 100 mL shake flasks with a total volume of 150 mL of LB broth as described in Section 2.2.2. Samples were taken at 3, 6, 9 and 12 hours and total protein determined by the Bradford Assay. Densitometry analysis was performed as described in Section 2.7.4.

SDS-PAGE electrophoresis was performed as described in Section 2.7.3, using the cell free lysate from both mutant strains alongside a number of other mutant strains of interest. TK subunit has a molecular weight of 72 KDa which corresponds to the thickest bands on the gel confirming its overexpression. As can be seen in Figure 3.5, mutant H461Y exhibited the highest TK expression in comparison with mutant R520Y and higher than the other TK mutants analysed.

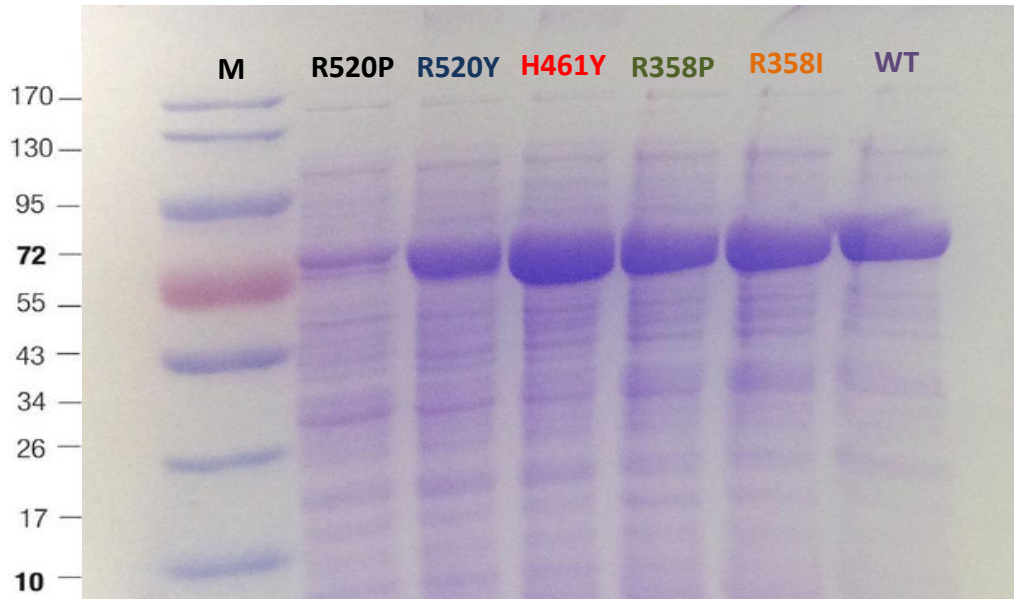

Figure 3.5. SDS-PAGE gel showing total protein expression of the different *E. coli* TK mutants. Experiment was performed as described in Section 2.7.3. Lane M is the protein marker, and the name of each mutant is written on top of the following lanes. The amount of protein loaded was the same for all lanes, showing that the H461Y mutant has the highest TK expression.

Finally, bioconversions using clarified lysates from R520Y and H461Y at different harvesting times were performed as described in Section 2.4.1. As shown in Table 3.1, the highest specific initial rate (Spr_0) for mutants R520Y and H461Y were reached at 6 hours. The highest total conversion yield of 65% (% mol/mol) was reached when H461Y was used, in comparison with the 36% total bioconversion yield obtained when R520Y was used. On the basis of these results, H461Y TK mutant was selected as the best for the production of L-glucoheptulose and it was used throughout the rest of the project.

Table 3.1. Specific initial rate and total bioconversion yield of TK R520Y and H461Y bioconversions from L-arabinose to L-glucoheptulose at different harvesting times

Harvest time (h)	Specific initial rate (μmol gmin^{-1})		Total conversion yield after 48 h of reaction (% mol/mol)	
	R520Y	**H461Y**	**R520Y**	**H461Y**
6	4.25 ± 0.01	4.53 ± 0.05	42	52
9	4.15 ± 0.11	2.69 ± 0.08	40	62
12	4.27 ± 0.01	3.36 ± 0.22	36	65

*Total conversion yield is based on the formula: $\%\ yield = \frac{[Glucohep]_{Actual}}{[Glucohep]_{Theorical}} * 100\ \%$; Where $[Glucohep]_{Actual}$ is the glucoheptulose concentration obtained by HPLC after 48 h of reaction, $[Glucohep]_{Theorical}$ is the expected concentration after complete bioconversion which, based on the stoichiometry of the reaction it is equal to the initial concentration of L-arabinose in the reaction.

3.3.2. Kinetic parameter quantification for the TK lysate catalysed bioconversion of L-arabinose and Li-HPA to L-glucoheptulose

As the transketolation follows a ping-pong bi-bi ordered mechanism with competitive inhibition for both substrates (Gyamerah & Willets, 1997), the King-Altman method (1956) was used for obtaining all the fundamental kinetic combinations and substrates multipliers needed for defining the rate equation for the reaction.

According to King-Altman, the reaction needs to be presented in a closed “box” format (Figure 3.6), which allows a better view of the four enzymatic species in the reaction. It shows where each substrate is added to the enzyme or enzymatic intermediate, as well as where each product is released from the enzyme or enzymatic intermediate.

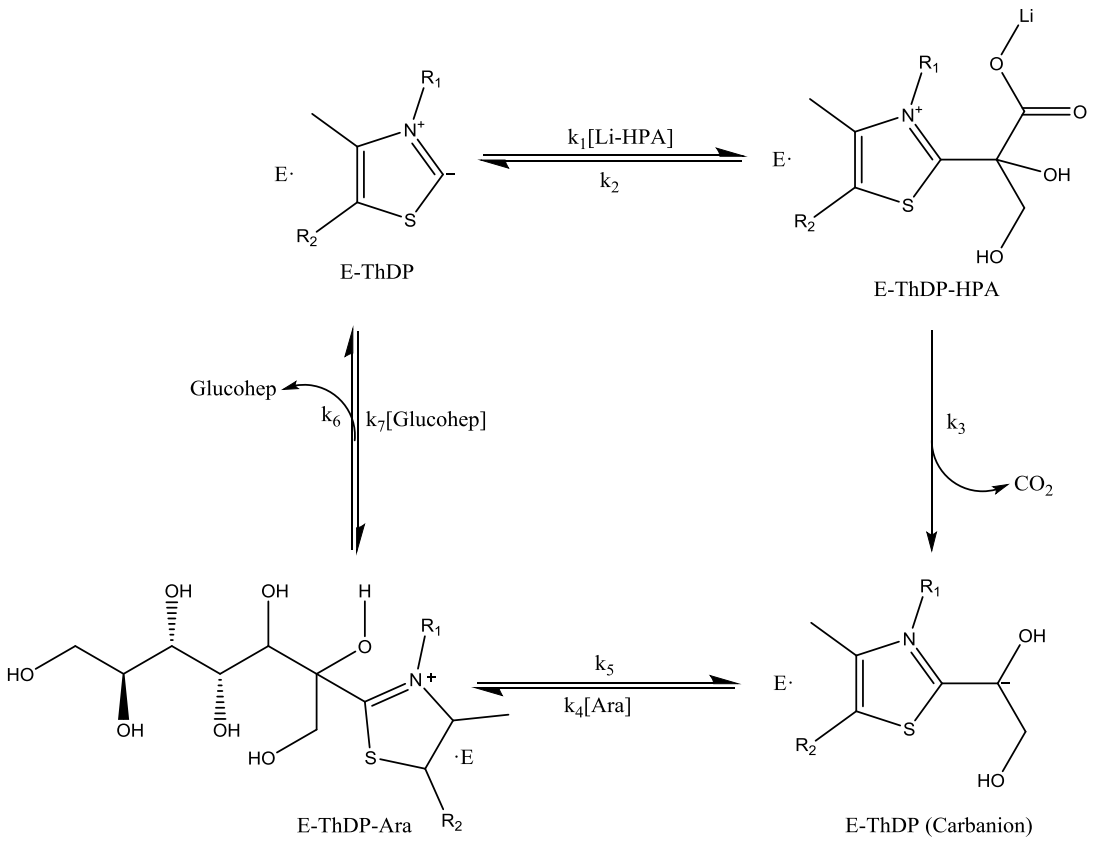

Figure 3.6. Proposed King-Altman scheme for the transketolation of L-arabinose to L-glucoheptulose.

Moreover, Figure 3.6 can be shown as a simple square illustration, called the "Master Pattern" (Figure 3.7), in which the four sides of the box represent the four sides of the reaction, and each of the corners represent the enzymatic species.

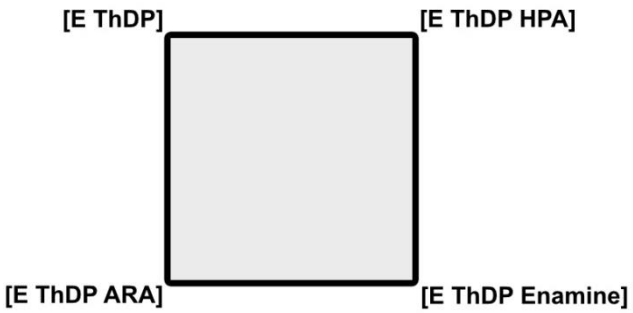

Figure 3.7. Master Pattern of the reaction presented in Figure 3.6 for rate derivation by the King-Altman Method.

The King-Altman method stipulates that all “patterns” (consisting only of lines from the Master Pattern) that connect each enzymatic species must be found, without containing any loops. According to this, each pattern will contain 1 line less than the total number of enzymatic species. Figure 3.8 shows all the patterns found in the TK reaction presented in Figure 3.7.

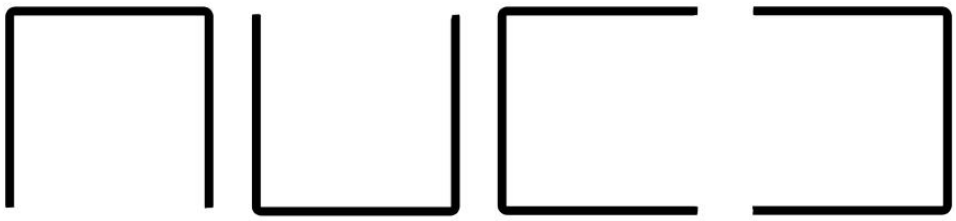

Figure 3.8. Patterns that connect every enzymatic species of the TK reaction shown in Figure 3.7.

For each of the enzymatic species and each pattern, the product of the rate constants in the pattern leading to that species can be written down with the combination of three arrows, all pointing to only one of the four species. Figure 3.9 shows all the patterns ending on each of the four enzymatic species. It is important to note that by using Li-HPA as one of the substrates, the reaction for obtaining the [E ThDP Enamine] intermediate is irreversible, as CO_2 is released from the reaction mix (Figure 3.6).

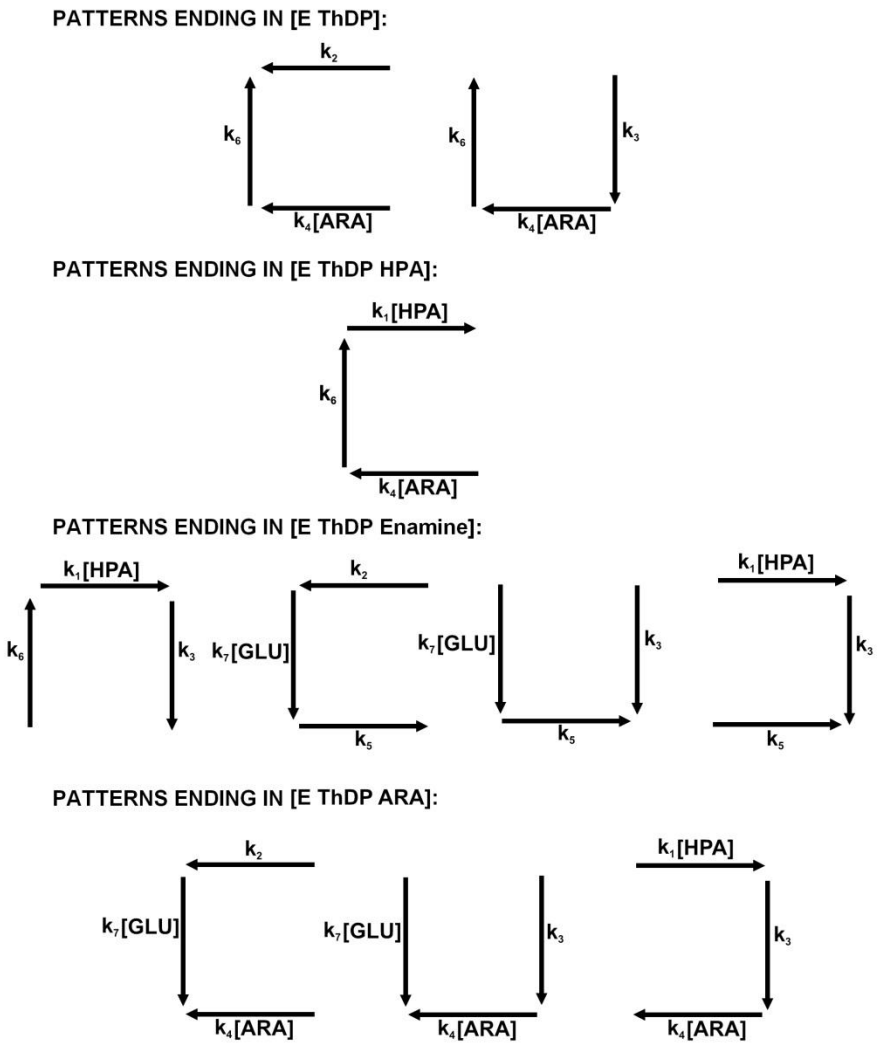

Figure 3.9. Patterns and kinetic combinations of the enzymatic species of the TK reaction shown in Figure 3.7 according to the King-Altman Model.

The fraction of each enzyme species ($[EX_i]/[E_t]$) in the steady-state mixture will be the sum of contributing kinetic constant combinations plus the substrate multipliers, divided by the sum of all kinetic constants combinations (Σ). Equations 3.1 to 3.4 show the steady-state concentrations of each of the enzymatic species based in Figure 3.9.

Eq.3.1

$$\frac{[E\ ThDP]}{[E_t]} = \frac{k_2 k_4 k_6 [ARA] + k_3 k_4 k_6 [ARA]}{\Sigma}$$

Eq.3.2

$$\frac{[E\ ThDP\ HPA]}{[E_t]} = \frac{k_1 k_4 k_6 [ARA][HPA]}{\Sigma}$$

Eq.3.3

$$\frac{[E\ ThDP\ Enamine]}{[E_t]} = \frac{k_1 k_3 k_6 [HPA] + k_2 k_5 k_7 [GLU] + k_3 k_5 k_7 [GLU] + k_1 k_3 k_5 [HPA]}{\Sigma}$$

Eq.3.4

$$\frac{[E\ ThDP\ ARA]}{[E_t]} = \frac{k_2 k_4 k_7 [ARA][GLU] + k_3 k_4 k_7 [ARA][GLU] + k_1 k_3 k_4 [HPA][ARA]}{\Sigma}$$

$$\begin{aligned}\Sigma = {} & k_2 k_4 k_6 [ARA] + k_3 k_4 k_6 [ARA] + k_1 k_4 k_6 [ARA][HPA] + k_1 k_3 k_6 [HPA] \\ & + k_2 k_5 k_7 [GLU] + k_3 k_5 k_7 [GLU] + k_1 k_3 k_5 [HPA] \\ & + k_2 k_4 k_7 [ARA][GLU] + k_3 k_4 k_7 [ARA][GLU] + k_1 k_3 k_4 [HPA][ARA]\end{aligned}$$

These equations derived from the King-Altman method are used for the algebraic derivation of the kinetic expression presented in Equation 3.5 for the reaction kinetics of the TK-mediated synthesis of L-glucoheptulose from L-arabinose and Li-HPA.

Eq.3.5

$$\frac{d[GLU]}{dt} = \frac{k_{cat} E_i [HPA][ARA]}{K_{ARA}[HPA]\left(1 + \frac{[HPA]}{K_{iHPA}}\right) + K_{HPA}[ARA]\left(1 + \frac{[ARA]}{K_{iARA}}\right) + [HPA][ARA] + \frac{K_{HPA}}{K_{iHPA}}[ARA][GLU] + \frac{K_{HPA}K_{iARA}}{K_{iGLU}}[GLU]}$$

Where [HPA], [ARA], and [GLU] represent the concentrations of lithium hydroxypyruvate, L-arabinose and L-glucoheptulose repectively. k_{cat} is the reaction rate constant; K_{HPA} and K_{ARA} are the Michaelis constants of the

reactants, Ki_{HPA}, Ki_{ARA} and Ki_{GLU} are the inhinition contants and Ei is the enzyme concentration in the bioconversion.

As described in Section 2.5, Chen et al. (2008) developed a new approach to bioconversion kinetic parameter identification based in a hybrid methodology that utilises the best features of linear (Lineweaver and Burk, 1934; Hofstee, 1952; Hofstee, 1959; Eisenthal and Cornish-Bowden, 1974; Dixon, 1953) and non-linear (Wilkinson, 1961; Downd and Riggs, 1965; Garfinkel et al., 1977; Ranaldi et al., 1999) methods. This new approach has been successfully applied for transketolase (Chen et al., 2008 and Chen et al., 2009) and transaminase bioconversions (Rios-Solis, et al., 2011).

The method is based on obtaining preliminary kinetic values, reducing the number of estimated parameters by the utilisation of basic linear methods. The preliminary kinetic data then will be used as initial values for a non-linear regression for obtaining the final kinetic parameters.

The approach followed consists of four main steps as shown in Figure 3.10, and are described as follows:

1. To determine the proportionality between initial reaction rate and enzyme concentration.
2. To obtain preliminary kinetic parameters by the utilisation of two sets of initial rates. One set of initial rates is obtained by varying the concentration of one substrate and maintaining the concentration of the other substrate fixed, and the other set is obtained by doing the opposite. All experiments are performed at a fixed protein or enzyme concentration.

3. To determine the preliminary full kinetic parameters by the non-linear regression of bioconversion progress curves at different enzyme and substrate concentrations.
4. To reconcile the kinetic parameters by a new non-linear regression of the progress curves, using all the preliminary kinetic parameters as initial values.

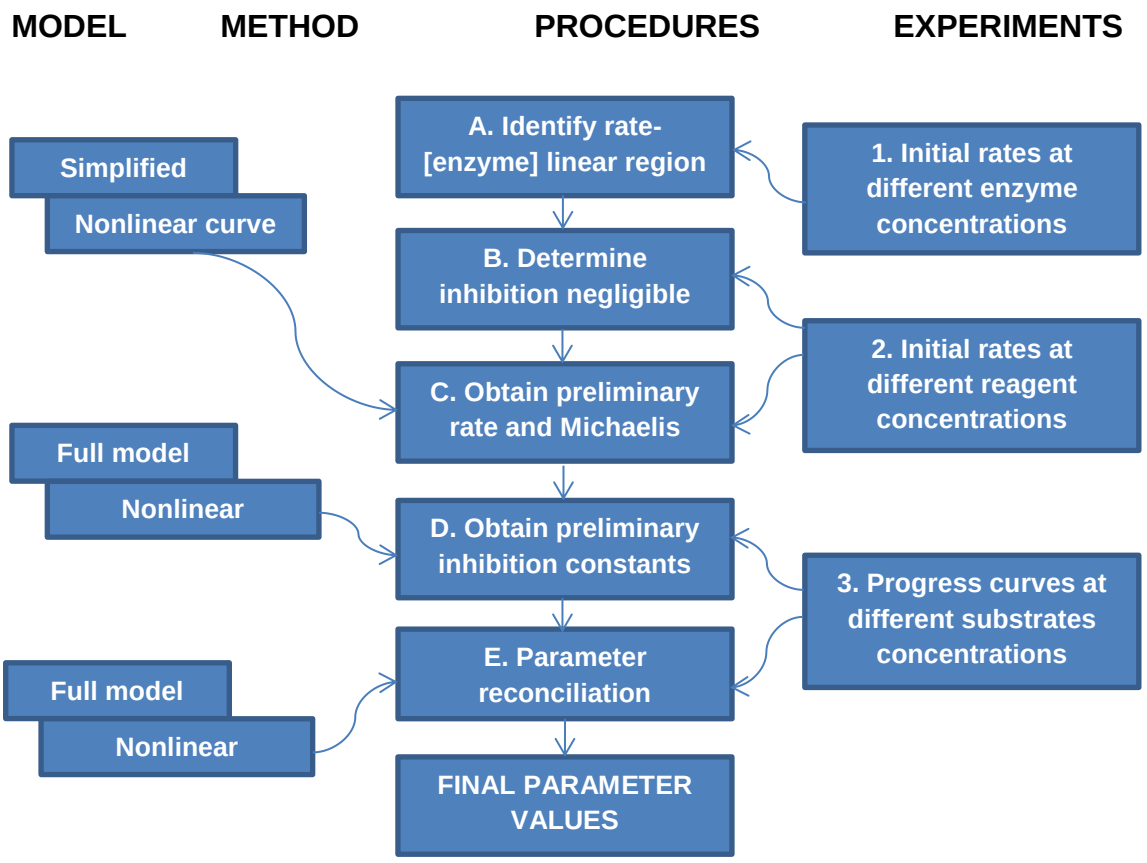

Figure 3.10. Schematic representation of the systematic procedure for rapid kinetic parameter identification.

In order to implement the non-linear regression and all the statistical analyses required for the method, a programme was developed (Appendix VII) using MatLab software (MathWorks, Natick, MA, USA).

3.3.2.1. Proportionality between initial reaction rate and protein concentration

Based on Figure 3.10, the first step on the approach for obtaining the kinetic parameters is to determine the linear region between protein concentration and initial reaction rate. This step is fundamental for ensuring that any change in enzyme concentration would contribute to the kinetic values (Chen et al., 2008).

The necessary experiments were performed as described in Section 2.5.1.1. An equimolar concentration of 33 mM was used for L-arabinose and Li-HPA, and lysate was used as biocatalyst at different concentrations in the reaction from 0.33 to 3.6 mg mL^{-1}. The linear relationship between lysate concentration and initial rate was maintained up to 3.6 mg mL^{-1} of protein in the reaction as can be seen in Figure 3.11. This concentration was used for all following experiments as this was the protein concentration obtained when using the lysate with no dilution.

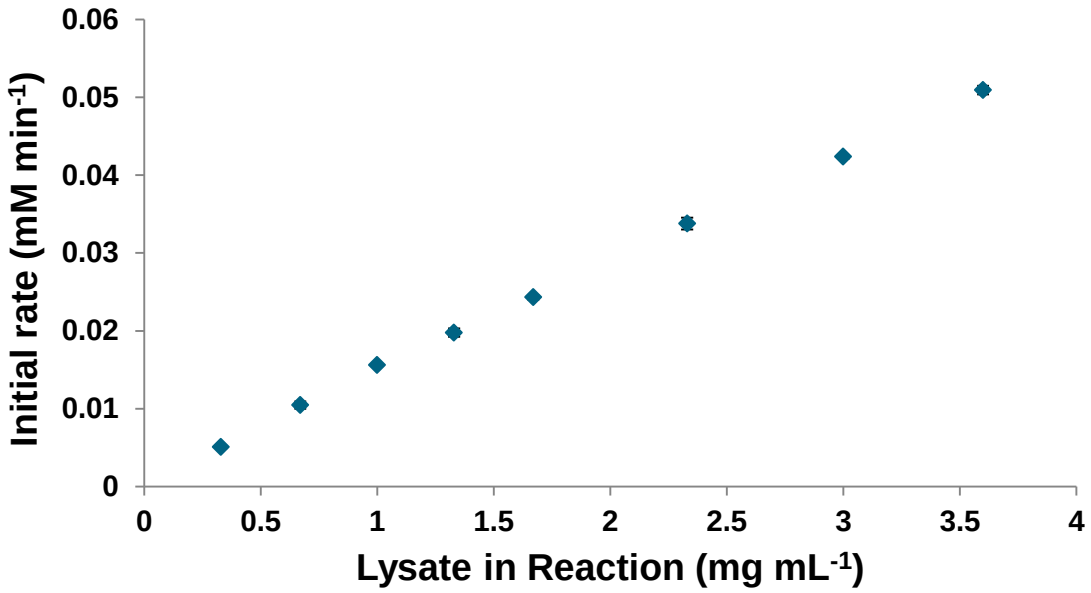

Figure 3.11. Initial rate of L-glucoheptulose formation as a function of total protein in the bioconversion of L-arabinose and Li-HPA to L-glucoheptulose. Reaction conditions: 33 mM Li-HPA, 33 mM L-arabinose, 1.7 ThDP, 6 mM $MgCl_2$, 450 rpm and 25 °C. Lysate was used at different concentrations in the reaction from 0.33 to 3.6 mg mL^{-1}. Experiments were performed as described in Section 2.4.1. Error bars represent one standard deviation of the mean (n=3).

3.3.2.2. Kinetic model of TK and initial rate experiments

The second step on the methodology shown in Figure 3.10 is to obtain two sets of initial reaction rate data. The first set was obtained by varying L-arabinose concentration while fixing Li-HPA concentration. The second set was obtained by varying Li-HPA concentration while maintaining L-arabinose at a fixed concentration.

For the first set, different L-arabinose concentrations were tried; at first a range from 5 to 30 mM was used, maintaining the linear behaviour between L-arabinose concentration and initial reaction rate. Higher L-arabinose concentrations were then tried up to 540 mM, obtaining the trend shown in Figure 3.12.

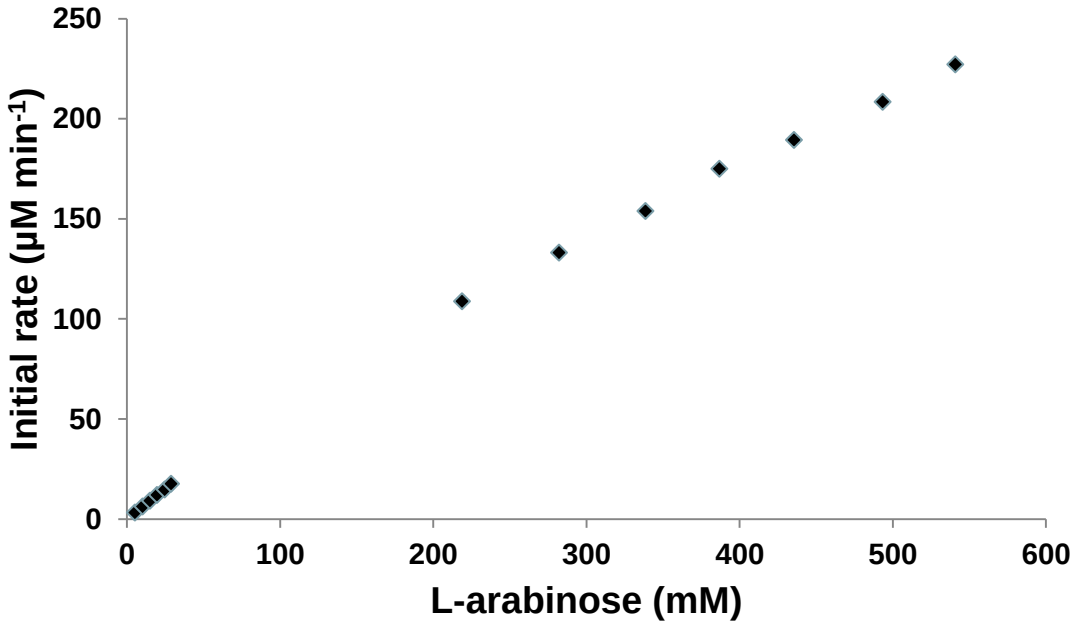

Figure 3.12. Initial rate of L-glucoheptulose formation as a function of initial L-arabinose concentration and a fixed Li-HPA concentration, using TK lysate. Reaction conditions: 30 mM Li-HPA, 1.7 ThDP, 6 mM $MgCl_2$, 450 rpm and 25 °C. L-arabinose was used in a range from 10 to 1000 mM. Experiments were performed as described in Section 2.5.1.2. Error bars represent one standard deviation of the mean (n=3).

Based on the results shown in Figure 3.12, little L-arabinose inhibition was found in the reaction, this means that there is no saturation of the TK active site up to the maximum substrate concentration tested. This is an important finding with regard to the potential for processing biorefinery streams containing high concentrations of L-arabinose.

For obtaining the second set of initial reaction rate data, L-arabinose concentration was fixed at 30 mM, and Li-HPA was varied at first between 5 – 10 mM, but these results showed a high degree of Li-HPA inhibition as the result was the same initial reaction rate for all Li-HPA concentrations used. Subsequently, a new range of Li-HPA concentrations was evaluated, from 0.2 to 10 mM, and it was found that Li-HPA shows reaction rate inhibition after 1 mM as shown in Figure 3.13.

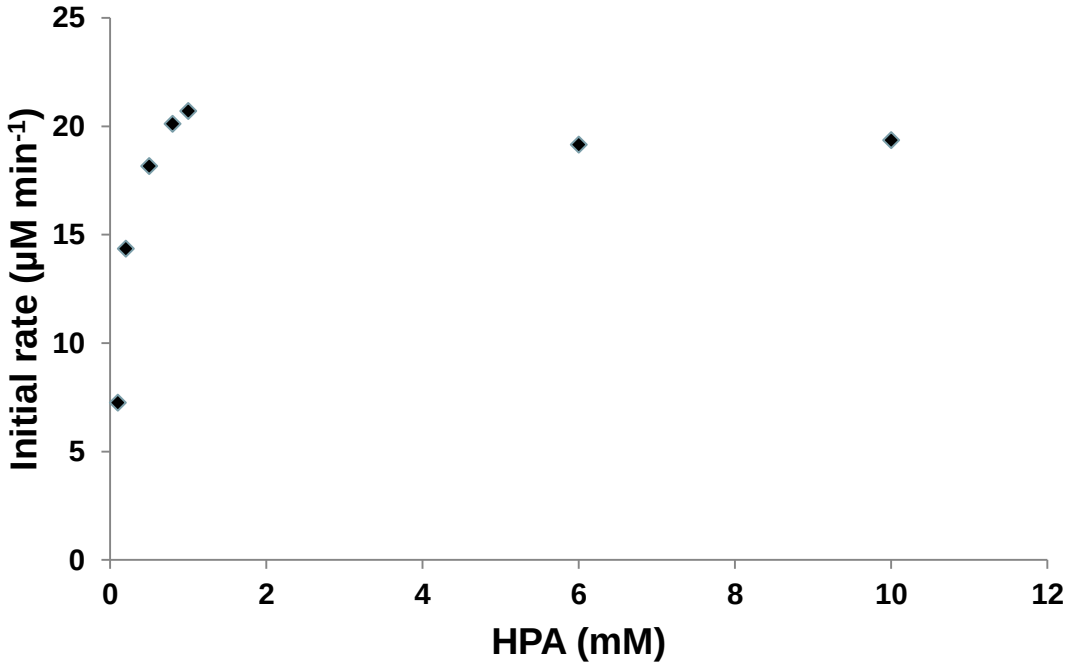

Figure 3.13. Initial rate of L-glucoheptulose formation as a function of initial Li-HPA concentration and a fixed L-arabinose concentration, using TK lysate. Reaction conditions: 30 mM L-arabinose, 1.7 mM ThDP, 6 mM $MgCl_2$, 450 rpm and 25 °C. HPA was used in a range from 0.2 to 10 mM. Experiments were performed as described in Section 2.5.1.2. Error bars represent one standard deviation of the mean (n=3).

The significant substrate inhibition that Li-HPA showed in the reaction could limit the productivity of any industrial bioconversion process. This would need to be overcome by the operation of fed-batch reactors (Rios-Solis, 2015) to maintain the level of Li-HPA in the reactor below inhibitory concentrations.

The other purpose of these two sets of initial reaction rate data was to find the linear region between substrate concentration and initial reaction rate, in order to operate in the range where no substrate inhibition is determinant. For L-arabinose the linear range utilised was from 5 to 55 mM, even when it could get up to 540 mM without losing the linear behaviour; while for the case of Li-HPA the linear range was found to be between 0.2 and 1 mM.

In order to estimate the initial kinetic parameters, linear plots of the data were subsequently performed using Equation 3.6, which is a modification of Equation 3.5 without inhibition constants, as reaction products are low and therefore product and substrates inhibition is negligible. The preliminary kinetic parameters for K_{HPA}, K_{ARA} and V_{MAX} were 2.86 mM, 1449.22 mM and 853.49 µM min^{-1} respectively. These values were used for the non-linear refinement of the progress curves detailed in the subsequent sections.

Eq.3.6

$$\frac{d[GLU]}{dt} = \frac{k_{cat}E_i[HPA][ARA]}{K_{ARA}[HPA] + K_{HPA}[ARA] + [HPA][ARA]}$$

3.3.2.3. Progress curves for kinetic parameter identification

The final experimental step on the methodology shown in Figure 3.10 was to obtain the full reaction progress curves of five different reactions at different substrate and enzyme concentrations, with the objective of including possible

substrate and product inhibition in the data analysis. A set of 5 different reactions were performed as described in Section 2.5.1.3., and samples were taken every 2 hours for 24 hours. This provided a total of thirteen sample points for maximizing the accuracy of fitting the mathematical model. The substrates and protein concentrations used are shown in Table 2.5.

Initial experiments were performed for 48 hours, but it was noticed that the reaction reached a plateau in 24 hours. The preliminary results for K_{HPA}, K_{ARA}, Ki_{HPA}, Ki_{ARA}, Ki_{GLU} based on a 24 hour reaction time were 2.86, 1449.22, 56, 1029, and 916 mM respectively, the value for k_{cat} was 127 min^{-1}. These preliminary data were used as initial guesses for the full kinetic model in order to obtain the final kinetic parameters.

The final model fit and parameter optimisation was obtained in MatLab (MathWorks, Natick, USA), using the pattern search algorithm available in the 'Genetic Algorithm and Direct Search Toolbox' with Maximun likehood, using the objective function defined in Equation 3.7, where *y* and $\hat{y}$ are experimental results and model predicted values, respectively; $y_{i,j}$ is the experimental result of the *j*th response variable in the *i*th experiment; N_j is the number of observations of the *j*th response variable, and *M* is the number of variables (Chen et al., 2008). The lower and upper bounds for all non-linear regressions were set at 0.0001 and 800.

Eq.3.7

$$\Phi = -\frac{1}{2}\sum_{j=1}^{M}\left[N_j(\ln(2\pi)+1) + N_j ln\left[\left(\frac{1}{N_j}\right)\sum_{i=1}^{N_j}\left(y_{i.j}-\hat{y}_{i,j}\right)^2\right]\right]$$

The global optimisation was achieved after a second run on the full kinetic model, and the final values for each kinetic parameter were: 1, 1200, 0.06, 247.5, and 8.5 mM for K_{HPA}, K_{ARA}, Ki_{HPA}, Ki_{ARA}, and Ki_{GLU} respectively. The final value for k_{cat} was 140 min^{-1}. Figure 3.14 shows a comparison of the experimental progress curves against the fitted mathematical model for a range of initial substrate concentrations, and the corresponding rate model is displayed in Equation 3.8. Model Predictions and residuals from the final model fit are shown in Section A of Appendix VIII.

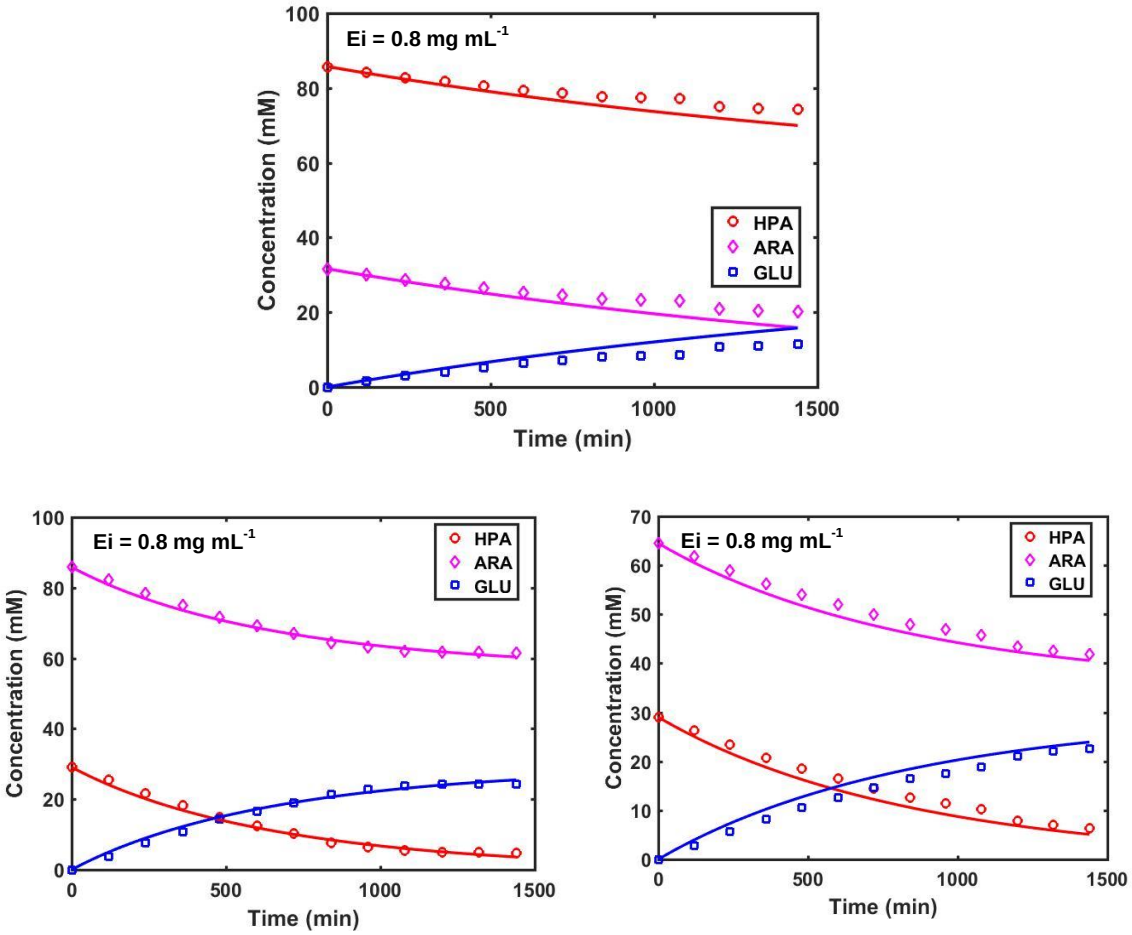

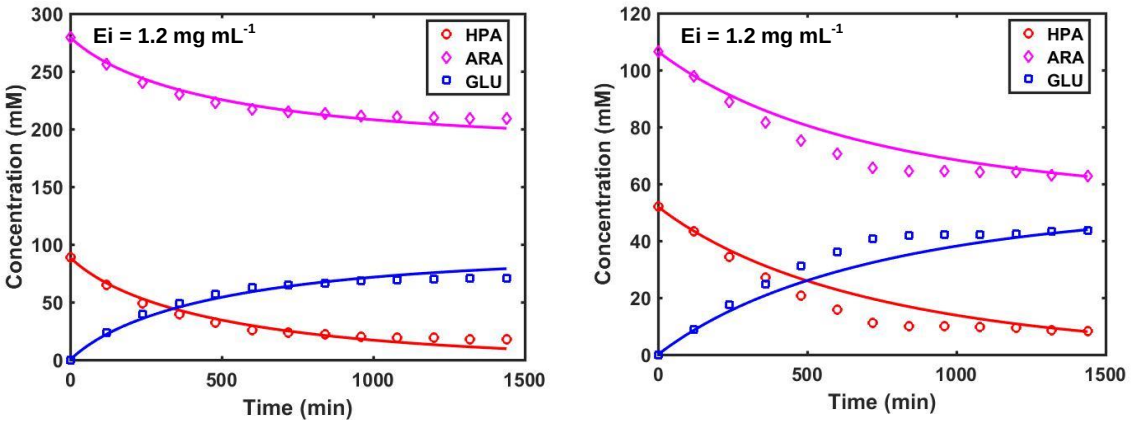

Figure 3.14. Comparison of experimental and fitted progress curves using different concentrations of lysate, Li-HPA, and L-arabinose for the TK synthesis of L-glucoheptulose. Lines show model predictions and dots represent the experimental data. Error bars represent one standard deviation of the mean (n=3).

Eq.3.8

$$\frac{d[GLU]}{dt} = \frac{140E_i[HPA][ARA]}{1200[HPA]\left(1+\frac{[HPA]}{0.06}\right)+[ARA]\left(1+\frac{[ARA]}{247.5}\right)+[HPA][ARA]+\frac{1}{0.06}[Ara][GLU]+29.12[GLU]}$$

Finally, a separate experiment was performed at substrate concentrations not used for parameter fitting in order to validate the predictive power of the model and suitability of the kinetic parameters obtained. The experiment was performed as described in Section 2.5.1.3, and the concentrations for L-arabinose and Li-HPA used were 34 and 26 mM respectively, and the lysate concentration in the reaction was 0.9 mg mL^{-1}. The fit of the model to the experimental data can be seen in Figure 3.15.

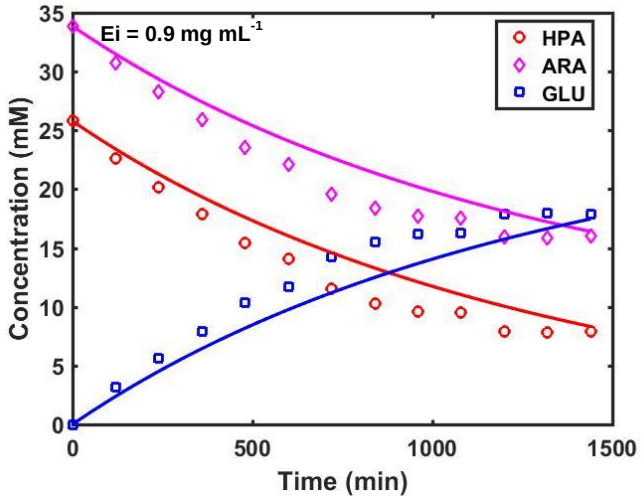

Figure 3.15. Verification of model predictions with an experimental set of data not included in the initial progress curve experiment. Reaction conditions: 34 mM L-arabinose, 26 mM Li-HPA, 1.7 mM ThDP, 6 mM $MgCl_2$, 0.9 mg mL^{-1} of lysate, 450 rpm and 25 °C. Lines show model predictions and dots represent the experimental data. Error bars represent one standard deviation of the mean (n=3).

3.3.3. Transaminase catalysed amination of L-glucoheptulose

As described in Section 1.6, the coupling of transketolase and transaminase bioconversions provides an elegant route for the synthesis of chiral polyaminoalcohols. For this reason, after optimising the TK-catalysed production of L-glucoheptulose, preliminary experiments were performed to explore the subsequent TAm-catalysed conversion of L-glucoheptulose to the corresponding polyaminoalcohol (Figure 1.13). Consequently, the production of transaminase was established along with the relationship between TAm activity and culture duration after induction. Moreover, an initial screen of available transaminases for the amination of L-glucoheptulose (among other sugars) was performed.

3.3.3.1. Transaminase production and optimisation

In order to explore the best conditions for transaminase formation, the CV2025 ω-transaminase was produced in *E. coli* pQR801, induced with 0.1 mM IPTG after 9 hours of incubation. Biocatalyst preparations in lysate form were prepared at 1, 2, 3, and 15 hours post induction and the TAm activity was assessed as described in Section 2.7.6. The growth and TAm activity profiles are shown in Figure 3.16.

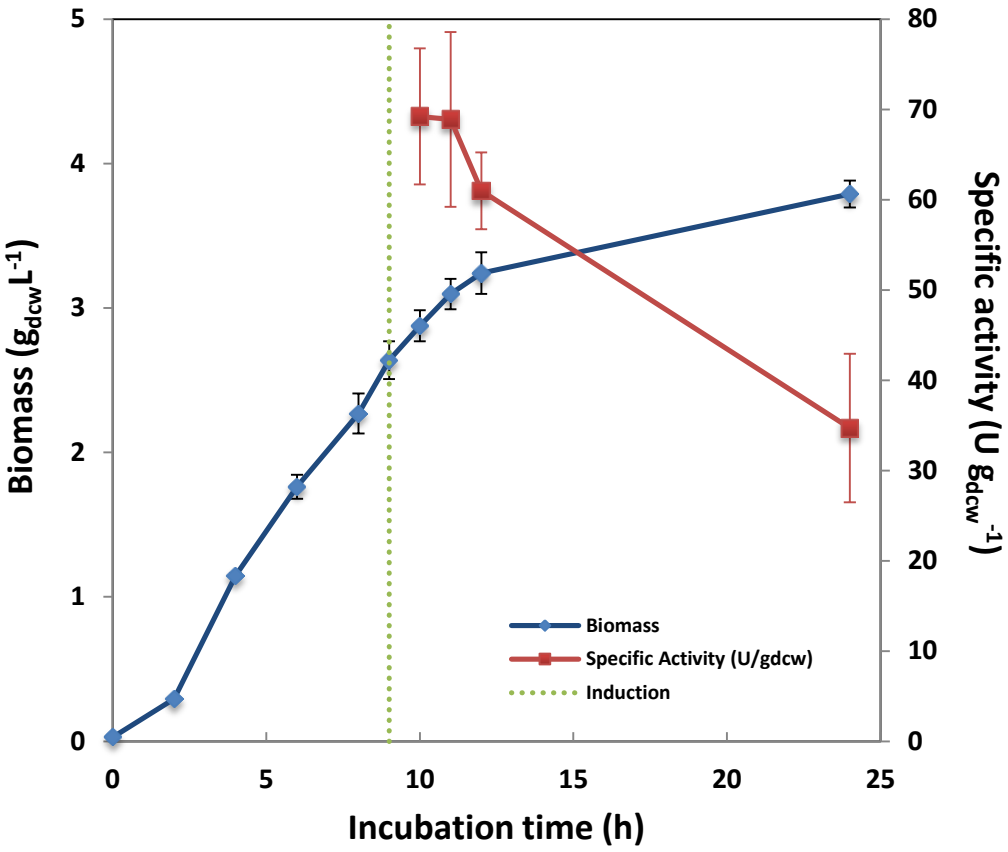

Figure 3.16. Growth kinetics and CV2025 TAm activity produced in *E. coli* pQR801 shake flask cultures. Fermentation was performed using CM media with induction by 0.1 mM IPTG after 9 hours of incubation as described in Section 2.2.2. Transaminase activity was quantified using methylbenzylamine (MBA) and pyruvate for the synthesis of L-alanine and acetophenone (AP) as described in Section 2.7.6. Error bars represent one standard deviation of the mean (n=3).

The calculated *E.coli* pQR801 maximum specific growth rate (μ) was 0.066 ± 0.003 h^{-1}, and the doubling time (dt) was 10.51 ± 0.49 hours. According to

Figure 3.16, transaminase activity reached its highest value 1-2 hours after induction when the cells were in the late exponential phase of growth.

3.3.3.2. Transaminase screening for L-glucoheptulose bioconversion

Colorimetric screening and MBA quantification methods were performed as described in Section 2.7.7, for exploring the amination of a range of ketose sugars, including L-glucoheptulose; the main product of the TK mediated upgrading of L-arabinose. Ten different amine acceptors were screened against six different transaminases. As shown in Figure 3.17, L-glucoheptulose was successfully accepted by the TAm encoded by pQR2191, achieving a 23% yield of conversion into the postulated (2*S*,3*S*,4*S*,5*R*)-6-aminoheptane-1,2,3,4,5,7-hexaol (AHH) product (Figure 1.14), using (*S*)-MBA as amino donor. Moreover, colorimetric analysis (Figure 3.17) demonstrated that the same TAm mutant can also use 2-(4-nitrophenyl)ethan-1-amine as amino donor for catalysing this bioconversion, based on the production of a red precipitate as described in Figure 2.2.

	Cv-TAm		*Rh*-TAm[a]		*Mv*-TAm		pQR2189[b]		pQR2191[b]		pQR2208[b]	
	EA	(S)-MBA	EA	(S)-MBA	EA	(R)-MBA	EA	(S)-MBA	EA	(S)-MBA	EA	(S)-MBA
D-GalAc		7%		n.a.		n.a		8%		29%		2%
L-arabinose		7%		16%		n.a.		6%		12%		1%
D-ribose		15%		14%		n.a.		12%		54%		3%
D-xylose		7%		28%		n.a.		4%		9%		n.d.
L-rhamnose		6%		6%		n.a.		n.d.		19%		n.d.
D-ribulose		9%		10%		45%		n.d.		12%		4%
D-fructose		1%		n.a.		40%		1%		31%		n.a.
L-sorbose		n.d.		n.a.		16%		1%		29%		n.a.
D-tagatose		n.d.		n.a.		22%		n.d.		24%		n.a.
L-glucohept		n.d.		n.a.		n.d.		n.d.		23%		n.a.
(+)		44%		75%		95%		74%		82%		62%
(-)		-		-		-		-		-		-

Figure 3.17. TAm catalysed reactions of various amine acceptors using 2-(4-nitrophenyl)ethan-1-amine (EA), and either *(R)*- or *(S)*-MBA as amine donors. Reaction conditions: 25 mM 2-(4-nitrophenyl)ethan-1-amine, or 20 mM MBA, 10 or 5 mM of the amino acceptor, 50 mM potassium phosphate buffer (pH=8), and clarified lysate, 45 ºC, 400 rpm, and 24 h of incubation. Buffer was used as negative control (-) and pyruvate as positive control (+). [a] Reaction at 30 °C. [b] Reaction in the presence of 25% of dimethyl sulfoxide (Adapted from Subrizi et al., 2019).

3.4. Discussion of results

3.4.1. Influence of substrates and enzyme preparation on reaction rates.

As shown in Figure 3.5 and Table 3.1, H461Y was found to be the best mutant for the production of L-glucoheptulose from all the TK mutants evaluated. However, it should be noted that the rate of this particular reaction is considerably slower than the reported by Chen et al. (2008, 2009) using propionaldehyde and glycolaldehyde as aldose acceptor respectively. In that case the reported reaction rates were of the order of mmol $L^{-1}min^{-1}$, while when using L-arabinose, reaction rates were in the order of µmol $L^{-1}min^{-1}$. The lower conversion rate could be due to the size differences between glycolaldehyde and propionaldehyde that are small molecules (60.052 g mol^{-1} and 58.08 g mol^{-1}, respectively), compared with L-arabinose (150.13 g mol^{-1}) that is almost twice their size and not a natural substrate for this enzyme. Further discussion about this is provided in the following sections.

On the other hand, by optimising cell growth and protein expression for the H641Y TK mutant, it was possible to improve the initial reaction rate compared with the experiments previously reported by Subrizi et al. (2016). For the same reaction conditions and TK mutant they reported an initial reaction rate of 18.3 µmol L^{-1} min^{-1}, while in this work an initial reaction rate of 50.9 µmol $L^{-1}min^{-1}$ could be reached.

3.4.2. Evaluation of kinetic parameters for the TK lysate catalysed reaction of L-arabinose and Li-HPA to L-glucoheptulose

As can be seen in Section 3.3.2.1, the first step towards kinetic parameters identification is to find the linear range between reaction rate and enzyme

concentration. Increasing enzyme concentration will not always result in a higher reaction rate, because of several physical limitations such as mass transfer into the active site (due to steric effect) or certain forms of inhibition (Ríos-Solís, 2012). For the TK reaction studied here it was found that protein concentrations up to 3.6 mg mL^{-1} could be used without losing proportionality with the reaction rate.

The second step of the experimental approach helped generate a deeper understanding of the reaction of interest by performing reactions at higher substrate concentrations. As can be seen in Figure 3.13, when changing Li-HPA concentration at a fixed concentration of L-arabinose, V_{MAX} was reached at 1 mM Li-HPA. A low value of K_{HPA} indicates that the active site of the enzyme has a high affinity for this substrate, so it is rapidly saturated and V_{MAX} is reached (Puri, 2002). As can be seen in Figure 3.18A, Li-HPA is the first substrate that attaches to the enzyme for delivering a ThDP-enamine intermediate that is stabilised by electron resonance, ready for nucleophilic attack to the L-arabinose. If the enzyme shows high affinity for the Li-HPA, this first stage of the reaction would be very fast.

On the other hand, as can be seen in Figure 3.12, when L-arabinose is varied at a fixed Li-HPA concentration no plateau is reached, this means that K_{ARA} is very high. The main conclusion of this experiment is that L-arabinose is not inhibitory to the reaction over the range of concentrations evaluated; it also means that a very high concentration of L-arabinose is needed for saturating the active site of the enzyme i.e. the active site has relatively poor affinity for the binding of this non-natural substrate. Figure 3.18B, shows the second stage of the overall

reaction that comprises nucleophilic attack of the carbanion to L-arabinose; a very high value of K_{ARA} shows that this step of the reaction is very slow.

In summary, no matter how fast the first stage of the reaction is, the overall reaction rate will be determined by the low affinity of the enzyme for the L-arabinose. Fundamentally, this is why the measured reaction rate is lower than when other aldose acceptors are used, such as glycoladehyde or propionaldehyde.

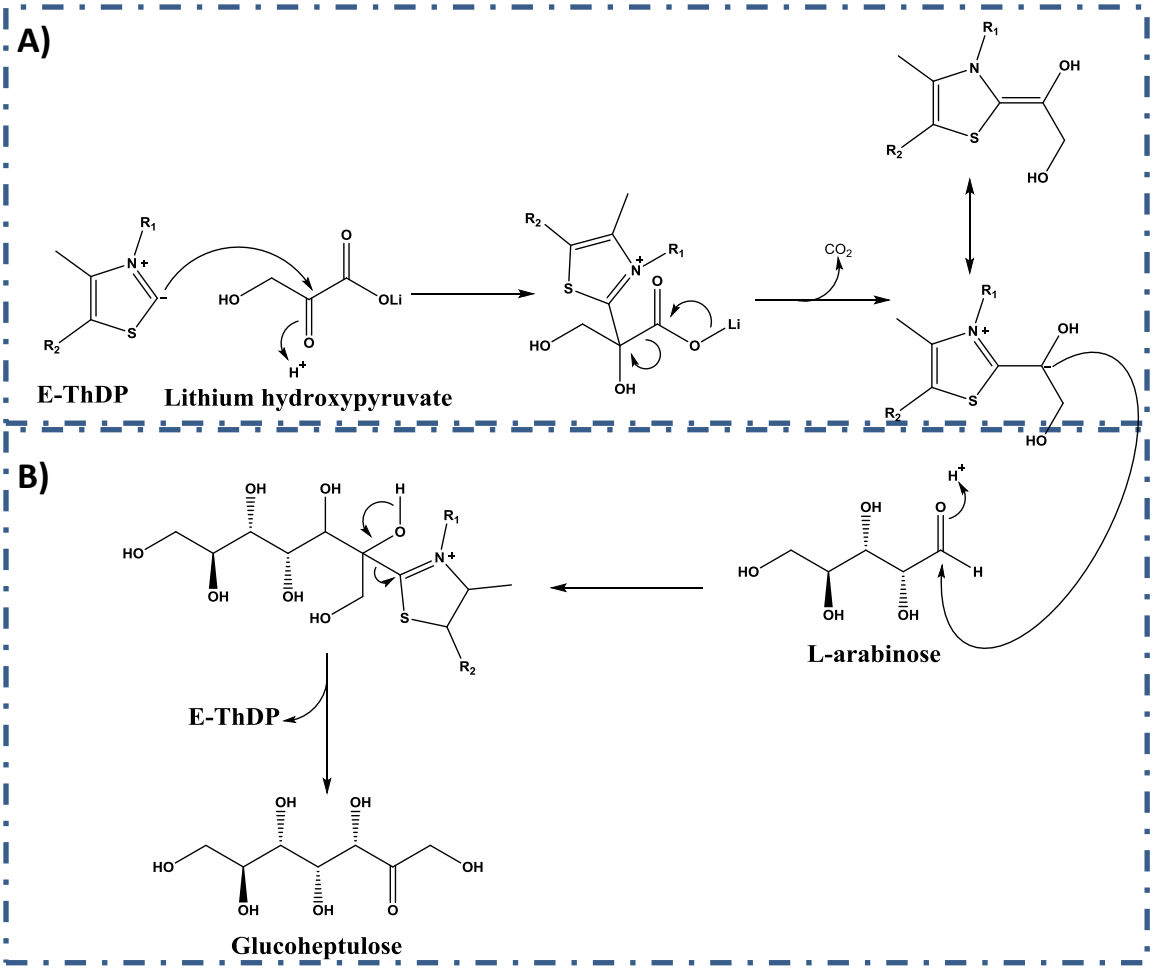

Figure 3.18. Reaction mechanism of the TK mediated bioconversion of Li-HPA and L-arabinose to L-glucoheptulose and CO_2. A) In the first stage of the reaction, Li-HPA is attached to the active site of the enzyme for producing a molecule of CO_2 and ThDP-enamine intermediate that is rapidly stabilised by electron resonance. B) In the second stage of the reaction, the stabilised carbanion attacks the carbonyl group on the L-arabinose for delivering the molecule of L-glucoheptulose.

This second step of the experimental approach was also helpful in order to define the “inhibition negligible” regions of both Li-HPA and L-arabinose on the reaction rate. The regions in which substrate inhibition is negligible were below 1 mM for Li-HPA and it was set to 55 mM for L-arabinose, even when no inhibition was found in the range tried. The first five initial reaction rate values of each set of experiments were used to obtain the preliminary values of V_{MAX}, K_{HPA}, and K_{ARA}, via linear regression and a simplified kinetic model.

In the final experimental step, 5 full progress curves were obtained at different substrates and protein concentrations (Figure 3.14). The objective of obtaining these progress curves was to ensure that any substrate and product inhibition phenomena were represented in the final non-linear regression for obtaining the full set of kinetic parameters. The substrates concentrations were chosen according to possible concentrations that might be used in an industrial bioconversion, and should be beyond inhibition regions found in previous experiments.

Final values for each kinetic parameter after reconciliation were: 1, 1200, 0.06, 247.5, and 8.5 mM for K_{HPA}, K_{ARA}, Ki_{HPA}, Ki_{ARA}, and Ki_{GLU} respectively, and the final value for k_{cat} was 140 min^{-1}. These values were validated by performing an extra experiment not included in the non-linear adjustment of the progress curves, shown in Figure 3.15. The fit of the experimental points to the model predictive curves was excellent for the three molecules of interest, which verified the kinetic parameters obtained.

Chen et al. (2008) obtained for the bioconversion of propionaldehyde (PROP) and HPA to 1,3-dihydroxypentan-2-one (DHP) the following kinetic parameters: 12, 98, 43, 625 and 681 mM for K_{HPA}, K_{PROP}, Ki_{HPA}, Ki_{PROP}, and Ki_{DHP}, with a

final value of 501 min^{-1} for k_{cat}. This difference could be due to the fact that Chen et al. used more natural substrates for the bioconversion which promotes a faster reaction, while L-arabinose is a non-natural substrate for TK and its 2.5-fold bigger than propionaldehyde which makes it more difficult to get to the active site of the enzyme. The relatively low value of K_{PROP} indicates that the enzyme shows more affinity for propionaldehyde than for L-arabinose, which means that DHP is released faster than L-glucoheptulose from the active site and it is reflected in the higher turnover number for the propionaldehyde bioconversion. Finally, the TK mutant used for each bioconversion is different and as clarified lysates were used in both experiments, there could be other reactions taking place that could interfere in the final kinetic parameter values.

3.4.3. Transaminase catalysed amination of L-glucoheptulose

As can be seen in Section 3.3.3, TAm activity was successfully optimised by inducing with 0.1 mM IPTG after 9 hours of incubation (Figure 3.16). Moreover, the TAm encoded by pQR2191 was successfully identified as being able to accept L-glucoheptulose as substrate for the production of (2S,3S,4S,5R)-6-aminoheptane-1,2,3,4,5,7-hexaol (Figure 3.17), using either 2-(4-nitrophenyl)ethan-1-amine or (*S*)-MBA as amino donors. However, further experiments need to be performed in order to optimise yield, and more TAm variants could be screened for the production of this particular polyaminoalcohol (Figure 1.14).

3.5 Summary

A TK mutant was selected for the bioconversion of Li-HPA and L-arabinose to L-glucoheptulose, an interesting ketoheptose not common in nature with high potential applications in hypoglycaemia and cancer. Mutant H461Y was

characterised and shown to have the highest bioconversion productivity and TK expression possible in order to facilitate further reaction optimisation.

According to Subrizi et al. (2016), the inner part of the substrate channel of the TK contains several Histidine residues; one of them is the H461 residue that interacts with the C-1 and C-2 hydroxyl groups of L-arabinose via polar interactions similar to the interactions with D-ribose-5-phosphate (one of the natural aldehyde acceptors of TK) in its cyclic five-membered ring form (cR5P). Those residues can also contribute to maintain close proximity and a suitable orientation of the substrate to the ThDP-enamine intermediate showed in Figure 3.18 for the second step of the bioconversion. Moreover the H461 residue interacts with the phosphate moiety of cR5P via hydrogen bonds and electrostatic interactions, making it an interesting residue for mutation to enhance TK activity towards non-phosphoryalted compounds such as L-arabinose. The H461Y mutation involved the change of a tyrosine (H) to a threonine (Y), which led to better acceptance of L-arabinose than the other mutants. This replacement of the positively charged tyrosine for an uncharged threonine has been previously reported to enhance activity towards non-phosphorylated polyhydroxylated substrates by Hibbert et al. (2007).

Moreover, a full kinetic model was obtained for the production of L-glucoheptulose when H461Y TK lysate is used as a biocatalyst, making use of a new hybrid approach that includes the best features of linear and non-linear methodologies for kinetic parameters identification (Figure 3.10). The kinetic parameters were validated with 5 progress curves, as well as one extra experimental data set not included in the non-linear analysis that originated the kinetic model.

It was found that it is possible to obtain the kinetic model of the reaction, even when the biocatalyst is added as lysate instead of pure TK.

The main bottlenecks identified for the reaction were the low Michaelis constant of Li-HPA, which results in inhibition at low concentrations, and the high Michaelis constant of L-arabinose that determines the rate of the overall reaction. Therefore, optimisation of the reaction can be explored when using high concentrations of L-arabinose and low Li-HPA concentrations.

Finally, L-glucoheptulose was successfully aminated by TAm encoded by pQR2191 into the postulated product AHH with 23% yield (Figure 3.17) when using (*S*)-MBA as amino donor. This opens the opportunity for AHH optimisation via different strategies as enzyme expression optimisation, bioconversion optimisation, kinetic parameters quantification, or directed evolution for increasing TAm affinity for L-glucoheptulose.

The kinetic parameters obtained in this chapter were for when clarified enzyme lysate is used, as this form of biocatalyst is most likely to be used in an industrial biorefinery. However, in order to understand the reaction kinetic better, the enzyme was also purified and the kinetic parameters determined and compare to lysate. This work is described in the following Chapter.

4. TK PURIFICATION AND KINETIC PARAMETER DETERMINATION FOR THE BIOCONVERSION OF L-ARABINOSE TO L-GLUCOHEPTULOSE USING PURE H461Y TK

4.1. Introduction

As previously described in Section 3.3.1, the TK mutant H461Y was selected as the best biocatalyst for the bioconversion of L-arabinose and Li-HPA to L-glucoheptulose. The apparent kinetic parameters for the enzyme in a clarified lysate form were determined and discussed in Section 3.4. In order to quantify the inherent kinetic parameters it was necessary to purify the enzyme prior to the kinetic parameter determination (Harris and Keshwani, 2009).

While it was initially thought that the mutant had been expressed with a His_6 tag to aid purification, this was discovered not to be the case. The expressed enzyme could not be purified on a Ni-NTA column as can be seen in Figure 4.1. No protein bands were found after Ni-NTA purification. Further sequencing of the mutant DNA confirmed the lack of the terminal histidine tails; hence a rapid, one-step purification via Ni-NTA columns was not initially possible.

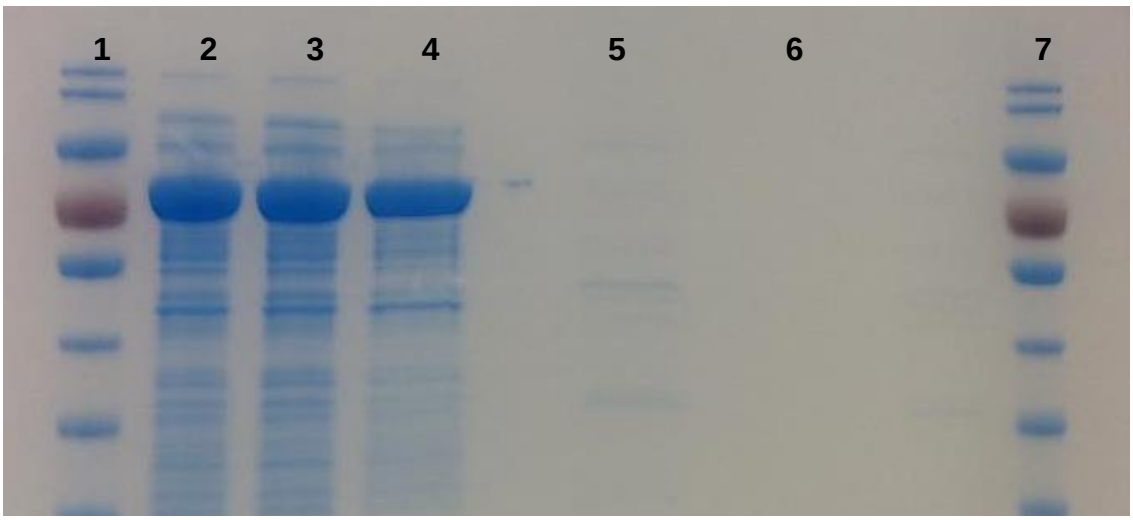

Figure 4.1. SDS-PAGE analysis of attempted Ni-NTA for TK purification. Experiment was performed as described in Section 2.7.3. Lane 1 and 7 contain the protein marker, lane 2 is H461Y lysate, lane 3 shows the filtered solution after passing the lysate through the Ni-NTA spin column, lane 4 is the flow through during the washing step, lane 5 is the elution solution before buffer exchange, and lane 6 is the protein solution after buffer exchange.

An alternative purification method was explored using precipitation of transketolase with ammonium sulphate (Section 2.2.4). This method was time-consuming and as can be seen in Figure 4.2, the final TK solution contained considerably less enzyme than the lysate. The highest TK concentration achieved with this method was 0.5 ± 0.06 mg mL^{-1}, which was around 6 times lower that the minimum concentration required for conducting the experiments planned for Chapter 4.

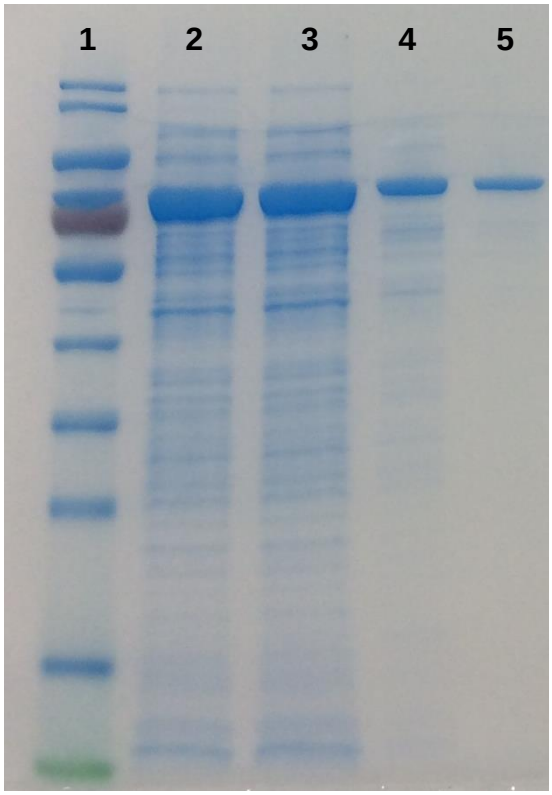

Figure 4.2. SDS-PAGE analysis of ammonium sulphate precipitation for TK purification. Experiment was performed as described in Section 2.7.3. Lane 1 contains the protein marker, lane 2 and 3 is H461Y lysate, lane 4 shows the final solution obtained after the purification process with ammonium sulphate, and lane 5 is the protein solution after buffer exchange.

In order to simplify and enhance TK purification, and be able to validate a kinetic model for L-glucoheptulose production using pure TK, the engineering of histidine purification tags on the mutant of interest had to be performed.

4.2. Aim and objectives

The aim of this chapter is to obtain the kinetic parameters of the reaction of Li-HPA and L-arabinose to L-glucoheptulose using the pure TK H461Y mutant as the biocatalyst. This approach will involve the successful purification of the TK from the H461Y TK mutant, the preparation of the pure TK for the bioconversion, as well as obtaining of the kinetic parameters of the reaction

based on the method used previously in Chapter 3. The key objectives of this chapter are thus:

- To sub-clone the H461Y TK gene into a new plasmid containing the histidine tail in order to achieve rapid Ni-NTA purification.
- To compare the initial reaction rate and total bioconversion yield of pure TK and TK lysate on the production of L-glucoheptulose.
- To determine the kinetic parameters for the pure TK mediated bioconversion of L-arabinose and Li-HPA to L-glucoheptulose, utilising the approach developed by Chen et al. (2006).

4.3. Results

4.3.1. Sub-cloning of H461Y TK gen into a new vector

In collaboration with Dr Maria Bawn from the UCL Department of Biochemical Engineering, the H461Y TK gene was sub-cloned into a new vector and it was confirmed by sequencing that the expressed TK contained a poly-histidine tail. This new mutant was termed H461Y-HT and all subsequent experiments involved the purified version of this mutant.

According to Velez et al. (2013), timing of induction, temperature shift and post-induction temperature are important variables for optimizing enzyme expression. Based on this, different culture conditions were subsequently tried in order to enhance production of the H461Y-HT mutant. These focused on changing the inducer concentration and culture time as shown in Table 4.1.

Table 4.1. Different induction strategies for maximizing expression of the His-tagged H461Y-HT TK mutant in *E. coli*

METHOD	IPTG (mM)	Incubation time before Induction (2.5 h)	Incubation time after induction (6 h)
1	1	37 ºC, 250 rpm	25 ºC, 200 rpm
2	1	37 ºC, 250 rpm	37 ºC, 250 rpm
3	0	37 ºC, 250 rpm	25 ºC, 200 rpm
4	0	37 ºC, 250 rpm	37 ºC, 250 rpm

As can be seen in Figure 4.3, when the H461Y-HT mutant was induced with 1 mM IPTG after 2.5 h of incubation and without changing incubation conditions after induction, TK production was maximized (Lane 3). A densitometry analysis was performed as described in Section 2.7.4., and it was found that H461Y-HT mutant produces approximately 30% (w/w) of transketolase within the total cell protein. This compared to a value of 36% for the non His-tagged version of the enzyme, this difference is due to the inherent inaccuracy of applying the densitometry analysis to lysates.

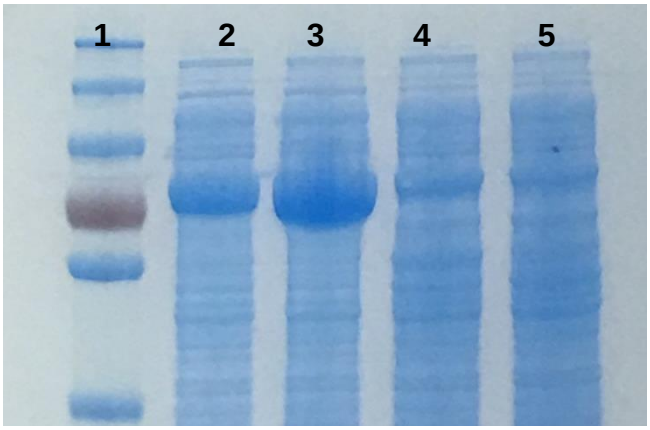

Figure 4.3. SDS-PAGE gel for TK purification using three different strategies for TK expression as specified in Table 4.1. Experiment was performed as described in Section 2.7.3. Lane 1 is the protein marker, lane 2 is the H461Y-HT lysate with induction at 1 mM IPTG after 2.5 h incubation at 37 °C and 250 rpm followed by a decrease in temperature to 25 °C and 200 rpm, lane 3 shows the H461Y-HT lysate induced at 1 mM IPTG after 2.5 hours incubation using constant temperature at 37 °C and 250 rpm, lane 4 shows the H461Y-HT lysate with no IPTG induction but a change in temperature after 2.5 h to 25 °C and 200 rpm, and lane 5 shows the H461Y-HT lysate with no induction and constant temperature at 37 °C and 250 rpm.

4.3.2. TK purification process development

The transketolase produced was subsequently purified using Ni-NTA spin columns as described in Section 2.2.5.1. Different wash buffers were used changing imidazole and NaCl concentrations in order to achieve the cleanest TK band. As can be seen in Figure 4.4, a wash buffer with 40 mM imidazole, 300 mM NaCl and 50 mM TRIS-HCl buffer (Lane 4), delivers the cleanest protein band, hence this buffer was used for future protein purifications.

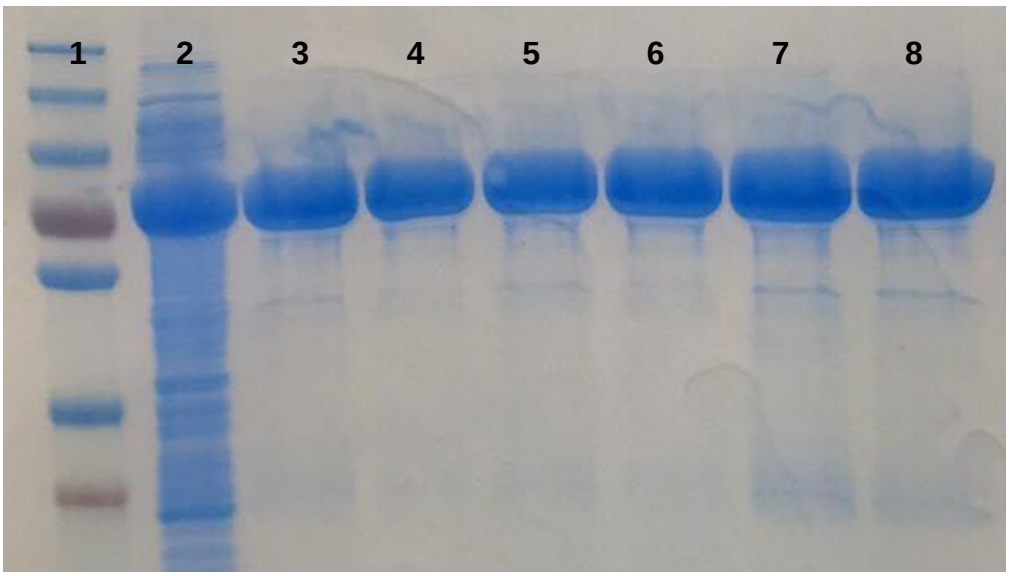

Figure 4.4. SDS-PAGE gel for TK purification using Ni-NTA spin columns and different wash and elution buffers. Experiment was performed as described in Section 2.7.3. Lane 1 is the protein marker, lane 2 is the H461Y-HT lysate, and lanes 2 to 8 are the final purified elution using different wash buffers. Experiments performed as described in Section 2.7.

Buffer exchange was next performed on all purified solutions using PD-10 Desalting columns (GE Healthcare, Sweden) as described in Section 2.2.5.3., in order to remove residual imidazole that could interfere in the enzymatic reaction by acting as a nucleophile (Frey and Hegeman, 2006).

A comparison between H461Y and H461Y-HT was then performed to assess differences in terms of initial reaction rate and total bioconversion yield. Experiments were performed as described in Section 2.4.1, and the results are shown in Table 4.2.

Table 4.2. Initial rate and specific initial rate of the conversion of Li-HPA and L-arabinose to L-glucoheptulose using H461Y and H461Y-HT TK mutants. Experiments were performed as described in Section 2.4.1

TK Used	Protein Loaded (mg)	Protein Concentration in Rx (g L^{-1})	R_0 (µmol $L^{-1}min^{-1}$)	SpR_0 (µmol $g^{-1}min^{-1}$)
H461Y-Lysate	1.54	2.56	17.95 ± 0.15	7 ± 0.06
H461Y-HT-Lysate	2.18	3.63	25.8 ± 0.1	7.1 ± 0.03
PURE TK	0.14	0.24	1.9	7.9

As can be seen in Table 4.2, the specific initial reaction rate (SpR_0) is similar when using H461Y or H461Y-HT in lysate, so the difference is negligible when using either of the two mutants. As expected, however the SpR_0 increases when using pure TK in comparison with lysate. This is because when using lysate there are other proteins in the reaction mix that could interfere with the bioreaction of interest.

4.3.3. Kinetic parameter quantification for the purified TK H461Y catalysed reaction of L-arabinose and Li-HPA to L-glucoheptulose

As outlined in Section 3.3.2, the new approach to bioconversion kinetic parameter identification developed by Chen *et al.* (2008), was again used to quantify the kinetic parameters of the pure TK H461Y mutant. For obtaining the kinetic parameters of this reaction the four steps shown in Figure 3.10 were followed as described as follows:

1. To determine the proportionality between initial reaction rate and TK concentration.
2. To obtain preliminary kinetic parameters by the utilisation of two sets of initial rates. One set consists in initial rates obtained by varying the concentration of one substrate and maintaining the concentration of the other substrate fixed, and the other set consists in initial rates obtaining by doing the opposite. All experiments need to be done at a fixed enzyme concentration.
3. Determination of the preliminary full kinetic parameters by the non-linear regression of progress curves at different enzyme and substrates concentrations.
4. Reconciliation of the kinetic parameters by a new non-linear regression of the progress curves, using all the preliminary kinetic parameters as initial values.

The MatLab software programme (MathWorks, Natick, MA, USA) was again used for determination of the kinetic parameters.

4.3.3.1. Proportionality between initial reaction rate and transketolase concentration

The first step on the approach for the obtaining of the kinetic parameters is to determine the linear region between protein concentration and initial reaction rate.

The experiment was performed as described in Section 2.5.1.1. An equimolar concentration of 33 mM was used for L-arabinose and Li-HPA, and pure TK was used as biocatalyst at different concentrations from 1.3 to 3.6 mg mL^{-1}. The linear relationship between lysate concentration and initial rate was maintained

up to 3.6 mg mL^{-1} of TK in the reaction as can be seen in Figure 4.5, thus this enzyme concentration was used for the following experiments.

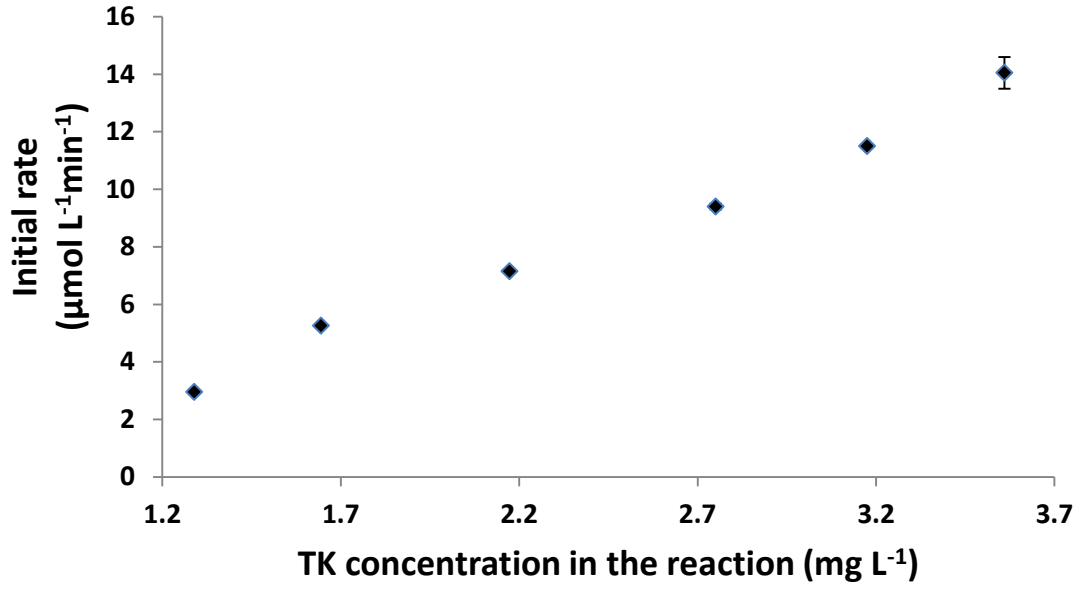

Figure 4.5. Initial rate of L-glucoheptulose formation as a function of pure TK in the bioconversion. Reaction conditions: 33 mM Li-HPA, 33 mM L-arabinose, 1.7 ThDP, 6 mM $MgCl_2$, 450 rpm and 25 °C. Pure TK was used from 1.3 to 3.6 mgTK mL^{-1}. Experiments were performed as described in Section 2.4.1. Error bars represent one standard deviation about the mean (n=3).

4.3.3.2. Kinetic model of TK and initial rate experiments

The second step on the methodology shown in Figure 3.10 is to obtain two sets of initial reaction rate data. The first initial set was obtained by varying L-arabinose concentration while fixing Li-HPA concentration. The second set was obtained by varying Li-HPA concentration while maintaining L-arabinose at a fixed concentration.

For the first set Li-HPA was fixed at 22 mM, and L-arabinose was varied from 10 to 150 mM, maintaining the linear behaviour between L-arabinose concentration and initial reaction rate as Figure 4.6 shows.

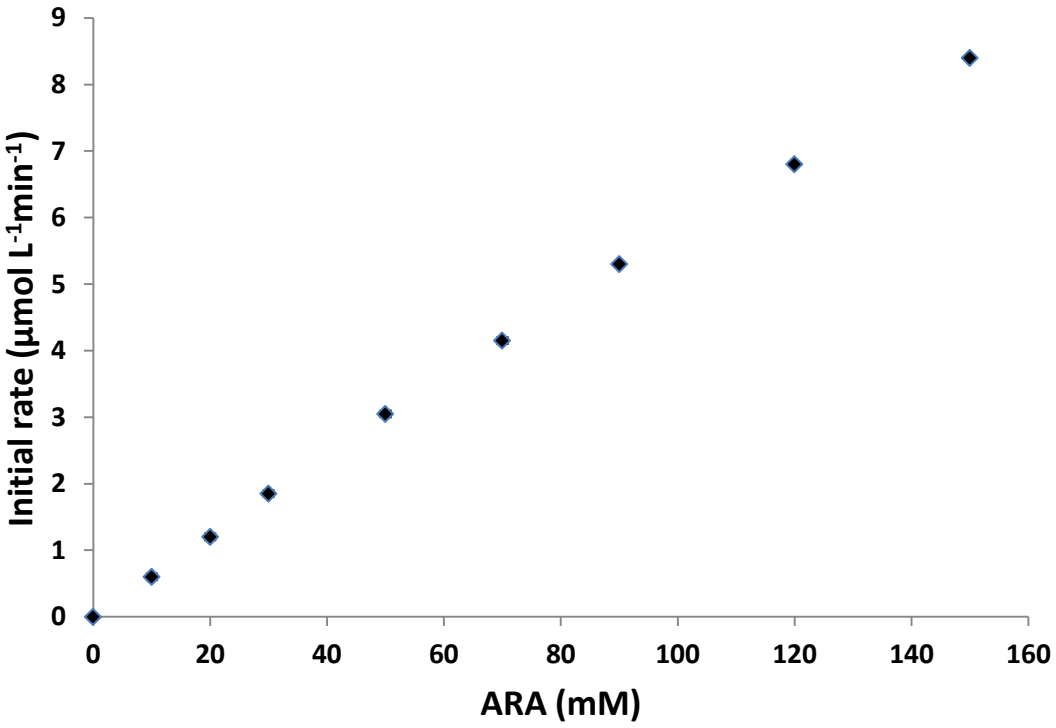

Figure 4.6. Initial rate of L-glucoheptulose formation as a function of initial L-arabinose concentration and a fixed Li-HPA concentration, using pure TK. Reaction conditions: 22 mM Li-HPA, 1.7 ThDP, 6 mM $MgCl_2$, 450 rpm and 25 °C. L-arabinose was used in a range from 10 to 150 mM. Experiments were performed as described in Section 2.5.1.2. Error bars represent one standard deviation of the mean (n=3).

Based on the results shown in Figure 4.6, no L-arabinose inhibition was found for this reaction. In order to obtain the second set of initial reaction rate data, L-arabinose concentration was fixed at 28 mM, and Li-HPA was varied from 0.2 to 10 mM. It was found that Li-HPA shows reaction inhibition after 0.6 mM as Figure 4.7 shows.

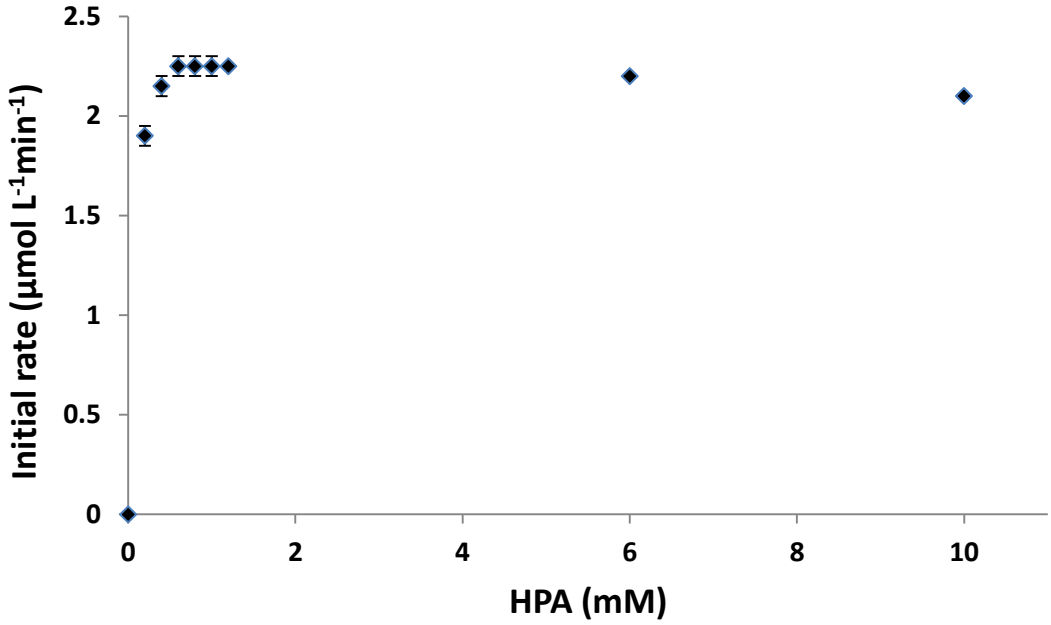

Figure 4.7. Initial rate of L-glucoheptulose formation as a function of initial Li-HPA concentration and a fixed L-arabinose concentration, using pure TK. Reaction conditions: 28 mM L-arabinose, 1.7 ThDP, 6 mM $MgCl_2$, 450 rpm and 25 °C. HPA was used in a range from 0.2 to 10 mM. Experiments were performed as described in Section 2.5.1.2. Error bars represent one standard deviation of the mean (n=3).

These two sets of initial reaction rates were used to find the linear region between substrate concentration and initial reaction rate, in order to work in the range where no substrate inhibition is present. For L-arabinose the linear range utilised was from 10 to 70 mM, while for the case of Li-HPA the linear range was much lower, between 0.2 and 0.6 mM.

Linear adjustment was successfully applied over the kinetic data for obtaining preliminary parameter values of K_{HPA}, K_{ARA} of 0.17 and 189.99 mM respectively, and a V_{MAX} of 15.33 µM min^{-1}, using Equation 3.6. These values were used for the non-linear adjustment of the progress curves detailed in the subsequent sections.

4.3.3.3. Progress curves for kinetic parameter identification

The final experimental step on the methodology shown in Figure 3.10 was to obtain the full progress curves of nine different reactions at different substrate and enzyme concentrations. A set of nine different reactions were performed as described in Section 2.5.1.3., and samples were taken every 2 hours for 24 hours of total reaction to obtain sufficient data for accurate curve fitting. The substrate and protein concentrations used are shown in Table 2.6.

The preliminary results for K_{HPA}, K_{ARA}, Ki_{HPA}, Ki_{ARA}, Ki_{GLU} were 0.17, 189.99, 37.32, 1010, and 713.23 mM respectively while the value for k_{cat} was 103.3 min^{-1}. These preliminary data were used as initial guesses for the full kinetic model for obtaining the final kinetic parameters. The optimisation was performed as described in Section 3.3.2.3. The lower and upper bounds for all non-linear regressions were set at 0.0001 and 800.

The global optimisation was achieved after a second run on the full kinetic model, and the final values for each kinetic parameter were: 1.84, 800, 1.0, 222.61, and 9.5 mM for K_{HPA}, K_{ARA}, Ki_{HPA}, Ki_{ARA}, and Ki_{GLU} respectively. The final value for k_{cat} was 137.1 min^{-1}. Figure 4.8 shows a comparison of the fitted progress curves, using these kinetic parameter values with the experimental data, and the corresponding rate model is displayed in Equation 4.1. Model Predictions and residuals from the final model fit are shown in Section B of Appendix VIII.

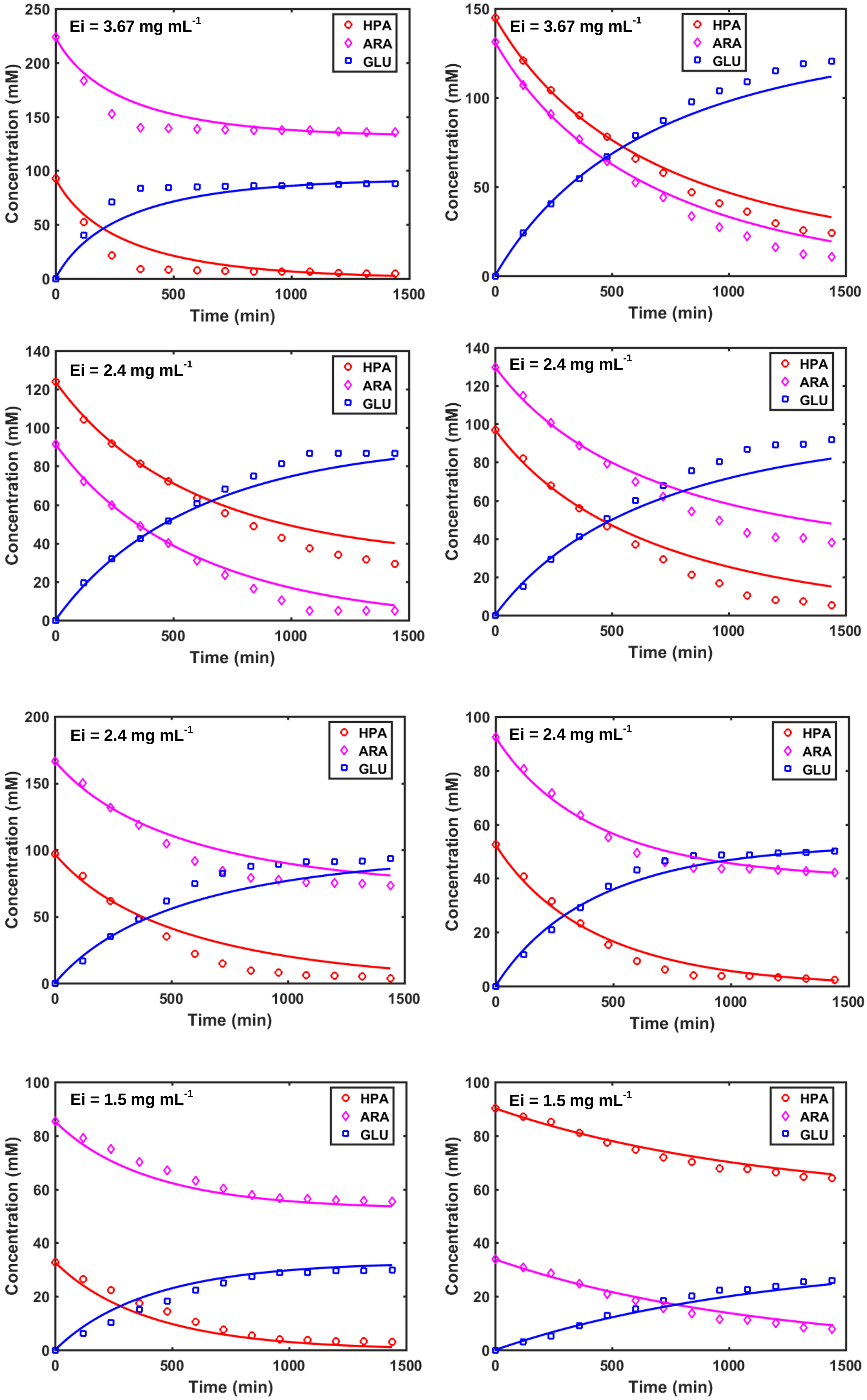
Ei = 3.67 mg mL-1
HPA
ARA
GLU
Concentration (mM)
Time (min)
Ei = 3.67 mg mL-1
HPA
ARA
GLU
Concentration (mM)
Time (min)
Ei = 2.4 mg mL-1
HPA
ARA
GLU
Concentration (mM)
Time (min)
Ei = 2.4 mg mL-1
HPA
ARA
GLU
Concentration (mM)
Time (min)
Ei = 2.4 mg mL-1
HPA
ARA
GLU
Concentration (mM)
Time (min)
Ei = 2.4 mg mL-1
HPA
ARA
GLU
Concentration (mM)
Time (min)
Ei = 1.5 mg mL-1
HPA
ARA
GLU
Concentration (mM)
Time (min)
Ei = 1.5 mg mL-1
HPA
ARA
GLU
Concentration (mM)
Time (min)

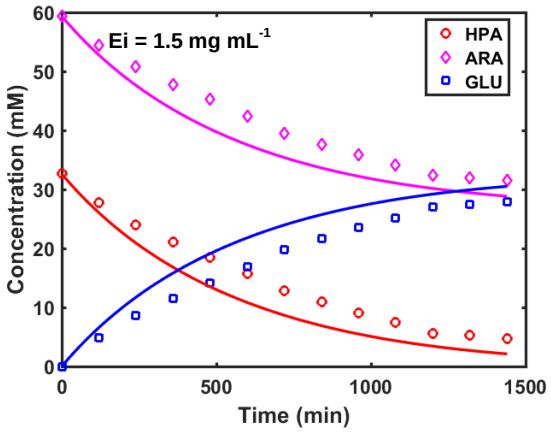

Figure 4.8. Comparison of experimental and fitted progress curves using different concentrations of purified H461Y-HT TK, Li-HPA, and L-arabinose for the synthesis of L-glucoheptulose. Lines show model predictions and dots represent the experimental data. Error bars represent one standard deviation of the mean (n=3).

Eq.4.1

$$\frac{d[GLU]}{dt} = \frac{137.1E_i[HPA][ARA]}{800[HPA](1+[HPA]) + 1.84[ARA]\left(1+\frac{[ARA]}{222.61}\right) + [HPA][ARA] + 1.84[ARA][GLU] + 43.12[GLU]}$$

As in Chapter 3, a final separate experiment was performed for validating the kinetic parameters obtained; this reaction progress curve was determined under conditions not included in the mathematical analysis. The experiment was performed as described in Section 2.5.1.3, the concentrations for L-arabinose and Li-HPA used were 34 and 33 mM respectively, and the TK concentration was 1.85 mg mL^{-1}. Figure 4.9 shows the good fit between the predictions of the model to the experimental data.

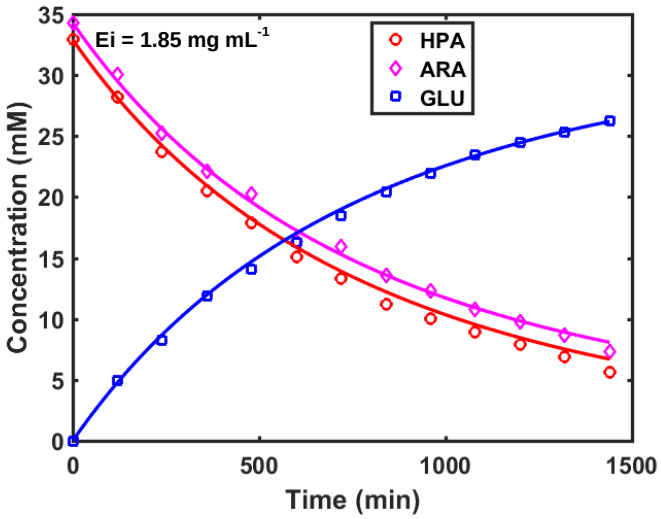

Figure 4.9. Verification of pure TK model predictions with an experimental set of data not included in the progress curves experiment. Reaction conditions: 34 mM L-arabinose, 33 mM Li-HPA, 1.7 mM ThDP, 6 mM $MgCl_2$, a final concentration of 1.85 mg mL^{-1} of purified H461Y-HT TK, 250 rpm and 25 ºC. Lines show model predictions and dots represent the experimental data. Error bars represent one standard deviation of the mean (n=3).

4.4. Discussion of results

4.4.1. TK purification

TK purification was achieved by sub-cloning the H461Y TK gene into a new vector containing a His_6 sequence. This new mutant was named H461Y-HT, and a preliminary optimisation of enzyme production was performed comprising of induction with IPTG 1 mM after 2.5 h of incubation. Using this process it was determined that the H461Y-HT mutant comprises 30% of total protein in *E. coli* and that a clarified lysate as well as the purified enzyme are able to undertake the bioconversion of Li -HPA and L-arabinose to L-glucoheptulose at a similar turnover number.

4.4.2. Kinetic parameters for the pure TK catalysed reaction of L-arabinose and Li-HPA to L-glucoheptulose

As can be seen in Section 4.3.3.1, the first step towards kinetic parameters identification is to find the linear range between reaction rate and enzyme concentration. It was found that for the reaction studied, protein concentration could get up to 3.6 mg TK mL^{-1} without losing proportionality with the reaction rate.

The second experimental step of the approach delivered similar results as when TK lysate was used (Section 3.3.2.2). As can be seen in Figure 4.6 and 4.7, no L-arabinose inhibition was found over the range of concentrations tested, and Li-HPA becomes inhibitory for the reaction at 1 mM when L-arabinose is kept at a fixed concentration. On the final experimental step, 9 full progress curves were obtained at different substrates and protein concentrations.

Final values for each kinetic parameter after reconciliation were: 1.84, 800, 1.0, 222.61, and 9.5 mM for K_{HPA}, K_{ARA}, Ki_{HPA}, Ki_{ARA}, and Ki_{GLU} respectively, and the final value for k_{cat} was 137.1 min^{-1}. These values were validated by performing an extra experiment not included in the non-linear adjustment of the progress curves, shown in Figure 4.9. The agreement between the experimental points to the model predictive curves was excellent for both substrates and product, which verified the kinetic parameters obtained.

4.5 Summary

A new version of the H461Y TK mutant studied in Chapter 3 was constructed which contained a His_6 purification tag on the N-terminus. This allowed rapid one-step purification of the TK with Ni-NTA beds. When it was originally found

that the H461Y mutant did not possess a His_6 tag, a number of attempts to purify the enzyme using a precipitation method were undertaken (Section 4.1). While the enzyme could be purified using this method, the purification process was time consuming and resulted in significant loss of enzyme during purification such that it was not possible to purify enough active enzyme to conduct the full set of kinetic parameter determination experiments.

This new mutant was termed as H461Y-HT and could be expressing at up to 30% of total protein in *E. coli*. Lysate bioconversions of L-arabinose and Li-HPA to L-glucohepulose using H461Y and H461Y-HT mutants delivered similar initial reaction rates. This suggests that inclusion of the His_6 tag does not alter the structure-activity of the H461Y TK enzyme. The one advantage of mutant H461Y over the H461Y-HT is that the latter requires IPTG for inducing TK production, which could be a drawback for its utilisation in industry or at large scale due to the expense of IPTG.

The full kinetic model for the new H461Y-HT mutant was obtained and the kinetic parameters determined are compared to the H461Y lysate in Table 4.3. This shows some differences that could be due to the interference of other proteins in the lysate during the evaluation of the kinetic parameters for the lysate model. However the differences are not considerable, which enables the possibility of the application of the lysate model at industry level, as this provides high activity and overcomes the need for expensive purification steps.

Table 4.3. Comparison of the kinetic parameters obtained for the bioconversion of L-arabinose and Li-HPA to L-glucoheptulose using H461Y lysate and Pure H461Y-HT TK as biocalatysts

Kinetic Parameter	H461Y TK Lysate	H461Y-HT pure TK
K_{HPA}	1 mM	1.84 mM
K_{ARA}	1200 mM	800 mM
Ki_{HPA}	0.06 mM	1.0 mM
Ki_{ARA}	247.5 mM	222.61 mM
Ki_{GLU}	8.5 mM	9.5 mM
k_{cat}	140 min^{-1}	137.1 min^{-1}

The main features of the reaction are the same as for when H461Y TK lysate is used as biocatalyst i.e., Li-HPA becomes inhibitory at low concentrations, and L-arabinose showed no inhibition at high concentrations. In Chapter 6, scale up and optimisation of the bioconversion process is explored in order to increase the productivity of the reaction.

As shown in Section 1.7.1, the other main sugar obtained after beet pulp saccharification is the D-galacturonic acid. Therefore, Chapter 5 was focused in exploring the bioconversion of D-galacturonic acid and Li-HPA to the corresponding octulose, an interesting building block for new pharmaceuticals.

5. TK CATALYSED UPGRADING OF D-GALACTURONIC ACID TO 2,3,4,5,6,8-HEXAHYDROXY-7-OXOOCTANOIC ACID

5.1. Introduction

D-galacturonic acid (DGA) is a hexose sugar that can be obtained after the saccharification of sugar beet pulp (Section 1.7.1); this could be used as well as L-arabinose as a sustainable substrate for the synthesis of chiral polyalcohols via TK biocatalysis. D-galacturonic acid is the second major component of sugar beet pulp after saccharification, with a percentage of 21.1% (Micard et al., 1996). The TK catalysed reaction of DGA and Li-HPA yields CO_2 and 2,3,4,5,6,8-hexahydroxy-7-oxooctanoic acid (OOA, Figure 5.1), an octulose non-common in nature that can be used as a building block for active pharmaceutical ingredients (APIs). It could also be further catalysed via transaminase for generating an aminated product useful for the preparation of branched polyhydroxypolyamides.

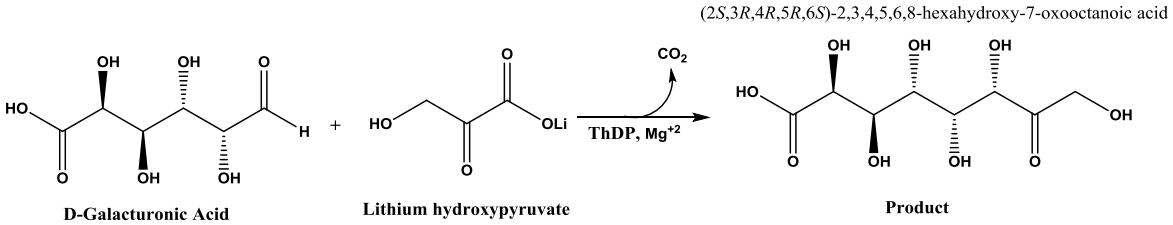

Figure 5.1. Reaction scheme of the TK catalysed reaction of DGA and Li-HPA to CO_2 and OOA.

To date, there have been no reported studies concerning bioconversion of DGA and Li-HPA to OOA, hence it is necessary to explore the possibility of achieving this bioconversion, and to quantify the reaction kinetics.

5.2. Aim and objectives

The aim of this chapter is to explore the transketolase catalysed upgrading of D-galacturonic acid to 2,3,4,5,6,8-hexahydroxy-7-oxooctanoic acid, and to obtain the kinetic parameters of this reaction using pure H461Y-HT TK as biocatalyst. This approach will involve the selection of the best conditions for the bioconversion, the measurement of OOA production, and obtaining the kinetic parameters of the reaction based on the toolbox developed by Chen et al. (2008). The key objectives of this chapter are thus:

- Evaluation of the feasibility of the bioconversion of DGA and Li-HPA to OOA using H461Y-HT transketolase.
- Comparison of the H461Y-HT TK affinity for L-arabinose and DGA.
- Evaluation of DGA consumption during the reaction of DGA and Li-HPA to OOA, using pure H461Y-HT TK as biocatalyst.
- Determination the kinetic parameters for the pure H461Y-HT TK mediated bioconversion of DGA and Li-HPA to OOA.

5.3. Results

5.3.1. Bioconversion of DGA to OOA using pure H461Y-HT TK

In Chapters 3 and 4, TK mutant H461Y was selected as the best biocatalyst for the bioconversion of L-arabinose to L-glucoheptulose and it was shown that the reaction kinetics were similar for both lysate and purified forms of the enzyme (Table 4.3). Being able to use the same TK mutant for the bioconversion of

DGA to OOA would help reduce enzyme costs at large scales. For this reason, reactions were performed using either H461Y-HT lysate or purified H461Y-HT TK along with 33 mM DGA, and 20 mM Li-HPA, in order to explore the feasibility of this bioconversion. As can be seen in Figure 5.2, more than 60% of the initial DGA was consumed after 24 h of reaction using either lysate or pure TK, which suggests that the TK mutant H461Y-HT can be successfully used as biocatalyst for the bioconversion of DGA to OOA. However, even when the DGA consumption is similar for lysate or pure TK, when using lysate some of the DGA is consumed by other proteins in the reaction mix over longer reaction times (>24 hours). For this reason, in order to validate OOA production, it would be preferable to use pure TK for the bioconversion.

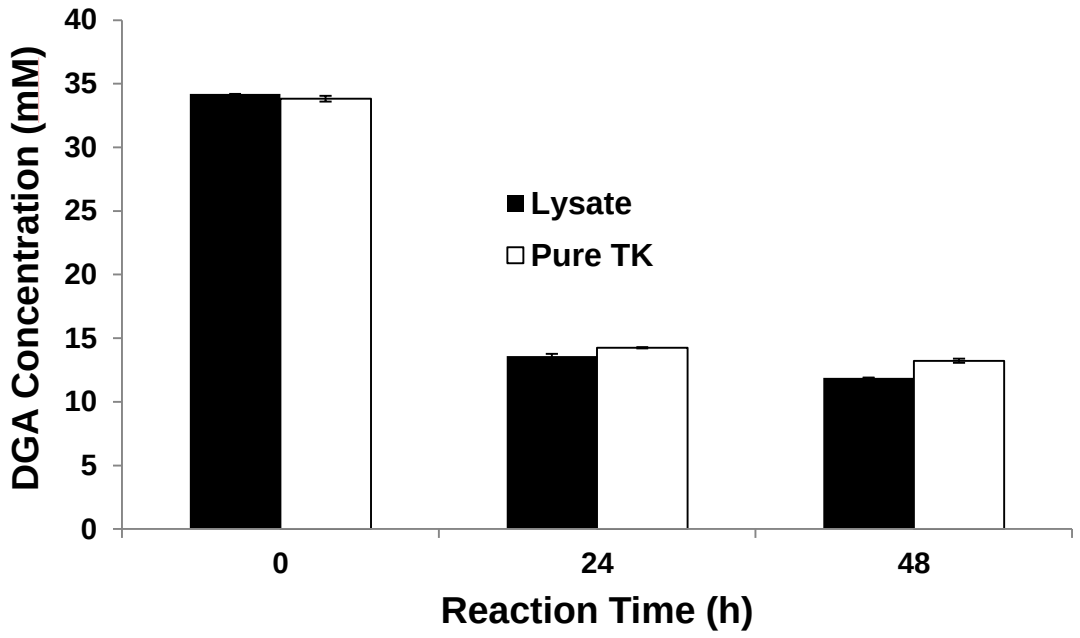

Figure 5.2. D-galacturonic acid consumption during the H461Y-HT TK mediated reaction of D-galacturonic acid and Li-HPA to the corresponding octulose (OOA), using lysate and pure TK. The reaction conditions were 33 mM DGA, 20 mM Li-HPA, 1.7 ThDP, 6 mM $MgCl_2$, 450 rpm and 25°C. Reactions were performed as described in Section 2.4.2. Error bars represent one standard deviation of the mean (n=3).

As the OOA is a novel molecule, there are no commercial available standards for its quantification. For this reason, DGA consumption was used for yield calculations in all further experiments as long as pure TK was used as the biocatalyst.

As can be seen in Figure 5.3, using pure H461Y-HT TK, the total yield for OOA synthesis (based in DGA consumption) was 93 and 98% at 24 and 48 hours respectively; these results are higher than the yields obtained for L-glucoheptulose production (Chapter 3), which suggests that mutant H461Y-HT TK has a higher affinity for DGA than for L-arabinose.

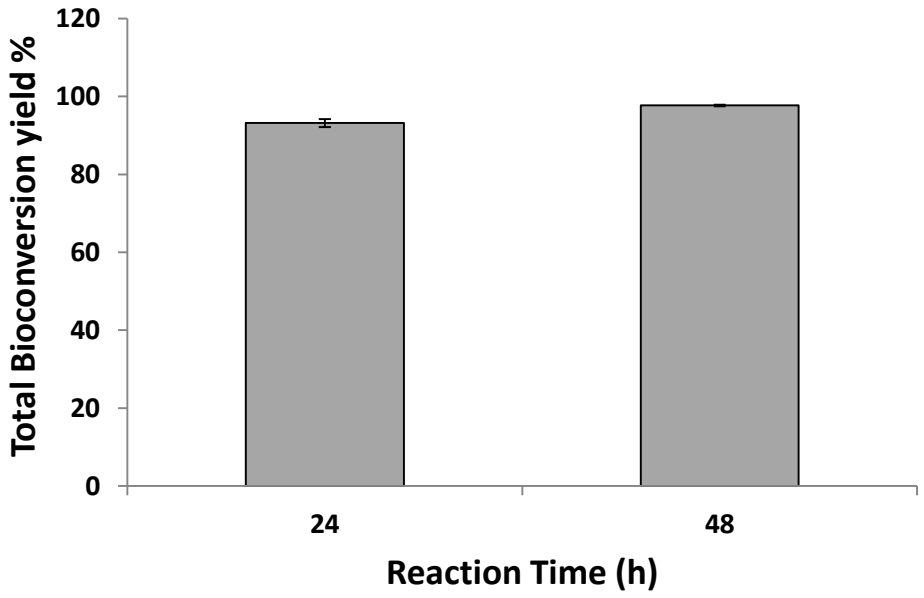

Figure 5.3. Total yield of the TK mediated reaction of D-galacturonic acid and Li-HPA to the corresponding octulose (OOA), using pure TK. The reaction conditions were 33 mM DGA, 20 mM Li-HPA, 1.7 ThDP, 6 mM $MgCl_2$, 450 rpm and 25°C. Reactions were performed as described in Section 2.4.2. Error bars represent one standard deviation of the mean (n=3).

5.3.2. Kinetic parameters identification for pure H461Y-HT TK catalysed reaction of DGA and Li-HPA to OOA

As before in Sections 3.3.2 and 4.3.3, the approach of Chen et al. (2008) was used to enable rapid bioconversion kinetic parameter quantification for the bioconversion of DGA and Li-HPA to OAA using pure TK as biocatalyst (Figure 5.1). For obtaining the kinetic parameters of this reaction the four steps shown in Figure 3.10 were followed as described previously in Section 4.3.3.

In order to implement the non-linear regression and all the statistical analyses required for the method, a programme was developed using MatLab software (MathWorks, Natick, MA, USA).

5.3.2.1. Proportionality between initial reaction rate and transketolase concentration

The experiment for determining the linear region between enzyme concentration and the initial reaction rate was performed as described in Section 2.5.2.1. An equimolar concentration of 30 mM was used for DGA and Li-HPA, and pure TK was used as biocatalyst at different concentrations from 0.5 to 3 mgTK mL^{-1}. TK was purified as described in Section 2.2.5. The results show that the linear relationship between enzyme concentration and initial bioconversion rate was maintained up to 3 mg mL^{-1} of TK in the reaction (Figure 5.4). For the following experiments, concentrations below 3 mg mL^{-1} of pure TK were used.

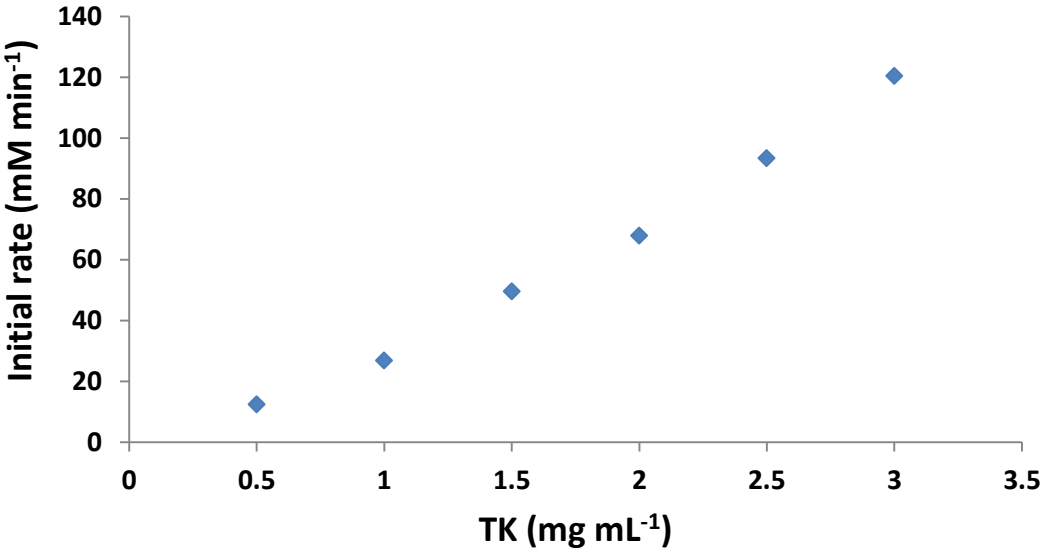

Figure 5.4. Initial rate of OOA formation as a function of pure H461Y-HT TK concentration in the bioconversion. Reaction conditions: 30 mM Li-HPA, 30 mM D-galacturonic acid, 1.7 ThDP, 6 mM $MgCl_2$, 450 rpm and 25 °C. Pure TK was used at 0.16, 0.31, 0.47, 0.63, 0.78, and 0.94 mgTK mL^{-1}. Experiments were performed as described in Section 2.5.2.1. Error bars represent one standard deviation of the mean (n=3).

5.3.2.2. Kinetic model of TK and initial rate experiments

The second step on the methodology shown in Figure 3.10 is to obtain two sets of initial reaction rate data. The first set was obtained by varying DGA concentration while fixing Li-HPA concentration. The second set was obtained by varying Li-HPA concentration while maintaining DGA at a fixed concentration.

For the first set, Li-HPA was fixed at 30 mM, and DGA was varied from 5 to 50 mM. It was found that a linear relationship between DGA concentration and initial reaction rate was maintained from 5 to 20 mM DGA as shown in Figure 5.5. For DGA concentrations higher than 20 mM the initial reaction rate decreased, which means that DGA exhibits inhibition after 25 mM in the reaction. This result is different for when L-arabinose was used as substrate

(Chapter 3 and Chapter 4), in which case L-arabinose did not exhibit inhibition to the reaction for concentrations up to 0.5 M.

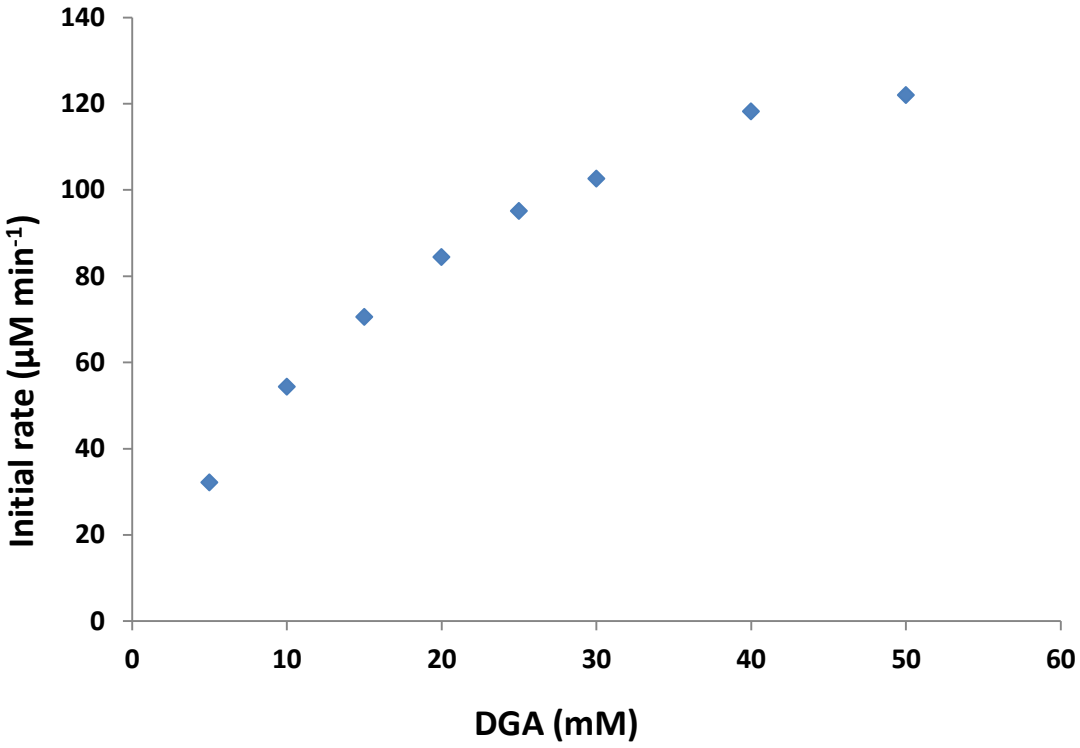

Figure 5.5. Initial rate of OOA formation as a function of initial DGA concentration and a fixed Li-HPA concentration, using pure H461Y-HT TK. Reaction conditions: 30 mM Li-HPA, 1.7 ThDP, 6 mM $MgCl_2$, 450 rpm and 25 °C. D-galacturonic acid was used in a range from 5 to 50 mM. Experiments were performed as described in Section 2.5.2.2. Error bars represent one standard deviation of the mean (n=3).

For obtaining the second set of initial reaction rates, DGA concentration was fixed at 30 mM, and Li-HPA was varied from 0.4 to 10 mM. Figure 5.6 shows that at concentrations above 2 mM HPA there is no further increase in reaction rate while at even higher Li-HPA concentrations the reaction rate fell further. This behaviour is similar to the results obtained for the bioconversion of L-arabinose to L-glucoheptulose, where Li-HPA exhibited inhibition at concentrations after 1 mM.

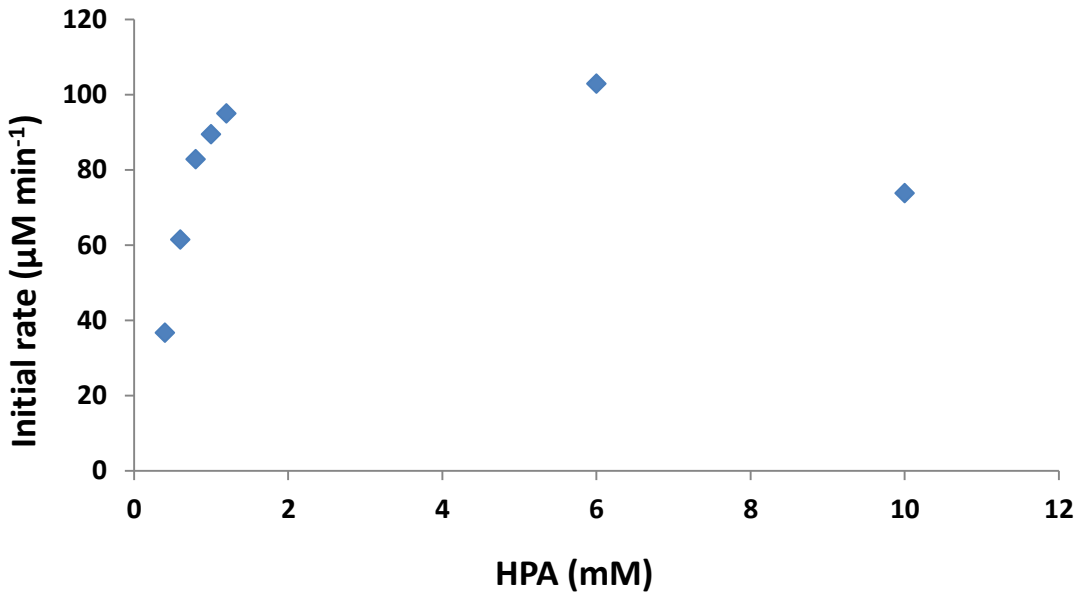

Figure 5.6. Initial rate of OOA formation as a function of initial Li-HPA concentration and a fixed D-galacturonic acid concentration, using pure H461Y-HT TK. Reaction conditions: 30 mM D-galacturonic acid, 1.7 ThDP, 6 mM $MgCl_2$, 450 rpm and 25 °C. HPA was used in a range from 0.2 to 10 mM. Experiments were performed as described in Section 2.5.2.2. Error bars represent one standard deviation of the mean (n=3).

These two sets of initial reaction rates were used to find the region between substrate concentration and initial reaction rate where no substrate inhibition is detected. For DGA the linear range utilised was from 5 to 20 mM, while for the case of Li-HPA the linear range was found to be between 0.4 and 1 mM.

A linear adjustment was successfully applied over the kinetic data using Equation 5.1 for obtaining a preliminary value of K_{HPA}, K_{DGA} of 2.4 and 90.6 mM respectively, and a V_{MAX} of 514.9 µM min^{-1}. These values were used as initial parameters for the non-linear adjustment of the progress curves detailed in the subsequent sections.

Eq.5.1

$$\frac{d[OOA]}{dt} = \frac{k_{cat}E_i[HPA][DGA]}{K_{DGA}[HPA] + K_{HPA}[DGA] + [HPA][DGA]}$$

5.3.2.3. Progress curves for kinetic parameter identification

The final experimental step in the methodology shown in Figure 3.10 was to obtain the full progress curves of reactions at different substrate and enzyme concentrations, with the objective of including possible substrate and product inhibition in the data analysis. A set of nine different reactions were performed as described in Section 2.5.2.3., and samples were taken every hour for 12 hours of reaction time, a total of thirteen sample points which helped maximizing the accuracy of fitting the mathematical model to the data and hence for quantification of the kinetic parameters. The combinations of substrate and protein concentrations used are shown in Table 2.7.

The preliminary results for K_{HPA}, K_{DGA}, Ki_{HPA}, Ki_{DGA}, Ki_{OOA} were 2.4, 90.6, 800, 800, and 156 mM respectively; the value for k_{cat} was 117 min^{-1}. These preliminary data were used as initial guesses for the full kinetic model for obtaining the final, revised kinetic parameters. The optimisation was performed as described in Section 3.3.2.3. The lower and upper bounds for all non-linear regressions were set at 0.0001 and 800.

The global optimisation was achieved after fitting the full kinetic model to the complete data set including both low and high substrate concentrations. The final values for each kinetic parameter were: 14.08, 28.35, 0.6517, 120.04, and 100.00 mM for K_{HPA}, K_{DGA}, Ki_{HPA}, Ki_{DGA}, and Ki_{GLU} respectively. The final value for k_{cat} was 2500 min^{-1}. Figure 5.7 shows the agreement between the experimental progress curves and the fit of the mathematical model based on these parameter values, and the corresponding rate model is displayed in Equation 5.2. Model Predictions and residuals from the final model fit are shown in Section C of Appendix VIII.

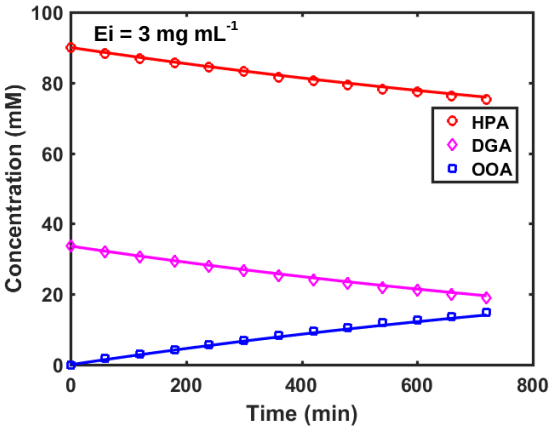
Ei = 3 mg mL-1
HPA
DGA
OOA
Concentration (mM)
Time (min)

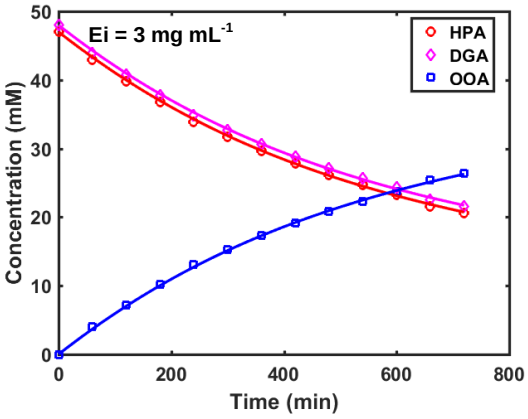
Ei = 3 mg mL-1
HPA
DGA
OOA
Concentration (mM)
Time (min)

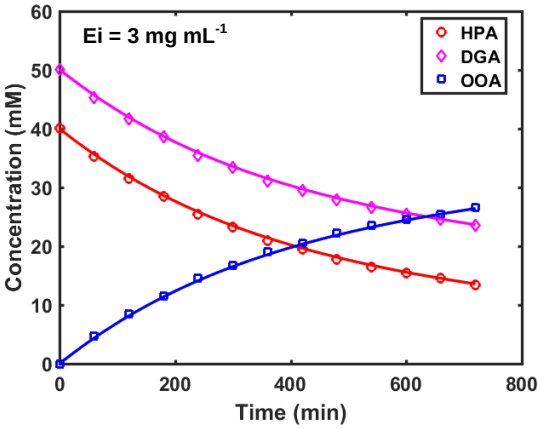
Ei = 3 mg mL-1
HPA
DGA
OOA
Concentration (mM)
Time (min)

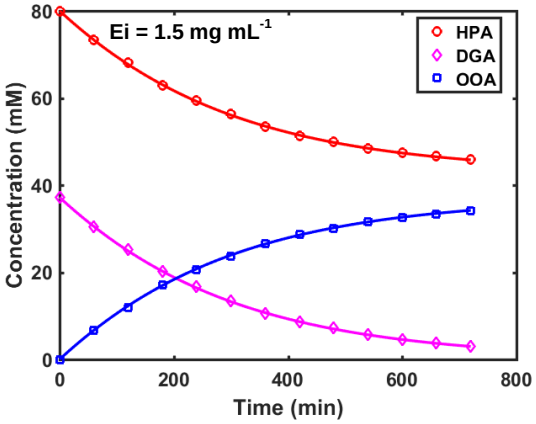
Ei = 1.5 mg mL-1
HPA
DGA
OOA
Concentration (mM)
Time (min)

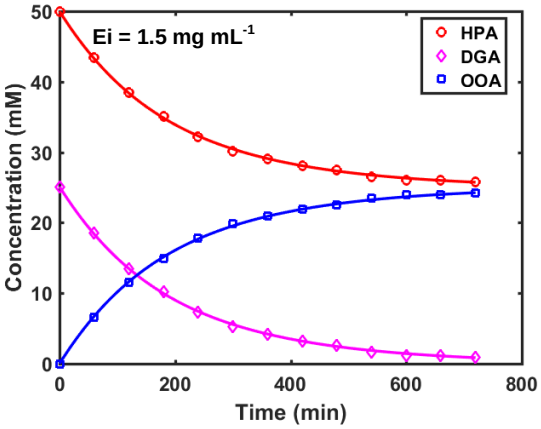
Ei = 1.5 mg mL-1
HPA
DGA
OOA
Concentration (mM)
Time (min)

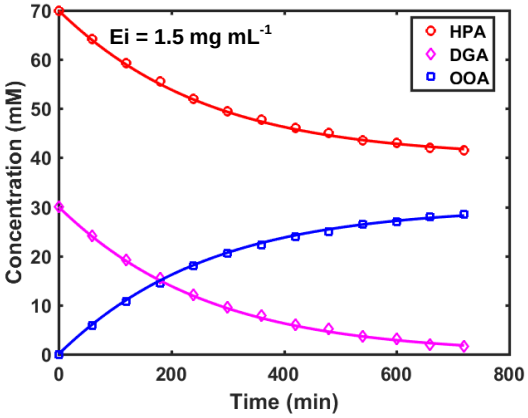
Ei = 1.5 mg mL-1
HPA
DGA
OOA
Concentration (mM)
Time (min)

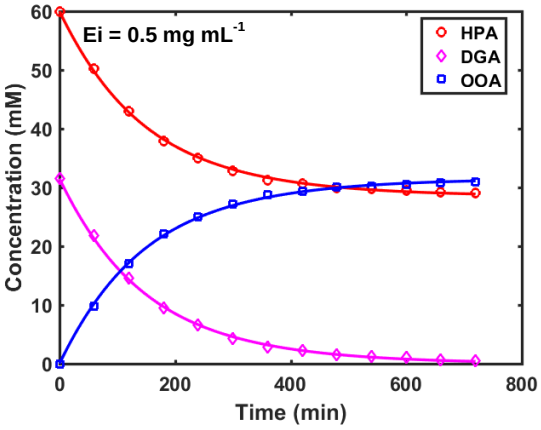
Ei = 0.5 mg mL-1
HPA
DGA
OOA
Concentration (mM)
Time (min)

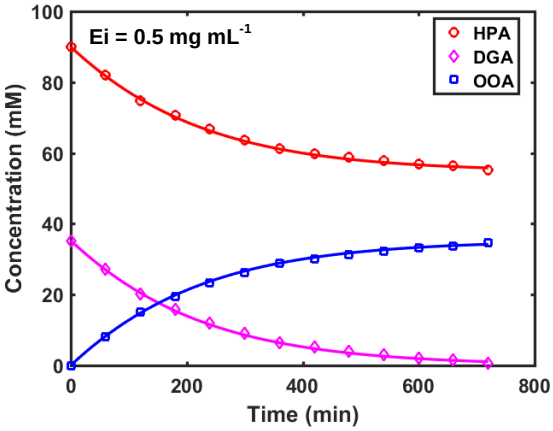
Ei = 0.5 mg mL-1
HPA
DGA
OOA
Concentration (mM)
Time (min)

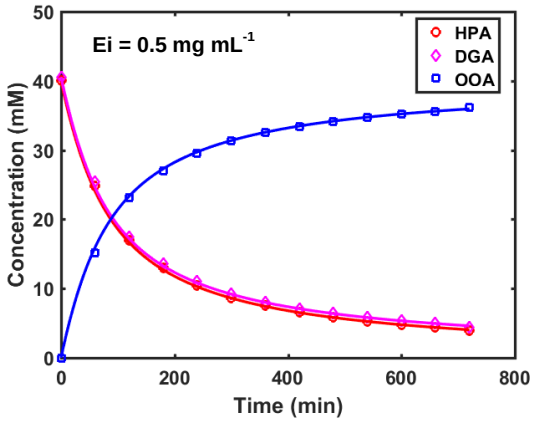

Figure 5.7. Comparison of the experimental and fitted progress curves using different concentrations of pure H461Y-HT TK, Li-HPA, and D-galacturonic acid for the synthesis of OOA. Lines show model predictions and dots represent the experimental data. Error bars represent one standard deviation of the mean (n=3).

Eq.5.2

$$\frac{d[OOA]}{dt} = \frac{2500E_i[HPA][DGA]}{28.35[HPA]\left(1+\frac{[HPA]}{0.65}\right)+14.1[DGA]\left(1+\frac{[ARA]}{120}\right)+[HPA][DGA]+21.7[DGA][OOA]+16.92[OOA]}$$

$$\frac{d[OOA]}{dt} = \frac{k_{cat}E_i[HPA][DGA]}{K_{DGA}[HPA]\left(1+\frac{[HPA]}{K_{iHPA}}\right)+K_{HPA}[DGA]\left(1+\frac{[DGA]}{K_{iDGA}}\right)+[HPA][DGA]+\frac{K_{HPA}}{K_{iHPA}}[DGA][OOA]+\frac{K_{HPA}K_{iDGA}}{K_{iOOA}}[OOA]}$$

As before, a separate experiment was performed to validate the kinetic parameters obtained using a combination of substrate and enzyme concentrations not included in the original mathematical curve fitting. The experiment was performed as described in Section 2.5.2.3. The DGA and Li-HPA concentration was 50 mM each, and the TK concentration was 1.35 mg mL^{-1}, the fit of the model to the experimental data can be seen in Figure 5.8.

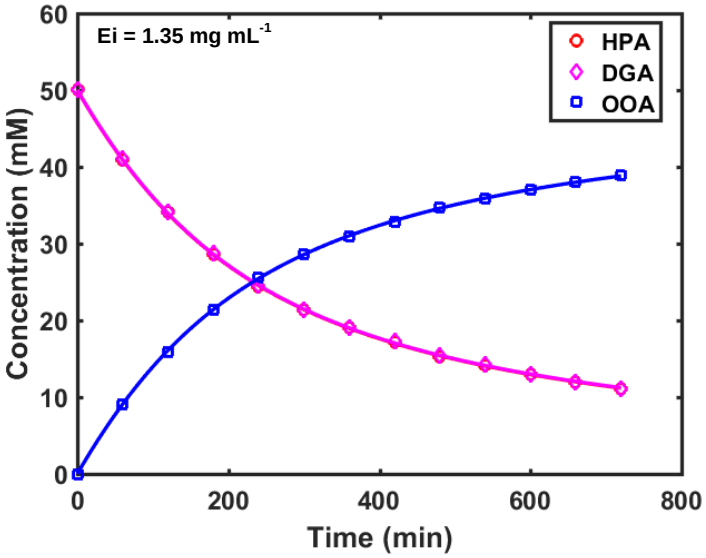

Figure 5.8. Verification of model predictions with an experimental set of data not included in the initial progress curves experiment. Reaction conditions: 50 mM DGA, 50 mM Li-HPA, 1.7 mM ThDP, 6 mM $MgCl_2$, and1.35 mg mL^{-1} of pure H461Y-HT TK, 450 rpm and 25 ºC. Lines show model predictions and dots represent the experimental data. Error bars represent one standard deviation of the mean (n=3).

5.4. Discussion of results

5.4.1. D-galacturonic acid bioconversion using H461Y-HT TK

The bioconversion of D-galacturonic acid to 2,3,4,5,6,8-hexahydroxy-7-oxooctanoic acid using pure H461Y-HT TK as biocatalyst was successfully achieved (Figure 5.2). Moreover, DGA was shown to be a more effective substrate for H461Y-HT TK than L-arabinose. More than 90% DGA bioconversion into OOA was achieved in 12 hours. This is greater than the yield achieved for L-arabinose after 48 hours of reaction (Table 3.1). This can be due to the higher affinity of the active site of the TK for DGA than for L-arabinose on the second half of the bioconversion (Figure 3.18), that allows the rapid release of OOA.

Furthermore, as well as with L-arabinose as substrate scheme, Li-HPA exhibits inhibition of the reaction at concentrations greater than 1 mM. This further suggests the establishment of a fed-batch reaction could be used in order to optimise OOA production, using low concentrations of fed Li-HPA.

5.4.2. Kinetic parameters for the pure TK catalysed reaction of D-galacturonic acid and Li-HPA to 2,3,4,5,6,8-hexahydroxy-7-oxooctanoic acid

As can be seen in Section 5.3.2.1, it was found that for the reaction studied, protein concentration could get up to 3 mgTK mL^{-1} without losing proportionality with the reaction rate, this was important to establish the enzyme concentration in further experiments.

During the second experimental step of the approach it was found that DGA and Li-HPA become inhibitory in the reaction when concentrations are higher than 20 and 1 mM respectively when the other substrate is kept fixed at 30 mM. With these results, preliminary kinetic values were obtained, resulting in a K_{HPA} and K_{DGA} of 2.4 and 90.6 mM respectively, and a V_{MAX} of 514.9 µM min^{-1}. These values were used as initial parameters for the non-linear adjustment of the 9 full progress curves designed in the last experimental step. The objective of obtaining these progress curves was to include any substrate and product inhibition on the final non-linear regression for the obtaining of the full set of kinetic parameters. The substrates concentrations were chosen according to possible concentrations used in the industry, and should be beyond inhibition regions found in previous experiments.

Final values for each kinetic parameter after reconciliation were: 14.08, 28.35, 0.6517, 120.04, and 100.00 mM for K_{HPA}, K_{DGA}, Ki_{HPA}, Ki_{DGA}, and Ki_{GLU}

respectively, and the final value for k_{cat} was 2500 min^{-1}. These values were validated by performing an extra experiment not included in the non-linear adjustment of the progress curves, shown in Figure 5.8. The adjustment of the experimental points to the model predictive curves was excellent for the three molecules of interest, which verified the kinetic parameters obtained.

5.5 Summary

The work developed in this Chapter has shown that it is possible to utilise H461Y-HT transketolase as biocatalyst for the bioconversion of Li-HPA and D-galacturonic acid to 2,3,4,5,6,8-hexahydroxy-7-oxooctanoic acid. It was discovered that H461Y-HT TK displayed better catalytic activity towards DGA than for L-arabinose; for this reason, the reaction can be completed in as less as 12 hours, when the full reaction using L-arabinose can last more than 24 hours. This suggests that a single TK enzyme source could be used in the first step of the biocatalytic upgrading of both of the major monosaccharide components of SBP (after glucose is removed for bioconversion to ethanol) (Section 1.7.1).

The full reaction kinetic model was obtained using 9 full progress curves, as well as utilising an independent experimental set not included in the methodology for determining the parameters. The main bottleneck of the reaction resulted in the high inhibition exhibited by Li-HPA; therefore, using a low concentration of Li-HPA in a fed-batch reaction system could improve OOA production. The need to overcome the inhibition of Li-HPA for both L-arabinose and D-galacturonic acid is a key feature of the bioconversions studied to date. Chapter 6 will explore the design of a fed-batch process for the synthesis of L-glucoheptulose and the optimisation of the feeding strategy.

6. SCALE UP OF L-GLUCOHEPTULOSE SYNTHESIS

6.1. Introduction

As previously described in Section 1.8, this thesis is contributing to a larger project focused on the enzymatic synthesis of chiral amino alcohols from an important UK renewable feedstock i.e. sugar beet pulp (Section 1.7.1). In Chapter 3 it was shown that H461Y TK mutant was able to convert one of the two major L-arabinose components of SBP (20.9%) into L-glucoheptulose (Figure 3.1). This was also shown to be true using the pure enzyme (Chapter 4). In Chapter 5, H461Y-HT TK mutant was identified that could convert the other major SBP pectin component, D-galacturonic acid (21.1%), into 2,3,4,5,6,8-hexahydroxy-7-oxooxtanoic acid (OOA). In order for these enzymatic processes to become sustainable and economic it would be necessary to increase their productivity i.e. the space-time yield of the reactions.

Based on discussions with various end-user companies, the production and optimisation of L-glucoheptulose has higher priority than the production of 2,3,4,5,6,8-hexahydroxy-7-oxooxtanoic acid from D-galacturonic acid. For this reason, the scale up of L-glucoheptulose production was further explored.

As shown in Chapter 3 (for the H461Y TK lysate) and in Chapter 4 (for the pure H461Y-HT TK), the main limitation on the synthesis of L-glucoheptulose is that HPA becomes inhibitory concentrations > 10 mM. It was hypothesised that this is caused, in part, by the slow reaction of L-arabinose with the ThDP-enamine intermediate in the second part of the overall reaction (Figure 3.18). For the

same reason L-arabinose exhibits no inhibition at even very high concentrations, > 500 mM.

For the industrial production of L-glucoheptulose it is necessary to enhance the concentration of the L-glucopheptulose product (to aid downstream processing) and the extent of substrate utilisation (for sustainability and economic reasons). From a bioprocess engineering perspective, it will also be important to demonstrate the synthesis of L-glucoheptulose at larger scales and in bioreactor formats. Therefore, a preparative scale reaction should be explored utilising lysate as biocatalyst (to minimize enzyme costs), high L-arabinose concentrations and in fed-batch mode to keep HPA concentrations below inhibitory levels.

6.2. Aim and objectives

L-arabinose is one of the major components of UK sugar beet pulp, and it can be released with high yield by a combination of mild steam explosion and chemical hydrolysis (Hamley-Bennet et al., 2016). It is therefore, sensible to focus on this SBP fraction for initial scale up studies. The aim of this Chapter is therefore to scale-up the synthesis of L-glucoheptulose, using L-arabinose, Li-HPA, and H461Y TK lysate, as well as to find the ideal reaction mode for optimising L-glucoheptulose production. To achieve this, the experimental results of Chapters 3 and 4 will be used to identify the ideal reaction mode for improving L-glucoheptulose production and minimizing the waste of the substrates on the reaction. The key objectives of this chapter are thus:

- To scale up the batch reaction from micro (0.6 mL) to preparative scale (50 mL).

- To explore the benefits of fed-batch operation, by the utilisation of high L-arabinose concentrations and identifying a suitable strategy for a Li-HPA feeding to maintain concentrations in the bioreactor below inhibitory levels.
- To identify the optimum bioconversion conditions for the preparative scale synthesis of L-glucoheptulose.

6.3. Results

6.3.1. Scale-up of the synthesis of L-glucoheptulose in batch mode

The synthesis of L-glucoheptulose from L-arabinose was scaled-up from 600 µL microscale reactions (Section 2.4.1) to a 50 mL working volume laboratory scale stirred tank bioreactor (Section 2.6). This represents an 84-fold increase in reaction volume. Table 6.1 shows the different conditions and bioreactors used for the micro and preparative scale synthesis.

Table 6.1. Comparison of the reaction conditions and bioreactors used for the scale-up of L-glucoheptulose synthesis from L-arabinose

Bioconversion Conditions	Microscale	Preparative Scale
Reactor Vessel	1.5 mL Eppendorf tubes	100 mL jacketed glass stirrer tank bioreactor
Temperature Control	Under plate heated platform	Circulating water bath
Mixing (rpm)	450	350
Mixing Device	Orbital shaking platform (6 mm diameter)	Magnetic stirrer bar
Working Reaction Volume	600 µL	50 mL
pH	7.0	7.0
pH Control	50 mM Tris-HCL Buffer	pH-STAT system with 0.1 mM NaOH

The temperature on the preparative scale reaction was maintained at 25 °C, using circulating water, and the pH was kept at 7 by the use of an automated pH-STAT system. This, controlled pH by the automated addition of a 0.1 M NaOH solution instead of the use of a 50 mM Tris-HCL buffer. At larger scales, this type of pH control is beneficial as it reduces the amount of salt present in the final reaction medium.

An initial batch reaction was set up in the pH-controlled, stirred bioreactor, using an equimolar concentration of 60 mM for Li-HPA and L-arabinose, and a H461Y

TK lysate concentration of 5.5 mg mL^{-1}. These conditions were chosen as 60 mM was the initial L-arabinose concentration that would be used for the fed-batch reaction mode.

As can be seen in Figure 6.1, the final L-glucoheptulose concentration was 13 mM (133 mg) and the final yield of product on substrate, $Y_{P/S}$ was around 22% after 120 hours. However, due to a combination of the labile nature of Li-HPA (Lorilliere et al., 2017) and the utilisation of lysate as biocatalyst (Harris and Keshwani, 2009), almost all the Li-HPA appeared to be consumed within 120 hours. Based on the known reaction stoichiometry, i.e. 1 mol of L-glucoheptulose is synthesised from 1 mol of L-arabinose, it is also clear that a considerable portion of L-arabinose (33%) was utilised by other enzymes in the crude TK lysate preparation.

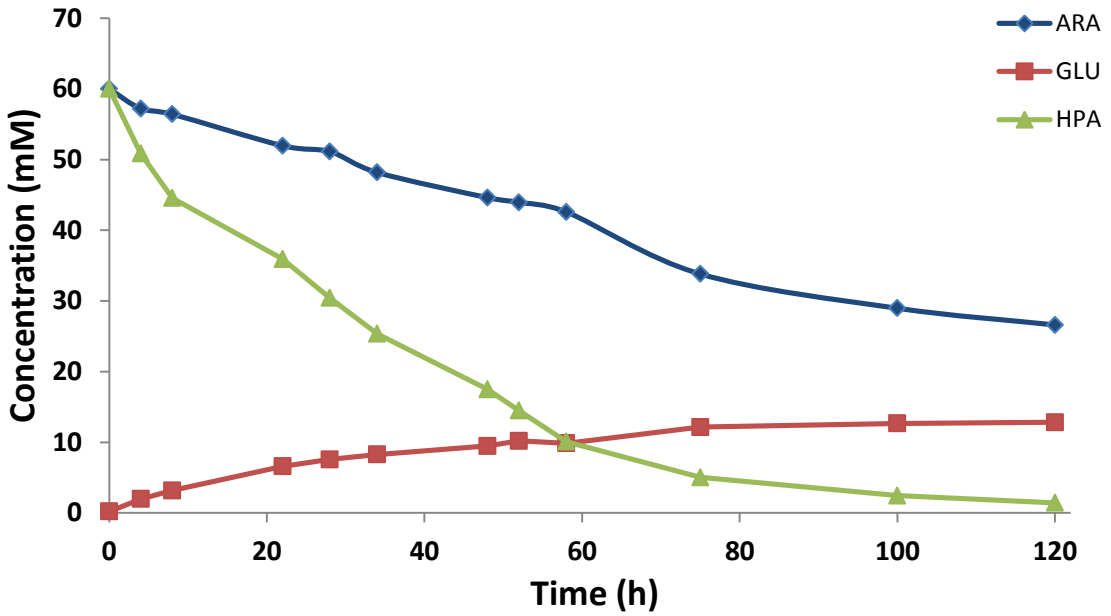

Figure 6.1. Batch bioconversion kinetics of L-glucoheptulose synthesis from L-arabinose and Li-HPA using H461Y TK lysate. Bioconversion performed in batch mode using a Ph-STAT system as described in Section 2.6. Initial substrate concentrations were 60 mM Li-HPA and 60 mM L-arabinose; total bioconversion time was 120 hours. A final L-glucoheptulose concentration of 13 mM was obtained. Error bars represent one standard deviation of the mean (n=3).

These results indicate that the bioconversion can be performed using NaOH addition for pH control, rather than buffer solutions, without any detriment. In order to optimise the utilisation of L-arabinose and decrease Li-HPA losses during the reaction, it is clear that a fed-batch operation should be considered.

6.3.2. Preparative scale of the synthesis of L-glucoheptulose in fed-batch mode

In order to overcome Li-HPA substrate inhibition on the reaction as well as the degradation of this substrate during the reaction, a fed-batch operating mode was investigated. Different feeding strategies were explored, and all experiments were performed under the preparative scale reaction conditions outlined in Table 6.1. The starting L-arabinose concentration was 60 mM for all cases.

According to Table 4.3, by maintaining a Li-HPA concentration below the Ki_{HPA}, it is assumed that substrate inhibition could be avoided. However, when concentration of 1 mM of HPA was used, all HPA was consumed within two hours of reaction with 8% bioconversion to L-glucoheptulose. Therefore, the first feeding strategy involved the addition of a Li-HPA solution to achieve a final overall concentration of 10 mM every 3 hours. As can be seen in Figure 6.2, three hours were not sufficient for all the Li-HPA to be consumed, which resulted in further accumulation of Li-HPA after each feeding time. As a consequence, there was significant inhibition of H461Y TK with a low overall productivity being achieved. The final L-glucoheptulose amount obtained was 89 mg, and Li-HPA accumulation up to 113 mg.

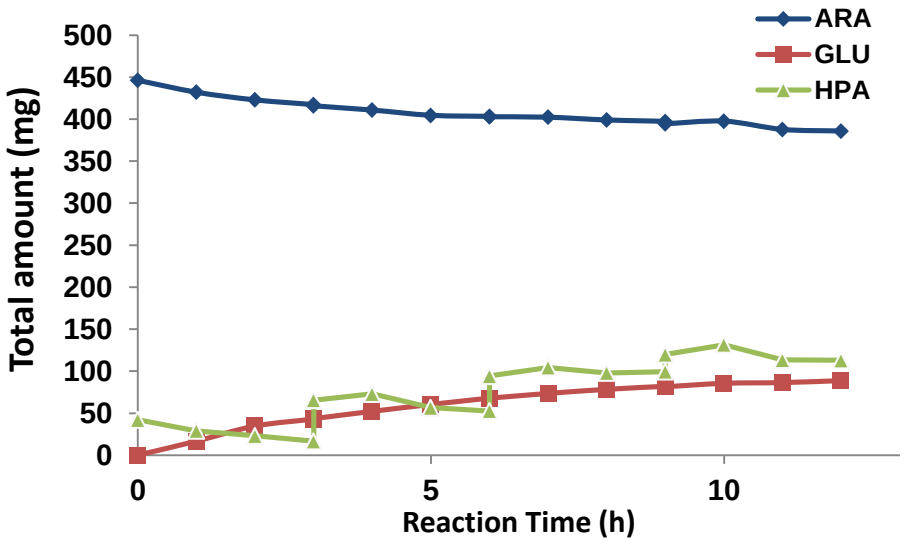

Figure 6.2. Total amount (in mg) of substrates and product during the fed-batch bioconversion of Li-HPA and L-arabinose to L-glucoheptulose. Bioconversion performed using a pH-STAT system as described in Section 2.6. Initial substrate concentration was 10 mM Li-HPA and 60 mM L-arabinose, with a feeding of Li-HPA every three hours up to 10 mM, total bioconversion time was 12 hours, and the final L-glucoheptulose obtained was 89 mg. Error bars represent one standard deviation of the mean (n=3).

The second strategy investigated for the fed-batch reaction involved the addition of a single shot of fresh H461Y TK lysate after 11 hours of reaction, in order to overcome any decrease in enzyme activity over time. The frequency of Li-HPA feeding was extended to 4 hours and the overall reaction time extended to 48 hours. As can be seen in Figure 6.3, there was Li-HPA accumulation as in previous experiments, leading to low levels of L-arabinose conversion. It can be seen, however, that the final low product concentration is not a consequence of TK activity loss, as the addition of fresh lysate did not improve L-arabinose production. The final amounts of L-arabinose and Li-HPA after 48 hours of were 133 and 212 mg respectively. The mass of L-glucoheptulose produced after 12 hours was 32.5 mg (less than that achieved in Figure 6.2) but this increased to 133 mg by extending the reaction time to 50 hours.

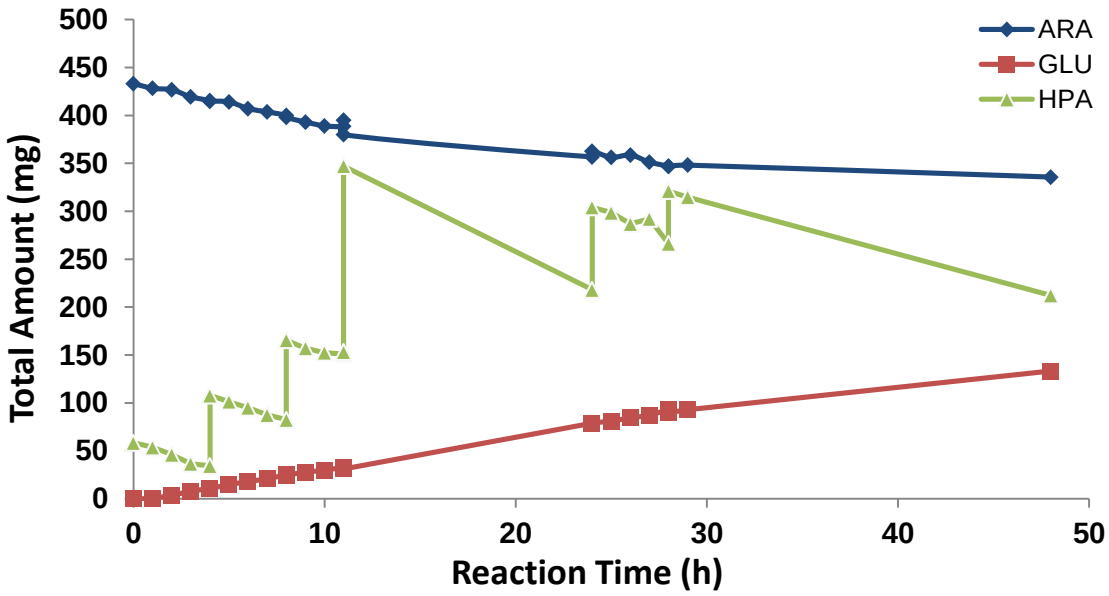

Figure 6.3. Total amount (in mg) of substrates and product during the fed-batch bioconversion of Li-HPA and L-arabinose to L-glucoheptulose. Bioconversion performed using a pH-STAT system as described in Section 2.6. Initial substrate concentration was 10 mM Li-HPA and 60 mM L-arabinose, with a feeding of Li-HPA every four hours up to 10 mM, fresh lysate was added after 11 hours of reaction, total bioconversion time was 48 hours, and the final L-glucoheptulose obtained was 133 mM. Error bars represent one standard deviation of the mean (n=3).

The third strategy for improving Li-HPA consumption and L-glucoheptulose production was to add Li-HPA aliquots to the reactor every 12 hours, for a total reaction time of 96 hours with a starting L-arabinose concentration of 60 mM. Figure 6.4 shows that a feeding interval of 12 hours is better strategy than those described above, leading to a final total mass of L-glucoheptulose product of 337 mg. The residual mass of Li-HPA was just 9 mg. Based on the reaction stoichiometry, 55% of the L-arabinose consumed was converted into L-glucoheptulose. This experiment demonstrated that keeping Li-HPA concentration at low levels, improves both its utilisation and the production of L-glucoheptulose.

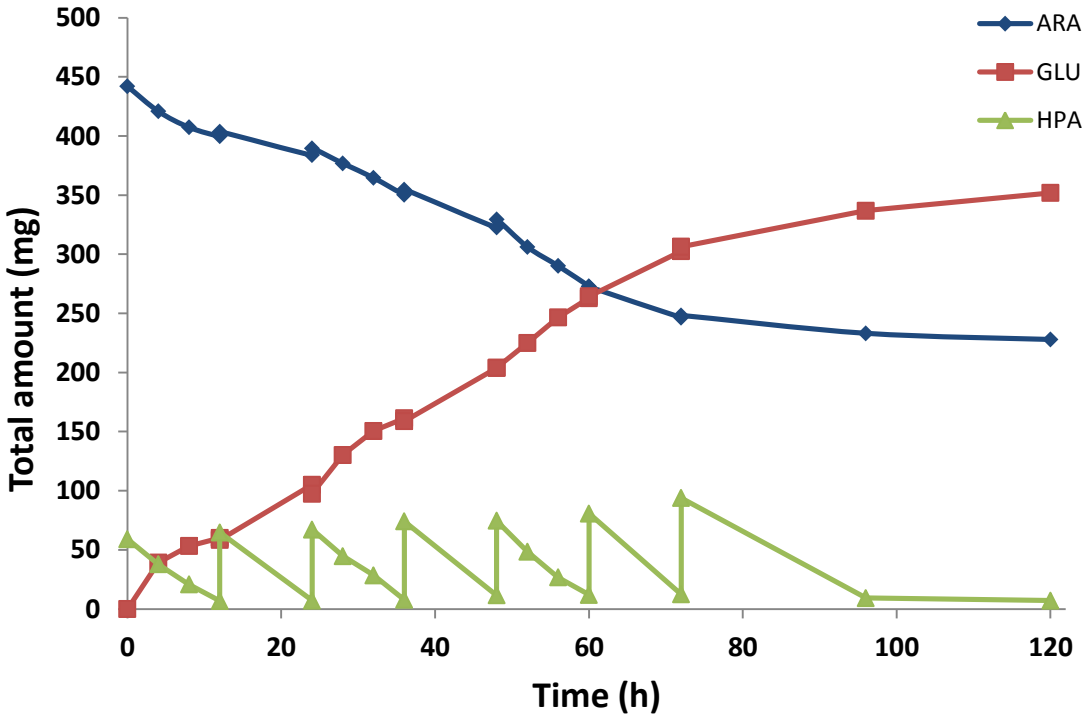

Figure 6.4. Total amount (in mg) of substrates and product during the fed-batch bioconversion of Li-HPA and L-arabinose to L-glucoheptulose. Bioconversion performed using a pH-STAT system as described in Section 2.6. Initial substrate concentration was 10 mM Li-HPA and 60 mM L-arabinose, with a feeding of Li-HPA every 12 hours up to 10 mM, total bioconversion time was 120 hours, and the final L-glucoheptulose production was 352 mg. Error bars represent one standard deviation of the mean (n=3).

After 96 hours, further samples were taken from the reactor. Figure 6.4 shows that the remaining Li-HPA was utilised for getting to a final L-glucoheptulose mass of 352 mg, this shows that the enzyme was still active over the extended reaction period and the bioconversion could be maintained for longer time.

Within a biorefinery context (Section 1.8), a further objective would be to achieve utilisation of L-arabinose at even higher concentrations which should be possible, considering that this substrate does not exhibit significant TK inhibition (Table 4.3). To explore this, a further fed-batch reaction was set up with an initial L-arabinose concentration of 111 mM, and a feeding time of Li-HPA of 12 hours over a total reaction time of 150 hours.

Figure 6.5 shows the bioconversion kinetics of the best fed-batch feeding strategy for the production of L-glucoheptulose. After 150 hours of reaction, nearly half a gram of L-glucoheptulose had been synthesised (482 mg). The residual masses of Li-HPA and L-arabinose were 37 mg and 35 mg respectively. This experiment also demonstrated the long-term stability of the H461Y TK over the full 150 hour bioconversion period.

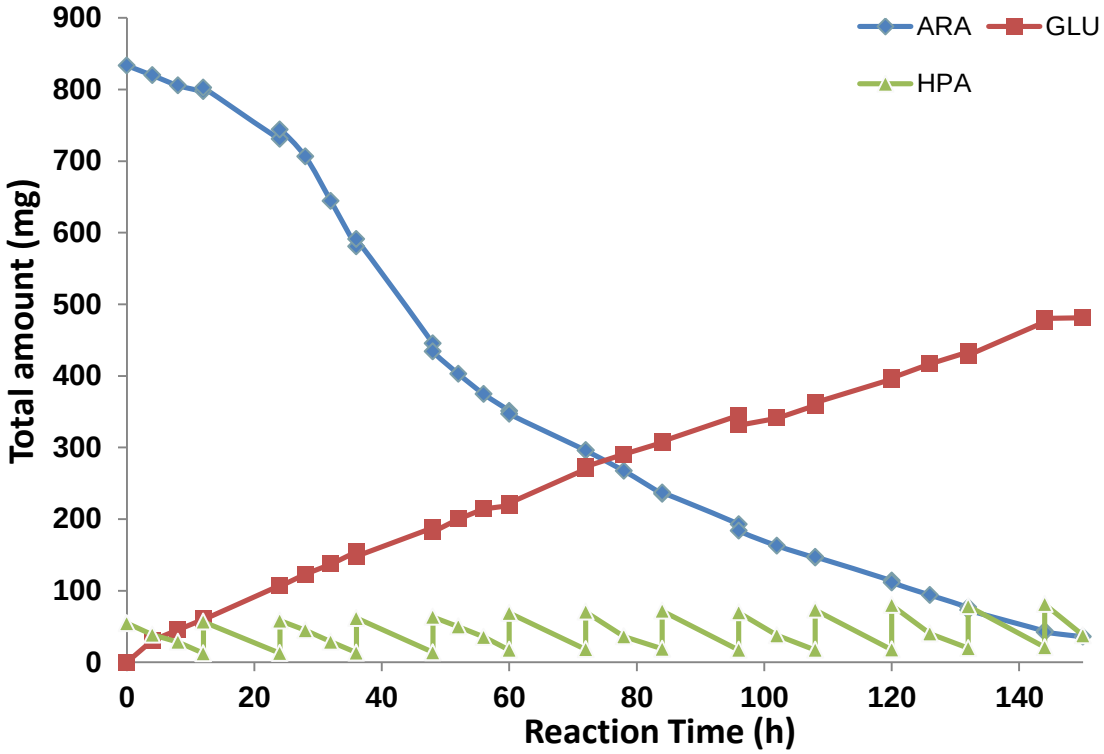

Figure 6.5. Total amount (in mg) of substrates and product during the fed-batch bioconversion of Li-HPA and L-arabinose to L-glucoheptulose. Initial substrate concentration was 10 mM Li-HPA and 111 mM L-arabinose, with a feeding of Li-HPA every 12 hours up to 10 mM, total bioconversion time was 150 hours, and the final L-glucoheptulose obtained was 482 mg. Error bars represent one standard deviation of the mean (n=3).

6.4. Discussion of results

During the different feeding strategies evaluated in this work, it was found that Li-HPA is utilised by other enzymes in the lysate apart from just TK (Figure 6.1). This leads to low levels of conversion of this expensive substrate into the main target product, L-glucoheptulose. For this reason, as well as the low Ki for Li-

HPA (Table 4.3), it is essential to maintain a low Li-HPA concentration during the reaction. Similarly, the results showed that L-arabinose was also converted by other enzymes in the lysate. These losses are considered negligible since the L-arabinose was in excess, is cheaply available in large quantities (Section 1.7.1) and it does not exhibit any inhibition over the synthesis of L-glucoheptulose (Table 4.3). As a result of the low affinity of the TK active site for L-arabinose (Section 3.4.2), the overall reaction rate is very slow, however this is compensated for, in part, by the long term stability of the enzyme which is seen to remain active for over 150 hours of operation. For these reasons, fed-batch operation over 150 hours with feeding of Li-HPA every 12 hours resulted in the best reported synthesis of L-glucoheptulose (Figure 6.5).

The optimised conditions for the production of L-glucoheptulose are: an initial concentration of L-arabinose of 111 mM, a feeding frequency of Li-HPA every 12 hours to give a maximum reactor concentration of 10 mM over a total reaction time of 150 hours.

6.5 Summary

In Chapters 3 and 4, the bioconversion of Li-HPA and L-arabinose to L-glucoheptulose was studied experimentally and the enzyme kinetic parameters quantified. These results showed that the main bottlenecks of the reaction were the high substrate inhibition of Li-HPA and the low affinity of the active site of the enzyme for L-arabinose (Table 4.3). For these reasons, the best approach for optimising the L-glucoheptulose synthesis was considered to be a fed-batch reaction with a high L-arabinose starting concentration and a low level of Li-HPA.

An optimised fed-batch operating strategy was thus developed (Figure 6.5) to enable efficient production of L-glucoheptulose at a preparative scale in a pH-STAT system. This operating strategy and the conditions identified could be a useful starting point for the establishment of L-glucoheptulose synthesis at industry commercial scales. A similar strategy could be employed for optimising the TK-catalysed synthesis of OOA from L-galacturonic acid as described in Chapter 5.

7. CONCLUSIONS AND FUTURE WORK

7.1. Overall conclusions

In this work the biocatalytic upgrading of L-arabinose and D-galacturonic acid, two of the main sugars obtained from sugar beet pulp after saccharification (Section 1.7.1) was achieved and optimised. The aim of this thesis was to characterise and model the bioconversion of L-arabinose and D-galacturonic acid, this was enabled by the succesfull selection of an efficient TK mutant for the bioconversion of the substrate of interest (Section 3.3.1, and Section 4.3.1), and the utilisation of a new hybrid modelling approach (Section 2.5) developed by Chen et al. (2008), that includes the best features of linear and non-linear methodologies for kinetic parameters identification.

The best TK enzyme for the bioconversion of L-arabinose and D-galacturonic acid to the corresponding polyalcohols was the H461Y mutant (Table 3.1). It was used primarily used in this work as a cell lysate because this form of biocatalyst is more suitable for industrial applications and at the same time provides high activity and overcomes the need for purification processes. Nevertheless, to facilitate more detailed study of the bioconversion kinetics, this mutant was successfully His_6 tagged to enable rapid purification via Ni-NTA columns (Section 4.3.1 and Section 4.3.2). This enabled the utilisation of pure transketolase preparation for enzyme kinetic parameter and stability determination (Section 4.3.3).

Kinetic models for the bioconversion of L-arabinose to L-glucoheptulose were established for both lysate and purified forms of transketolase (Section 3.3.2

and Section 4.3.3). These indicated similar results for the kinetic parameters suggesting that the TK biocatalyst can be used either as lysate or pure enzyme.

Also, it was found that the overall reaction rate for the L-glucoheptulose production is determined by the low affinity of the enzyme for the L-arabinose (Section 3.4.2); this was suggested by the high values of K_{ARA} obtained (Table 4.3) which causes the slow release of the L-glucoheptulose in the second stage of the reaction (Figure 3.18B). Moreover, these kinetic parameters also indicate that Li-HPA becomes inhibitory at low concentrations around 1 mM (Table 4.3).

Moreover, L-glucoheptulose was successfully accepted by the TAm encoded by pQR2191, achieving a 23% yield of conversion into the postulated product (2*S*,3*S*,4*S*,5*R*)-6-aminoheptane-1,2,3,4,5,7-hexaol (Figure 1.13) when using (*S*)-MBA as amino donor (Figure 3.17). This result opens the possibility of establishing a coupled TK-TAm bioconversion for the production of AHH from L-arabinose.

In order to utilise the other major monosaccharide component of SBP, the upgrade of D-galacturonic acid (DGA) to 2,3,4,5,6,8-hexahydroxy-7-oxooctanoic acid (OOA) was achieved utilising the same TK mutant (Section 3.3.1) as was used for the bioconversion of L-arabinose to L-glucoheptulose (Chapters 3 and 4). It was found that using pure TK (Section 4.3.1), a total bioconversion yield of 93 and 98% was achieved after 24 and 48 hours respectively (Section 5.3.1). This suggests that TK mutant H461Y has higher affinity for DGA than for L-arabinose which is confirmed by the lower value of K_{DGA} (Section 5.4.2) compared to the values of K_{ARA} obtained for the L-arabinose kinetic models (Table 4.3). Furthermore, the kinetic parameters for the bioconversion of DGA to OOA using H461 TK as biocatalyst were obtained (Section 5.4.2), where the

main bottleneck was, as well as for the L-arabinose reaction system, that Li-HPA exhibits inhibition of the reaction at concentrations above 1 mM (Figure 5.5).

Finally, with the purpose of demonstrating that all these enzymatic processes can become sustainable and economic from a bioprocess engineering perspective, the optimisation of the more studied bioconversion in this work was explored at preparative scale utilising a pH-STAT system and a fed-batch bioreaction mode (Chapter 6). L-glucoheptulose production was optimised using a fed-batch mode, starting with high L-arabinose concentrations (more than 100 mM), with a feeding of Li-HPA every 12 hours to up to a maximum concentration of 10 mM. Using this methodology it was possible to obtain a total of 500 mg of L-glucoheptulose after 150 hours (Figure 6.5).

In summary, the kinetic models obtained on this project will help to establish the principle for biocatalytic design and operation of the production of L-glucoheptulose and 2,3,4,5,6,8-hexahydroxy-7-oxooctanoic acid utilising one single TK mutant. The models offer an insight of the expected productivity of these chiral molecules at higher scales and help to design suitable feeding strategies. If the results of this work are going to be used in the industry, an economic analysis should be realised in order to optimise not only production but also resource utilisation.

It is expected that in the future a major proportion of the fine chemical industry will rely on sustainable processes in order to preserve non-renewable resources, and reduce waste and contamination (Section 1.7). The results on this thesis are meant to provide a useful tool towards the establishment, optimisation, and the scaling up of this kind of industrial processes.

7.2. Future work

The findings of this project have established kinetic models for the optimised production of L-glucoheptulose (Equation 3.2 and Equation 4.1) and 2,3,4,5,6,8-hexahydroxy-7-oxooctanoic acid (Equation 5.2). These are two polyalcohols of industrial importance for the production of active pharmaceutical ingredients. Moreover, initial screening results suggest that it may be possible to produce (2*S*,3*S*,4*S*,5*R*)-6-aminoheptane-1,2,3,4,5,7-hexaol via the TAm catalysed reaction of L-glucoheptulose using the TAm encoded by pQR2191. However future work is needed in order to optimise the production in economic terms. A complete list of future work is outlined below:

- In terms of D-galacturonic acid upgrade with transketolase, as mentioned in Section 5.3.1., to date there are no commercial available standards for the 2,3,4,5,6,8-hexahydroxy-7-oxooctanoic acid. For this reason, future studies are needed in order to purify this molecule from the reaction mix or producing it by chemical synthesis. This would allow proper measurement of the reaction product and the exploration of its transamination.
- Future studies are needed in order to upgrade the polyalcohols obtained from L-arabinose and D-galacturonic acid to get the corresponding polyaminoalcohols, which are also important chiral molecules for the pharmaceutical industry.
- Optimisation of the synthesis of AHH optimisation is needed in order to improve the yield achieved in this work. This could involve further enzyme expression optimisation, bioconversion optimisation, kinetic parameters quantification or directed evolution.

- As seen in Section 3.4.2., H461Y TK has little affinity for the L-arabinose, which derives in slow reaction rates. It would be necessary to improve this affinity by the use of protein engineering in order to optimise time and resources in L-glucoheptulose production.
- Taking into account that H461Y TK could catalyse effectively L-arabinose and D-galacturonic acid, it would be interesting in terms of industry processes to assess the bio conversion of galactose, rhamnose and the other minor saccharides obtained from sugar beet pulp using either TK or other enzymes.
- Further research could be performed in order to find a different TK mutant for DGA bioconversion, for cases in which a specific bioconversion is preferred in SBP samples that could contain a mixture of L-arabinose and D-galacturonic acid.
- Future research is needed in order to set up and optimise the production of aminopolyols from L-arabinose and D-galacturonic acid by the coupling of TK and TAm.
- In terms of industry application, future work is needed for assessing TK and TAm bioconversion of the actual saccharification streams from sugar beet pulp, to evaluate the enzyme activity with two or more substrates in the same reaction mix.
- In order to take advantage of the use of pure TK, future work could be done for cloning the H461Y TK gene in another plasmid (in which overexpression of the enzyme could be constitutive) for avoiding the use of IPTG. Also, the optimisation of a purification method that does not include the use of Ni-NTA beads could be explored. Moreover, enzyme

reutilisation methods should be explored, as protein immobilisation techniques which also could improve enzyme stability.

- As Li-HPA is the most expensive substrate of the bioconversions studied on this work, future research is needed in order to produce this substrate via the utilisation of enzymes, or *in situ* during the bioconversion of interest.

8. REFERENCES

Abdul Halim, A., Szita, N. & Baganz, F., 2013. Characterization and multi-step transketolase-ω-transaminase bioconversions in an immobilized enzyme microreactor (IEMR) with packed tube. *Journal of Biotechnology*, 168(4), pp.567–575.

Adams, J.P. et al., 2010. *Practical Methods for Biocatalysis and Biotransformations (Chapter 1: Biotransformations in Small-Molecule Pharmaceutical Development)*.

Baud, D. et al., 2015. A rapid, sensitive colorimetric assay for the highthroughput screening of transaminases in liquid or solid-phase. *Chemistry Communications*, 51, pp.17225-17228.

Bawn, M. et al., 2018. One-pot, two-step transaminase and transketolase synthesis of L-glucoheptulosefrom L-arabinose. *Enzyme and Microbial Technology.*, 116, pp.16-22.

Birrel, J.A. & Jacobsen, E. N. 2013. A Practical Method for the Synthesis of Highly Enantioenriched trans-1,2-Amino Alcohols. *Organic Letters.*, 15(12), pp.2895-2897.

Berlowska, J. et al., 2015. A low-cost method for obtaining high-value bio-based propylene glycol from sugar beet pulp. *Royal Society of Chemistry Advances.*, 5(3), pp.2299–2304.

Board, M., et al., 1995. High Km Glucose-phosphorylating (Glucokinase) activities in a range of tumor Cell lines and Inhibition of Rates of Tumor Growth by the Specific Enzyme Inhibitor Mannoheptulose. *Cancer Research*, 55, pp.3278-3285.

British Sugar, 2011. *UK Beet Sugar Industry. Sustainability Report 2011*.

Brunhuber, N.M. & Blanchard, J.S., 1994. The biochemistry and enzymology of amino acid dehydrogenases. *Critical reviews in biochemistry and molecular biology*, 29(6), pp.415–467.

Bulos, B. & Handler, P., 1965. Kinetics of Beef Heart Glutamic-Alanine Transaminase. *The Journal of Biological Chemistry*, 240(8), pp.3283–3294.

Cardenas-Fernandez, M. et al., 2018. Continuous enzymatic hydrolysis of sugar beet pectin and L-arabinose recovery within an integrated biorefinery. *Bioresource Technology*, 269, pp.195–202.

Cardenas-Fernandez, M. et al., 2017. An integrated biorefinery concept for conversion of sugar beet pulp into value-added chemicals and pharmaceutical intermediates. *Faraday Discuss*, 202, pp.415-431.

Chamy, R. et al., 1994. Acid hydrolysis of sugar beet pulp as pretreatment for fermentation. *Bioresource Technology*, 50(2), pp.149–152.

Chang, T.M., 1988. Artificial Cells as Bioreactive Biomaterials. *Journal of Biomaterials Applications*, 3(July), pp.116–125.

Chen, B.H. et al., 2009. An efficient approach to bioconversion kinetic model generation based on automated microscale experimentation integrated with model driven experimental design. *Chemical Engineering Science*, 64(2), pp.403–409.

Chen, B.H. et al., 2006. Reaction modelling and simulation to assess the integrated use of transketolase and ω-transaminase for the synthesis of an aminotriol. *Biocatalysis and Biotransformation*, 24(6), pp.449–457.

Chen, H.M., Fu, X. & Luo, Z.G., 2015. Properties and extraction of pectin-enriched materials from sugar beet pulp by ultrasonic-assisted treatment combined with subcritical water. *Food Chemistry*, 168, pp.302–310.

Chi, Y., Scroggins, S.T. & Fréchet, J.M.J., 2008. One-pot multi-component asymmetric cascade reactions catalyzed by soluble star polymers with highly branched non-interpenetrating catalytic cores. *Journal of the American Chemical Society*, 130(20), pp.6322–6323.

Chou, I.C. & Voit, E.O., 2009. Recent developments in parameter estimation and structure identification of biochemical and genomic systems. *Mathematical Biosciences*, 219(2), pp.57–83.

Clark, J., Macquarrie, D. & Holland, H.L., 2002. Chapter 9 : Biocatalysis. , pp.188–205.

Coughlan, M.P. et al., 1986. Energy from Biomass : Saccharification of Beet Pulp Using Fungal Enzymes. *Annals of the New York Academy of Sciences*, 469, pp.294–303.

Dalby, P. et al., 2009. Protein and pathway engineering in biocatalysis. *Chimica Oggi*, 27, pp.10–21.

Demirjian, D.C., Shah, P.C. & Moris-Varas, F., 1999. Screening for Novel Enzymes. In F. W. Prof. Dr. Wolf-Dieter Fessner, A. Archelas, D. C. Demirjian, R. Furstoss, H. Griengl, K. -E. Jaeger, E. Morís-Varas, R. Öhrlein, M. T. Reetz, J.-L. Reymond, M. Schmidt, S. Servi, P. C. Shah, W. Tischer, ed. *Biocatalysis - From Discovery to Application*. Elsevier Ltd, pp. 1–29.

DiCosimo, R., McAuliffe, J., Poulose, A.J. & Bohlmann, G. 2013. Industrial use of immobilized enzymes. *Chemical Society Reviews*, 42, pp.6437-6474.

Dixon, M., 1953. The determination of enzyme inhibitor constants. *Biochemical Journal*, 55, pp.170–171.

Doig, S.D. et al., 2002. The use of microscale processing technologies for quantification of biocatalytic Baeyer-Villiger oxidation kinetics. *Biotechnology and Bioengineering*, 80(1), pp.42–49. Available at: http://doi.wiley.com/10.1002/bit.10344.

Down, J.E. & Riggs, D.S., 1965. A comparison of estimates of Michaelis-Menten kinetic constants from various linear transformations. *Journal of Biological Chemistry,* 240, pp.863–869.

Duetz, W. a. & Witholt, B., 2001. Effectiveness of orbital shaking for the aeration of suspended bacterial cultures in square-deepwell microtiter plates. *Biochemical Engineering Journal*, 7(2), pp.113–115.

Eisenthal, R., Cornish-Bowden, A., 1974. Direct linear plot—new graphical procedure for estimating enzyme kinetic-parameters. *Biochemical Journal*, 139, pp.715–720.

Ferrer, M., Martínez-Abarca, F. & Golyshin, P.N., 2005. Mining genomes and "metagenomes" for novel catalysts. *Current Opinion in Biotechnology*, 16(6), pp.588–593.

Findrik, Z., 2009. Overview on Reactions with Multi-enzyme Systems. *Chemical and Biochemical Engineering Quarte*, 23(4), pp.545–553.

Franssen, M.C.R., Kircher, M. & Wohlgemuth, R., 2010. Industrial Biotechnology in the Chemical and Pharmaceutical Industries. *Industrial Biotechnology: Sustainable Growth and Economic Success*, pp.323–350.

Frey, P.A. & Hegeman, A.D., 2006. *Enzymatic reaction mechanisms*. New York: Oxford University Press. pp.16–19.

Fu, a Y. et al., 1999. A microfabricated fluorescence-activated cell sorter. *Nature biotechnology*, 17(11), pp.1109–11.

Garfinkel, L., et al., 1977. Systems-analysis in enzyme-kinetics. *Critical Reviews in Bioengineering*, 2, pp.329–361.

Gasperini, C. & Ruggieri, S. 2012. Development of oral agent in the treatment of multiple sclerosis: how the first available oral therapy, fingolimod will change therapeutic paradigm approach. *Chemical Papers*, 62(5), pp.509–515.

Gigac, J., Fišerová, M. & Rosenberg, M., 2008. Improvement of paper strength via surface application of sugar beet pectin. *Drug Design, Development and Therapy*, 6, pp.175-186.

Gruber, P. et al, 2018. Enzymatic synthesis of chiral amino-alcohols by coupling transketolase and transaminase-catalyzed reactions in a cascading continuous-flow microreactor system. *Biotechnology and Bioengineering.*, 115, pp.586-596.

Gyamerah, M. & Willetts, A.J., 1997. Kinetics of overexpressed transketolase from *Escherichia coli* JM 107/pQR 700. *Enzyme Microbial Technology*, 20, pp.127-134.

Hailes, H.C., Dalby, P.A. & Lye, G.J., 2009. Biocatalytic approaches to ketodiols and aminodiols. *Chimica Oggi*, 27, pp.28–31.

Halim, M. et al., 2014. Microscale methods to rapidly evaluate bioprocess options for increasing bioconversion yields: Application to the ω-transaminase synthesis of chiral amines. *Bioprocess and Biosystems Engineering*, 37(5), pp.931–941.

Hamley-Bennett, C. et al., 2016. Selective fractionation of sugar beet pulp for release of fermentation and chemical feedstocks; optimisation of thermo-chemical pre-treatment. *Bioresource Technology,* 209, pp. 259–264..

Hanes C. S., 1932 Studies on plant amylases. I. The effect of starch concentration upon the velocity of hydrolysis by the amylase of germinated barley. *Biochemical Journal,* 26, pp.1406–1421.

Harris, T.K. & Keshwani, M.M., 2014. Measurement of Enzyme Activity. *Methods in Enzymology*, 463, pp.57–71.

Hibbert, E.G. et al., 2005. Directed evolution of biocatalytic processes. *Biomolecular Engineering*, 22(1-3), pp.11–19.

Hofstee B. H. J.,1952. On the evaluation of the constant-Vm and constant-Km in enzyme reactions. *Science*, 116, pp.329–331.

Hofstee B. H. J., 1959. Non-inverted versus inverted plots in enzyme kinetics. *Nature*, 184, pp.1296–1298.

Hyun, Y.L. & Davidson, V.L., 1995. Mechanistic studies of aromatic amine dehydrogenase, a tryptophan tryptophylquinone enzyme. *Biochemistry*, 34(3), pp.816–823.

Ingram, C.U. et al., 2006. One-Pot Synthesis of Amino-Alcohols Using a De-Novo Transketolase and β-Alanine: Pyruvate Transaminase Pathway in Escherichia Coli. *Biotechnology and Bioengineering*, 96(3), pp.559–569.

Jemli, S., Ayadi-Zouari, D., Ben Hilma, H. & Bejar, S. 2016. Biocatalysts: application and engineering for industrial purposes, Critical Reviews in Biotechnology. *Critical reviews in Biotechnology*, 36(2), pp.246–258.

Jiménez-González, C. & Woodley, J.M., 2010. Bioprocesses: Modeling needs for process evaluation and sustainability assessment. *Computers and Chemical Engineering*, 34(7), pp.1009–1017.

Kalaitzakis, D. & Smonou, I., 2010. A two-step, one-pot enzymatic synthesis of 2-substituted 1,3-diols. *Journal of Organic Chemistry*, 75(24), pp.8658–8661.

Kaulmann, U. et al., 2007. Substrate spectrum of ω-transaminase from Chromobacterium violaceum DSM30191 and its potential for biocatalysis. *Enzyme and Microbial Technology*, 41(5), pp.628–637.

King, E.L. & Altman, C., 1956. A Schematic Method of Deriving the Rate Laws for Enzyme-Catalyzed Reactions. *Journal of Physical Chemistry*, 60(10), pp.1375–1378.

König, S. et al., 1994. Specificity of coenzyme binding in Thiamine diphosphate-dependent enzymes. Crystal structures of yeast transketolase in complex with analogs of Thiamine diphosphate. *The Journal of Biological Chemistry*, 269, pp.10879–10882.

Koszelewski, D., Tauber, K., et al., 2010. Omega-Transaminases for the synthesis of non-racemic ??-chiral primary amines. *Trends in Biotechnology*, 28(6), pp.324–332.

Koszelewski, D., Göritzer, M., et al., 2010. Synthesis of optically active amines employing recombinant ω-transaminases in E. coli cells. *ChemCatChem*, 2(1), pp.73–77.

Krämer, S.D. & Testa, B., 2008. The Biochemistry of Drug Metabolism – An Introduction part 6. *Chemistry & Biodiversity*, 5(12), pp.2465–2578.

Kwon, S.J. & Ko, S.Y., 2002. Synthesis of statine employing a general syn-amino alcohol building block. *Tetrahedron Letters*, 43(4), pp.639–641.

Leijdekkers, a. G.M. et al., 2013. Enzymatic saccharification of sugar beet pulp for the production of galacturonic acid and arabinose; a study on the impact of the formation of recalcitrant oligosaccharides. *Bioresource Technology*, 128, pp.518–525.

Li, C. et al., 1993. Further purification and characterization of a multienzyme complex for DNA synthesis in human cells. *Journal of cellular biochemistry*, 53(4), pp.405–419.

Lin, G.Q., Zhang, J.G. & Cheng, J.F., 2011. Overview of Chirality and Chiral Drugs. *Chiral Drugs: Chemistry and Biological Action*, pp.3–28.

Lineweaver H, Burk D., 1934. The determination of enzyme dissociation constants. *Journal of the American Chemical Society*, 56, pp.658–666.

Lorilliere M. et al., 2017. One-pot, two-step cascade synthesis of naturally rare L-erythro (3S,4S) ketoses by coupling a thermostable transaminase and transketolase. *Green Chemistry.* 19, pp.425–435.

Lombardo, M.E. et al., 1989. Glutamate:4,5-dioxovaleric acid transaminase from Euglena gracilis. Kinetic studies. *European journal of biochemistry / FEBS*, 182(3), pp.657–660.

Lye, G.J. et al., 2003. Accelerated design of bioconversion processes using automated microscale processing techniques. *Trends in Biotechnology*, 21(1), pp.29–37.

Martinez-Torres, R.J., 2008. *Characterisation of the structural stability of transketolase under biocatalytically relevant conditions*. University College London.

Matosevic, S., Szita, N. & Baganz, F., 2011. Fundamentals and applications of immobilized microfluidic enzymatic reactors. *Journal of Chemical Technology and Biotechnology*, 86(3), pp.325–334.

McArthur IV, G.H. & Fong, S.S., 2010. Toward engineering synthetic microbial metabolism. *Journal of Biomedicine and Biotechnology*, 2010.

Mehta, P.K. & Christen, P., 1994. Homology of 1-aminocyclopropane-1-carboxylate synthase, 8-amino-7-oxononanoate synthase, 2-amino-6-caprolactam racemase, 2,2-dialkylglycine decarboxylase, glutamate-1-semialdehyde 2,1-aminomutase and isopenicillin-N-epimerase with aminotransferases. *Biochemical and Biophysical Research Communications*, 198(1), pp.138–143.

Mehta, P.K., Hale, T.I. & Christen, P., 1993. Aminotransferases: demonstration of homology and division into evolutionary subgroups. *European journal of biochemistry / FEBS*, 214(2), pp.549–561.

Meyer, A., Pellaux, R. & Panke, S., 2007. Bioengineering novel in vitro metabolic pathways using synthetic biology. *Current Opinion in Microbiology*, 10(3), pp.246–253.

Micard, V., Renard, C.M.G.C. & Thibault, J.F., 1996. Enzymatic saccharification of sugar-beet pulp. *Enzyme and Microbial Technology*, 19(3), pp.162–170.

Micheletti, M. et al., 2006. Fluid mixing in shaken bioreactors: Implications for scale-up predictions from microlitre-scale microbial and mammalian cell cultures. *Chemical Engineering Science*, 61(9), pp.2939–2949.

Micheletti, M. & Lye, G.J., 2006. Microscale bioprocess optimisation. *Current Opinion in Biotechnology*, 17(6), pp.611–618.

Mitra, R.K. & Woodley, J.M., 1996. A useful assay for transketolase in asymmetric syntheses. *Biotechnology Techniques*, 10(3), pp.167–172.

Morris, K.G. et al., 1996. Transketolase from Escherichia coli: A practical procedure for using the biocatalyst for asymmetric carbon-carbon bond synthesis. *Tetrahedron Asymmetry*, 7(8), pp.2185–2188.

Muller, Y. a et al., 1993. A thiamin diphosphate binding fold revealed by comparison of the crystal structures of transketolase, pyruvate oxidase and pyruvate decarboxylase. *Structure (London, England : 1993)*, 1(2), pp.95–103.

Murzin, D., 2008. Sustainable Chemical Technology Through Catalytic Multistep Reactions. *Chemical Engineering Research and Design*, 86, pp.1002–1010.

Miyake, Y. et al., 1995. Serine palmitoyltransferase is the primary target of a sphingosine-like immunosupressant, ISP-1/Myriocin. *Biochemical and Biophysical Research Communications*, 211 (2), pp.396-403.

Panke, S., Held, M. & Wubbolts, M., 2004. Trends and innovations in industrial biocatalysis for the production of fine chemicals. *Current Opinion in Biotechnology*, 15(4), pp.272–279.

Patel, R.N., 2018. Biocatalysis for synthesis of pharmaceuticals. *Bioorganic and Medicinal Chemistry*, 26, pp.1252-1274.

Patel, R.N., 2001. Biocatalytic synthesis of intermediates for the synthesis of chiral drug substances. *Current Opinion in Biotechnology*, 12(6), pp.587–604.

Pohl, M., Sprenger, G. a. & Müller, M., 2004. A new perspective on thiamine catalysis. *Current Opinion in Biotechnology*, 15(4), pp.335–342.

Pollard, D.J. & Woodley, J.M., 2007. Biocatalysis for pharmaceutical intermediates: the future is now. *Trends in Biotechnology*, 25(2), pp.66–73.

Puri, D., 2002. Textbook of Medical Biochemistry, 3rd Ed., *Elsevier*. pp.111–114.

Ranaldi, F. et al., 1999. What students must knoow about the determination of enzyme kinetic parameters. *Biochemical Education*, 29, pp.87–91.

Richard, J.P. et al., 2011. The PLP cofactor: Lessons from studies on model reactions. *Biochimica et Biophysica Acta - Proteins and Proteomics*, 1814(11), pp.1419–1425. Available at: http://dx.doi.org/10.1016/j.bbapap.2010.12.007.

Rios-Solis, L. et al., 2011. A toolbox approach for the rapid evaluation of multi-step enzymatic syntheses comprising a “mix and match” E. coli expression system with microscale experimentation, 29(May), pp.192–203.

Rios-Solis, L., 2012. *Microscale evaluation of De Novo Engineered whole cell Biocatalysts*. University College London.

Rios-Solis, L. et al., 2015. Modelling and optimisation of the one-pot, multi-enzymatic synthesis of chiral amino-alcohols based on microscale kinetic parameter determination. *Chemical Engineering Science*, 122(June 2014), pp.360–372.

Rios-Solis, L. et al., 2013. Non-linear kinetic modelling of reversible bioconversions: Application to the transaminase catalyzed synthesis of chiral amino-alcohols. *Biochemical Engineering Journal*, 73, pp.38–48.

Santacoloma, P.A., 2011. Multienzyme-Catalyzed Processes : Next-Generation Biocatalysis Abstract (5), pp.203–212.

Schmid, a et al., 2001. Industrial biocatalysis today and tomorrow. *Nature*, 409(6817), pp.258–268.

Schulze, B. & Wubbolts, M.G., 1999. Biocatalysis for industrial production of fine chemicals, *Current Opinion in Biotechnology,* 10, pp.609–615.

Sehl, T. et al., 2015. Multi-step synthesis strategies towards 1,2-amino alcohols withspecial emphasis on phenylpropanolamines. *Journal of Molecular Catalysis B: Enzymatic*, 114, pp.65-71.

Sheldon, R. A., 2007. Enzyme immobilization: The quest for optimum performance. *Advanced Synthesis and Catalysis*, 349(8-9), pp.1289–1307.

Sheldon, R.A., 2008. Enzyme - Catalyzed Cascade Reactions. In E. Garcia-Junceda, ed. *Multi-Step Enzyme Catalysis: Biotransformations and Chemoenzymatic Synthesis*. Wiley.

Shin, J.S. & Kim, B.G., 1999. Asymmetric synthesis of chiral amines with omega-transaminase. *Biotechnology and bioengineering*, 65(2), pp.206–211.

Shin, J.S. & Kim, B.G., 2001. Comparison of the omega-transaminases from different microorganisms and application to production of chiral amines. *Bioscience, biotechnology, and biochemistry*, 65(8), pp.1782–1788.

Shin, J.S. & Kim, B.G., 2002. Exploring the active site of amine:pyruvate aminotransferase on the basis of the substrate structure-reactivity relationship: How the enzyme controls substrate specificity and stereoselectivity. *Journal of Organic Chemistry*, 67(9), pp.2848–2853.

Sin, G., Woodley, J.M. & Gernaey, K. V., 2009. Application of modeling and simulation tools for the evaluation of biocatalytic processes: A future perspective. *Biotechnology Progress*, 25(6), pp.1529–1538.

Smith, M. et al., 2010. A Multidisciplinary Approach Toward the Rapid and Preparative-Scale Biocatalytic Synthesis of Chiral Amino Alcohols: A Concise Transketolase-/omega-Transaminase-Mediated Synthesis of (2S,3S)-2-Aminopentane-1,3-diol.*Organic Process Research and Development*, 14(1), pp.99–107.

Smith, M. a., King, P.J. & Grimm, B., 1998. Transient-state kinetic analysis of Synechococcus glutamate 1- semialdehyde aminotransferase. *Biochemistry*, 37(1), pp.319–329.

Smithies, K. et al., 2009. Stereoselectivity of an ω-transaminase-mediated amination of 1,3-dihydroxy-1-phenylpropane-2-one. *Tetrahedron Asymmetry*, 20(5), pp.570–574.

Soetaert, W. & Vandamme, E.J., 2010. The Scope and Impact of Industrial Biotechnology. *Industrial Biotechnology*, pp.1–16.

Spagnuolo, M. et al., 1997. Synergistic effects of cellulolytic and pectinolytic enzymes in degrading sugar beet pulp. *Bioresource Technology*, 60(3), pp.215–222.

Sprenger, G. A., Schörken, U., Sprenger, G. & Sahm, H., 1995. Transketolase A of *Escherichia coli* K12. Purification and properties of the enzyme from recombinant strains. *European Journal of Biochemistry*, 230, pp.525-532.

Sprenger, G. A. & Pohl, M., 1999. Synthetic potential of thiamin diphosphate-dependent enzymes. *Journal of Molecular Catalysis B: Enzymatic*, 6(3), pp.145–159.

Stahl, S., Greasham, R. & Chartrain, M., 2000. Implementation of a rapid microbial screening procedure for biotransformation activities. *Journal of Bioscience and Bioengineering*, 89(4), pp.367–371.

Stewart, J.D., 2001. Dehydrogenases and transaminases in asymmetric synthesis. *Current Opinion in Chemical Biology*, 5(2), pp.120–129.

Stitt, M. et al., 2002. Steps towards an integrated view of nitrogen metabolism. *Journal of experimental botany*, 53(370), pp.959–970.

Straathof, A.J., Panke, S. & Schmid, A., 2002. The production of fine chemicals by biotransformation. *Current opinion in biotechnology*, 13, pp.548–556.

Subrizi, F. et al, 2016. Transketolase catalysed upgrading of L-arabinose: the one-step stereoselective synthesis of L-glucoheptulose. *Green Chemistry*, 18, pp.3158-3165.

Subrizi, F. et al, 2019. Aminopolyols from Carbohydrates: Amination of Sugars and Sugar-Derived Tetrahydrofurans with Transaminases. *Angewandte Chemie*, 131, pp.3894-3898.

Suhartini, S., Heaven, S. & Banks, C.J., 2014. Comparison of mesophilic and thermophilic anaerobic digestion of sugar beet pulp: Performance, dewaterability and foam control. *Bioresource Technology*, 152, pp.202–211.

Tao, J., Zhao, L. & Ran, N., 2007. Recent advances in developing chemoenzymatic processes for active pharmaceutical ingredients. *Organic Process Research and Development*, 11(2), pp.259–267.

Taylor, P.P. et al., 1998. Novel biosynthetic approaches to the production of unnatural amino acids using transaminases. *Trends in Biotechnology*, 16(10), pp.412–418.

Tufvesson, P., Lima-Ramos, J., Norblad, M. & Woodley, J.M., 2011. Guidelines and Cost Analysis for Catalyst Production in Biocatalytic Processes. *Organic Process Research & Development*, 15, pp.266-274.

Tyo, K.E., Alper, H.S. & Stephanopoulos, G.N., 2007. Expanding the metabolic engineering toolbox: more options to engineer cells. *Trends in Biotechnology*, 25(3), pp.132–137.

Velez, A. M., et al., 2013. Enhanced production of recombinant thermo-stable lipase in Escherichia coli at high induction temperature, *Protein Expression and Purification*, 90, pp.96-103.

Wang, J. & Lu, W., 2011. CHIRAL DRUGS VIA BIOCATALYTICAL APPROACHES.

Waschke, D., et al., 2012. Synthesis of Fluorinated Ketoheptoses as Specific Diagnostic Agents, *European Journal of Organic Chemustry*, 2012, pp.948-959.

Werpy, T. & Petersen, G., 2004. *Top Value Added Chemicals from Biomass Volume I — Results of Screening for Potential Candidates from Sugars and Synthesis Gas Top Value Added Chemicals From Biomass Volume I: Results of Screening for Potential Candidates*, Tech. Rep. U.S. Department of Energy.

Wilkinson, G. N., 1961. Statistical identifications in enzyme kinetics. *Biochemical Journal,* 80, pp.324–332.

Wikner C., U. Nilsson, L. Meshalkina, C. Udekwu, Y. Lindqvist, and G. Schneider.1997. Identification of catalytically important residues in yeast transketolase. *Biochemistry*. 36:15643-9.

Wohlgemuth, R., 2010. Biocatalysis—key to sustainable industrial chemistry. *Current Opinion in Biotechnology*, 21(6), pp.713–724.

Woodley, J.M., 2006. Choice of biocatalyst form for scalable processes. *Biochemical Society transactions*, 34(Pt 2), pp.301–303.

Woodley, J.M., 2008. New opportunities for biocatalysis: making pharmaceutical processes greener. *Trends in Biotechnology*, 26(6), pp.321–327.

Wu, Q. & Tao, J., 2012. Biocatalysis. In W. Zhang & C. J. Berkeley W., eds. *Green Techniques for Organic Synthesis and Medical Chemistry.* John Wiley & Sons, Ldt.

Yilmaz, E., 2014. Assessment of the role of agricultural wastes in aggregate formation and their stability. *Journal of Environmental Management*, 144, pp.93–100.

Zhang, L. et al., 2014. Emulsification properties of sugar beet pectin after modification with horseradish peroxidase. *Food Hydrocolloids*, 43, pp.107–113.

Zheng, Y. et al., 2013. Dilute acid pretreatment and fermentation of sugar beet pulp to ethanol. *Applied Energy*, 105, pp.1–7.

Ziemiński, K. et al., 2014. Effects of hydrothermal pretreatment of sugar beet pulp for methane production. *Bioresource Technology*, 166, pp.187–193.

APPENDIX I: Calibration plot of biomass as a function of OD_{600} absorbance

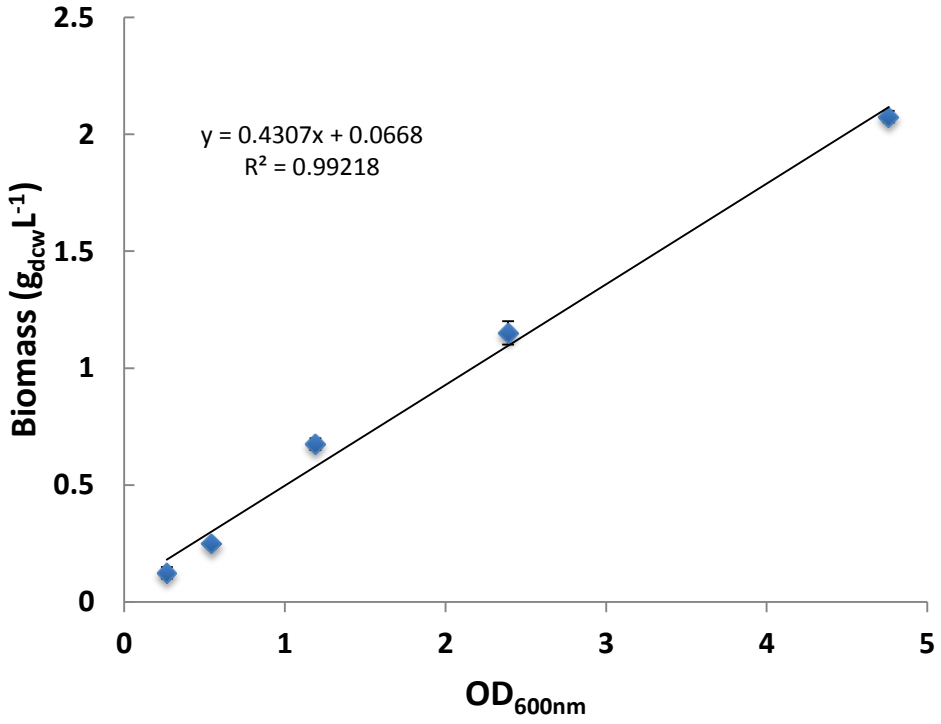

Figure A1. Calibration curve of *E.* coli biomass concentration (dry cell weight) as a function of OD_{600nm}. Assay was performed as described in Section 2.7.1. Error bars represent one standard deviation about the mean (n=3). Solid line was fitted by linear regression (R^2=0.992).

APPENDIX II: Calibration plot of BSA concentration as a function of OD_{600} absorbance

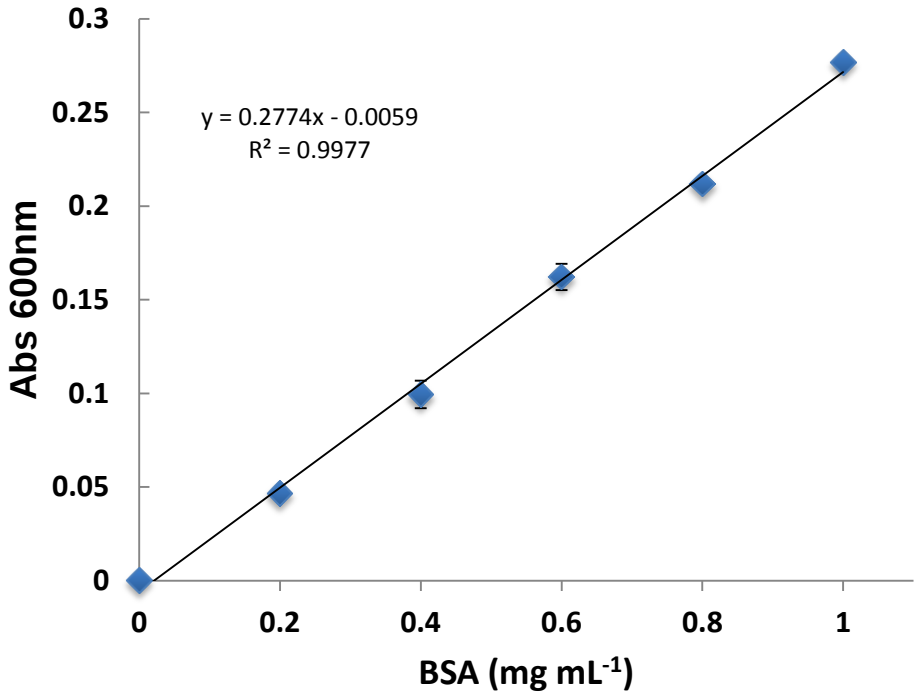

Figure A2. Calibration curve of BSA as a function of OD_{600nm}. Assay was performed as described in Section 2.7.2. Error bars represent one standard deviation about the mean (n=3). Solid line was fitted by linear regression (R^2=0.998).

APPENDIX III: Densitometry assay calibration plot

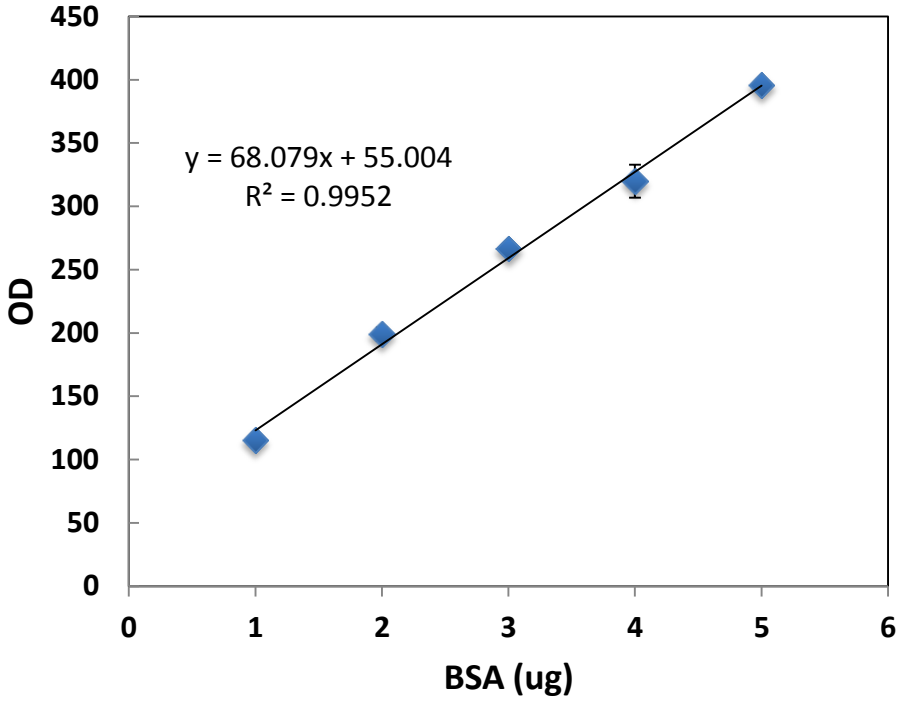

Figure A3. Calibration curve of BSA concentration as a function of optical density. Assay was performed as described in Section 2.7.4. Error bars represent one standard deviation about the mean (n=3). Solid line was fitted by linear regression (R^2=0.995).

APPENDIX IV: Sample HPLC chromatograms for analysis of L-arabinose bioconversion kinetics

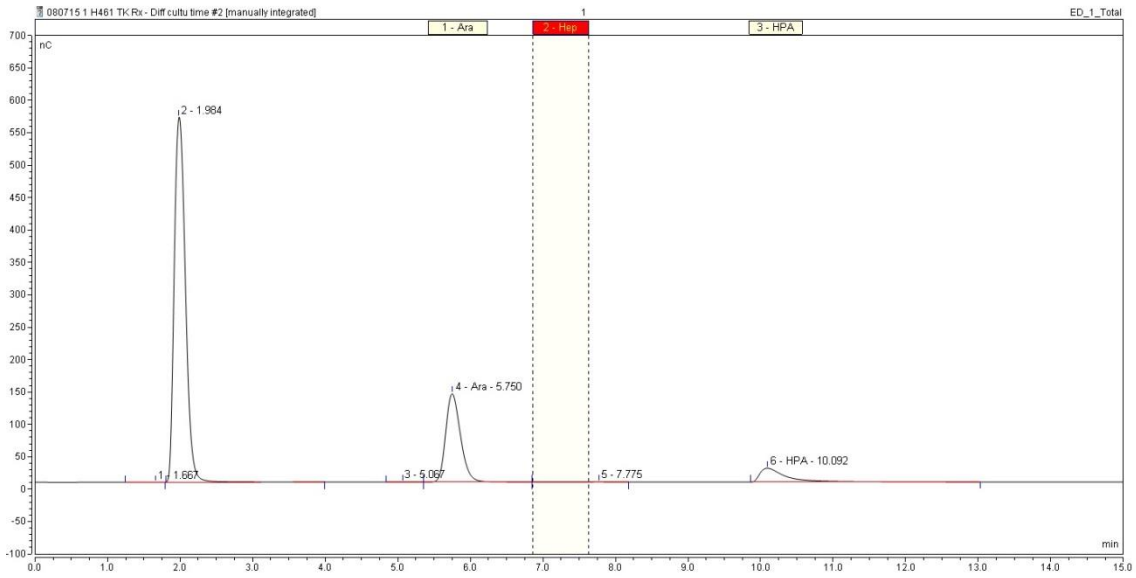

Figure A4.1. Chromatogram of a sample taken at time zero of bioconversion of L-arabinose to L-glucoheptulose. Bioconversion was performed as described in Section 2.4, and HPLC analysis is described in Section 2.7.5. Retention times are 5.75 min, 7.78 min and 10.09 min for L-arabinose, L-glucoheptulose and HPA respectively.

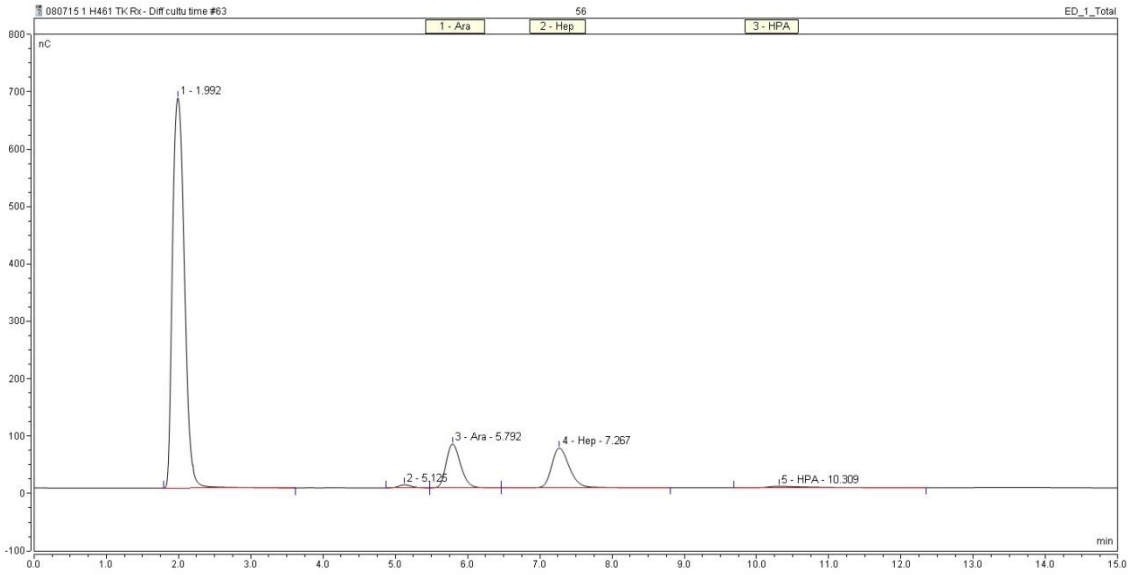

Figure A4.2. Chromatogram of a sample taken at 48 hours of bioconversion of L-arabinose to L-glucoheptulose. Bioconversion was performed as described in Section 2.4, and HPLC analysis is described in Section 2.7.5. Retention times are 5.75 min, 7.78 min and 10.09 min for L-arabinose, L-glucoheptulose and HPA respectively.

APPENDIX V: HPLC calibration curves for quantification of L-arabinose bioconversion kinetics

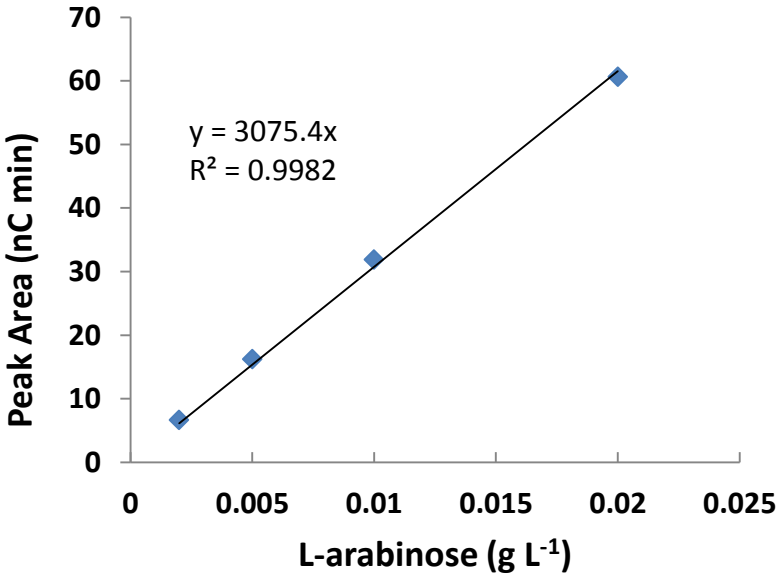

Figure A5.1. Calibration curve of L-arabinose in function of peak area for quantification by HPLC analysis (See Section 2.7.5). Solid line was fitted by linear regression (R^2=0.998).

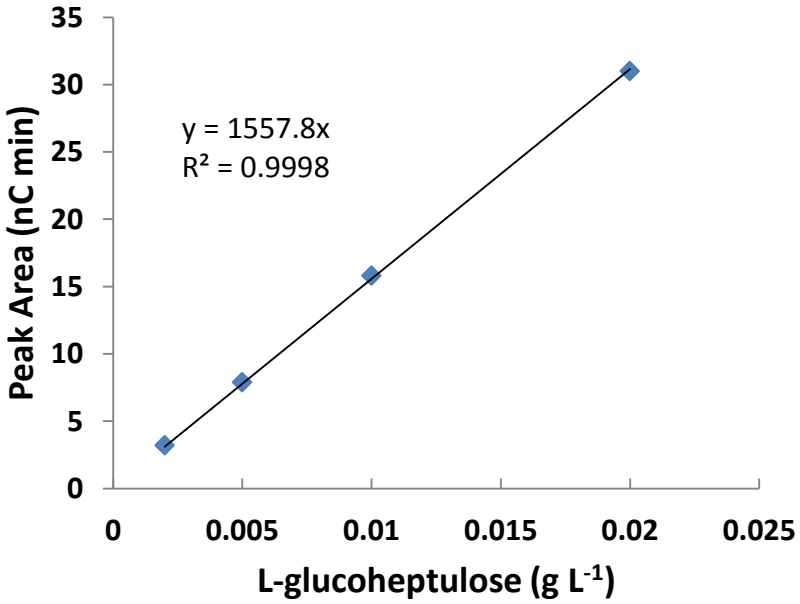

Figure A5.2. Calibration curve of L-glucoheptulose in function of peak area for quantification by HPLC analysis (See Section 2.7.5). Solid line was fitted by linear regression (R^2=0.999).

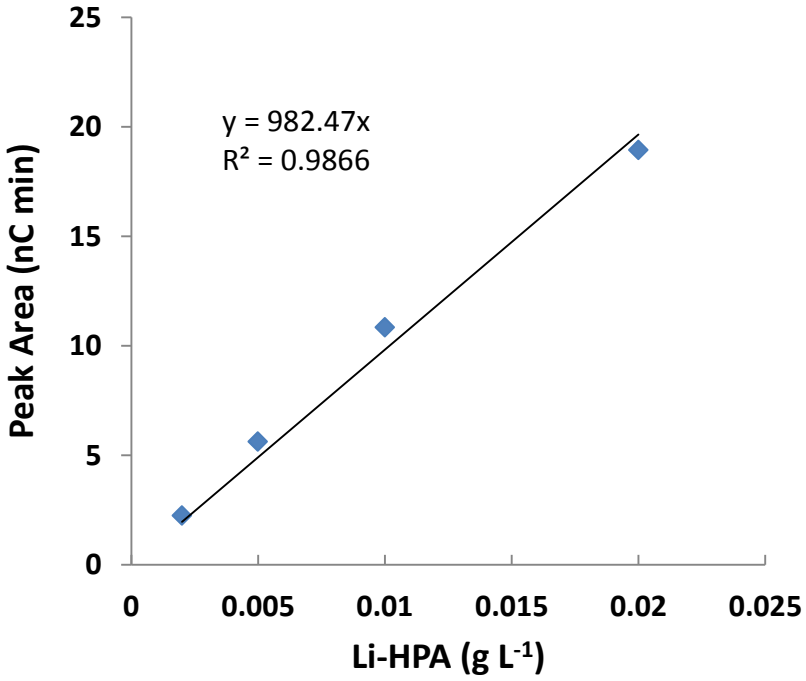

Figure A5.3. Calibration curve of Li-HPA in function of peak area for quantification by HPLC analysis (See Section 2.7.5). Solid line was fitted by linear regression (R^2=0.987).

APPENDIX VI: HPLC calibration curves for quantification of D-galacturonic acid bioconversion kinetics

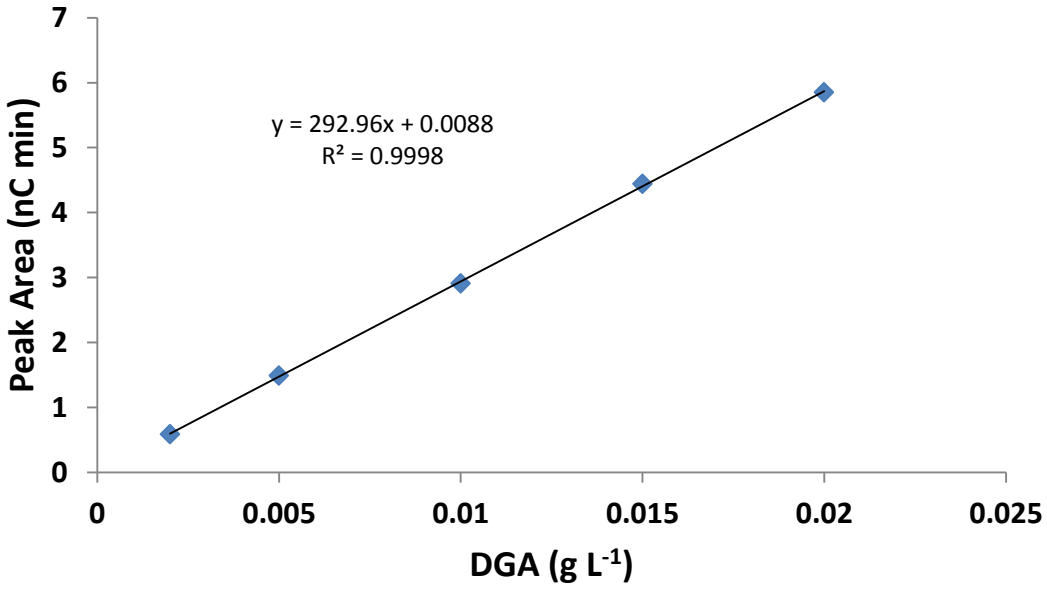

Figure A6.1. Calibration curve of DGA as a function of peak area for quantification by HPLC analysis (See Section 2.7.5). Solid line was fitted by linear regression (R^2=0.9998).

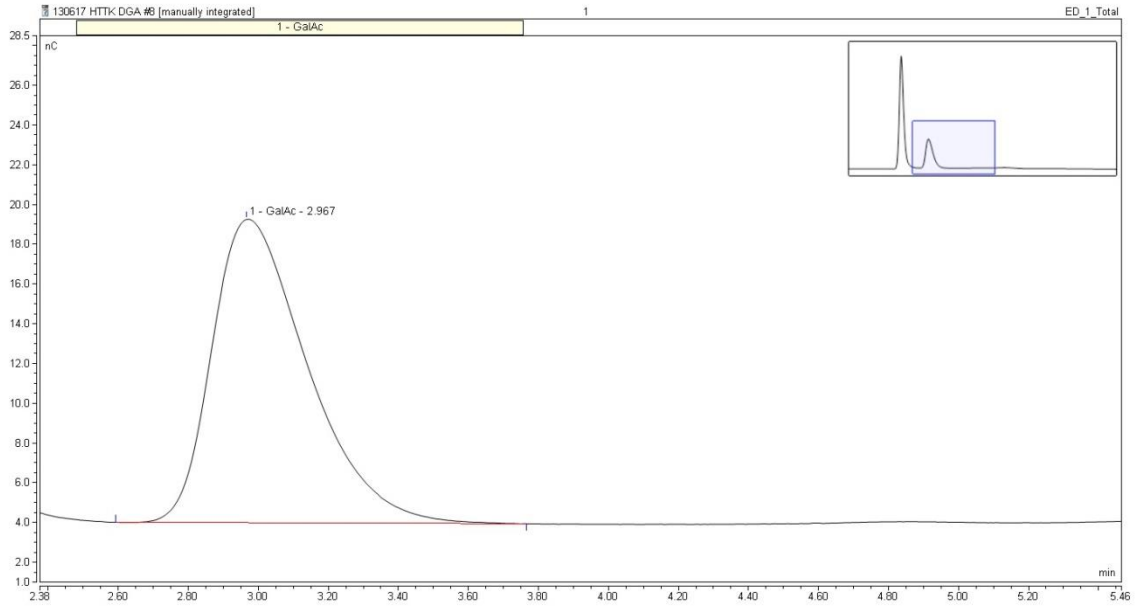

Figure A6.2. Chromatogram of a sample taken at time zero of bioconversion of DGA to OOA. Bioconversion was performed as described in Section 2.4.2, and HPLC analysis is described in Section 2.7.5.2. Retention time is 2.97 min for OOA.

APPENDIX VII: MatLab Code for Kinetic Parameters Estimation

In order to apply the procedure illustrated in Figure 3.10, a code was developed using MatLab software (MathWorks, Natick, MA, USA), for automatically perform all the non-linear regressions required for obtaining the kinetic parameters. The complete programme is reported below.

```
function ParaEst

close all;


format bank;

% Intial setup
NumDataSet = 10;                          % Number of
progress curves
NumSample(1:NumDataSet) = [13 13 13 13 13 13 13 13 13
13];


Data_Filename1 = 'InhibitionCurve'
Data_Filename2 = 'ProgressCurvesUpdated';
Result_File = 'Result';



% Call the programmes in the software
Result_Filename = strcat(Result_File,'.xls');

[Theta0, Theta] =
PE3(NumDataSet,NumSample,Data_Filename1,Data_Filename2
,Result_Filename);
```

```
StringTitle =
{'Kcat(1/min)','Ka(mM)','Kb(mM)','Kib(mM)','Kia(mM)','
Kiq(mM)'; ...
    Theta(1) Theta(2) Theta(3) Theta(4) Theta(5)
Theta(6)};

String1 = {'Initial'};
String2 = {'Final'};

xlswrite(Result_Filename,
StringTitle,'Parameters','D4');
xlswrite(Result_Filename, String1,'Parameters','C5');
xlswrite(Result_Filename, String2,'Parameters','C6');
xlswrite(Result_Filename, Theta0,'Parameters','D5');
xlswrite(Result_Filename, Theta, 'Parameters','D6');

------------------------------------------------------------
---

function Theta = PE1(Data_Filename)


% Intial setup
% Parameter Estimation
    Theta0 = [3.11 0.17 189.99];     % Initial values
for Kcat, Ka and Kb
    LB = [1 1 1];             % Lower bound
    UB = [50 50 50];      % upper bound

% Read experimental data
Data = xlsread(Data_Filename);

    CHPA = Data(:,1);
    CGA  = Data(:,2);
    Rate = Data(:,3);
    Ei   = Data(1,4);

    [NumSample,~] = size(CHPA);

% options group for different optimisers
    foptions =
optimset('Display','iter','MaxIter',2000);

    [Theta,~]= fmincon(@(x)
ObjFunc(x,CHPA,CGA,Rate,Ei,NumSample),Theta0,[],[],[],
[],LB,UB,[],foptions);

% ======== Objective Function ========
function Func = ObjFunc(C,CHPA,CGA,RateE,Ei,NumSample)
```

```
A = 0.0;

for I = 1:NumSample
    y = [CHPA(I) CGA(I)];
    RateC(I)= Kinetics(y,C,Ei);

    A = A + (RateC(I)-RateE(I))^2;

end % for I

Func = A;

% ========  Kinetics Model ========
function R = Kinetics(y,Para,Ei)
% Simplified (no inhibition terms) kinetic model

    Kcat = Para(1);        % Rate constant   [1/min]
    Ka  = Para(2);         % Michaelis constant of HPA
[mM]
    Kb  = Para(3);         % Michaelis constant of ARA
[mM]

% y(1) -- HPA concentration
% y(2) -- GA  concentration

    Vmax = Kcat*Ei;
    V = Kb*y(1)+Ka*y(2)+y(1)*y(2);
    R = Vmax*y(1)*y(2)/V;

 ------------------------------------------------------
----

function Theta =
PE2(NumDataSet,NumSample,NumPara,RatePara,Data_Filenam
e)


% Read experimental data
Data = xlsread(Data_Filename);

for I = 1:NumDataSet
    for J = 1:NumSample(I)
        Ei(I) = Data((I-1)*NumSample(I)+J,5);
        Time(I,J) = Data((I-1)*NumSample(I)+J,1);
        CHPA(I,J) = Data((I-1)*NumSample(I)+J,2);
        CGA(I,J)  = Data((I-1)*NumSample(I)+J,3);
        CERY(I,J) = Data((I-1)*NumSample(I)+J,4);
    end
end
```

```
Lstep = 1;

% Initial values for parameters
    Theta0(1:NumPara) =1000; %[32.01 2.863 1449.2 1 1
1];
    LB(1:NumPara) = 0.01;
    UB(1:NumPara) = 80000;

% Finding optimum parameters

    options =
optimset('Display','iter','MaxFunEvals',2000); %
,'MaxIter', 10);
    [Theta,~]= fmincon(@(x)
ObjFunc(x,Time,CHPA,CGA,CERY,Ei,NumDataSet,NumSample,R
atePara),Theta0,[],[],[],[],LB,UB,[],options);

% ================== Objective Function
==================
function Func =
ObjFunc(C,Time,CHPA,CGA,CERY,Ei,NumDataSet,NumSample,R
atePara)

Lstep = 1;

F = 0.0;
A(NumDataSet) = 0.0;

for I = 1:NumDataSet
    tspan = [0:Lstep:Time(I,NumSample(I))];
    Y0 = [CHPA(I,1),CGA(I,1),CERY(I,1)];

    sol =ode45(@(t,y)
TKKine2(t,y,C,Ei(I),RatePara),tspan,Y0);
    Y = deval(sol,Time(I,:));

    for J = 1:NumSample(I)
        EHPA(J) = (Y(1,J)-CHPA(I,J))^2;
        EGA(J)  = (Y(2,J)-CGA(I,J))^2;
        EERY(J) = (Y(3,J)-CERY(I,J))^2;
        A(I) = A(I) + EHPA(J) + EGA(J) + EERY(J);
    end % for J

    F = F + A(I);
end % for I

Func = F;
return
```

```
-----------------------------------------------------------------------------------------------
-----

function [Theta0, Theta] = PE3(NumDataSet,NumSample,
...
    Data_Filename1,Data_Filename2,Result_Filename)

close all

% Intial setup
NumPara2 = 3;          % Number of parameter to be
estimated (for Ki)
NumPara3 = 6;          % Number of parameter to be
estimated (for complete model)
NumComponent = 3;      % Number of Reaction component,
here is HPA, GA, ERY
NumPara= 6;
Theta1 = PE1(Data_Filename1);
RatePara = Theta1;

Theta2 =
PE2(NumDataSet,NumSample,NumPara2,RatePara,Data_Filena
me2);

Theta0 = double(int16([Theta1 Theta2]));

Lstep = 1;

% Read experimental data
Data = xlsread(Data_Filename2);

for I = 1:NumDataSet
    for J = 1:NumSample(I)
        Time(I,J) = Data((I-1)*NumSample(I)+J,1);
        CHPA(I,J) = Data((I-1)*NumSample(I)+J,2);
        CGA(I,J)  = Data((I-1)*NumSample(I)+J,3);
        CERY(I,J) = Data((I-1)*NumSample(I)+J,4);
        Ei(I)     = Data((I-1)*NumSample(I)+J,5);
    end
end

for I = 1:NumDataSet
    Conc(I,1,:) = CHPA(I,:);
    Conc(I,2,:) = CGA(I,:);
    Conc(I,3,:) = CERY(I,:);
end

% Initial values for parameters
```

```
    LB(1:NumPara3) = [1 1 1 1 1 1];
    UB(1:NumPara3) = [800 800 800 800 800 800];
% Finding optimum parameters
    psoptions =
psoptimset('Display','iter','MaxIter',200000,'MaxFunEv
als', 2000000);

%    [Theta01,Func]= ...
%       patternsearch(@(x)
ObjFunc(x,Ei,Time,Conc,NumDataSet,...
%
NumComponent,NumSample),Theta0,[],[],[],[],LB,UB,[],ps
options);

    Theta001 = Theta0;
    options =
optimset('Display','iter','MaxFunEvals',2000,'tolfun',
10E-15,'tolx',10E-15); % ,'MaxIter', 10);
    [Theta,~]= fmincon(@(x)
ObjFunc(x,Ei,Time,Conc,NumDataSet,NumComponent,NumSamp
le),Theta001,[],[],[],[],LB,UB,[],options);

% ======== Plotting the result comparison ========
NC = Theta;
Lstep = 1;

for I = 1:NumDataSet
    tspan = [0:Lstep:Time(I,NumSample(I))];
    Y0 = [CHPA(I,1),CGA(I,1),CERY(I,1)];

    [t,y] =ode45(@(t,y)
TKKine3(t,y,NC,Ei(I)),tspan,Y0);

    figure(I)
    plot(Time(I,:),CHPA(I,:),'ro','LineWidth',2)
    hold on
    plot(Time(I,:),CGA(I,:),'md','LineWidth',2)
    plot(Time(I,:),CERY(I,:),'bs','LineWidth',2)
    plot(t,y(:,1),'r-','LineWidth',2)
    plot(t,y(:,2),'m-','LineWidth',2)
    plot(t,y(:,3),'b-','LineWidth',2)
    hold off

    xlabel('Time (min)','fontsize',14,
'fontweight','bold')
    ylabel('Concentration (mM)','fontsize',14,
'fontweight','bold')
```

```
    set(gca, 'fontsize',14, 'fontweight','bold',
'LineWidth',2);
    legend('HPA','ARA','GLU','Location','best');

%    for J = 1:NumSample
%        fprintf(fid, '%6.2f %12.8f %12.8f %12.8f
%12.8f\n', ...
%
Time(I,J),YY(1,J),YY(2,J),YY(3,J),YY(4,J));
%    end
end

% Write experiment data, model prediction and
residuals into data file
for I = 1:NumDataSet
    tspan = [0:Lstep:Time(I,NumSample(I))];
    Y0 = [CHPA(I,1),CGA(I,1),CERY(I,1)];

    sol =ode113(@(t,y)
TKKine3(t,y,NC,Ei(I)),tspan,Y0);
    Y = deval(sol,Time(I,:));

    Residual1(I,:) = CHPA(I,:) - Y(1,:);
    Residual2(I,:) = CGA(I,:)  - Y(2,:);
    Residual3(I,:) = CERY(I,:) - Y(3,:);

    for J = 1:NumSample(I)
        T1(J+(I-1)*NumSample(I)) = Time(I,J);
        C1(J+(I-1)*NumSample(I)) = CHPA(I,J);
        Y1(J+(I-1)*NumSample(I)) = Y(1,J);
        R1(J+(I-1)*NumSample(I)) = Residual1(I,J);

        C2(J+(I-1)*NumSample(I)) = CGA(I,J);
        Y2(J+(I-1)*NumSample(I)) = Y(2,J);
        R2(J+(I-1)*NumSample(I)) = Residual2(I,J);

        C3(J+(I-1)*NumSample(I)) = CERY(I,J);
        Y3(J+(I-1)*NumSample(I)) = Y(3,J);
        R3(J+(I-1)*NumSample(I)) = Residual3(I,J);
    end
end% I

StringMatrix = {'Time', 'HPA-E', 'HPA-P', 'Residual-
1', 'GA-E', ...
    'GA-P', 'Residual-2', 'ERY-E',  'ERY-P',
'Residual-3'};

xlswrite(Result_Filename,StringMatrix,'Comparison','A1
');
```

```
DataMatrix = [T1;C1;Y1;R1;C2;Y2;R2;C3;Y3;R3]';

xlswrite(Result_Filename,
DataMatrix,'Comparison','A2');

% ================== Objective Function
==================
function Func = ObjFunc(CC,Ei,Time,Conc, ...
                        NumDataSet,NumResp,NumSample)

Lstep = 1;

F = 0.0;
MaxNum = max(NumSample(1:NumDataSet));
A(1:MaxNum) = 0.0;

for I = 1:NumDataSet
    tspan = [0:Lstep:Time(I,NumSample(I))];
    Y0(1:NumResp+1) = [Conc(I,1:NumResp,1) 1];
    YExp(:,:) = Conc(I,:,:);

    sol =ode45(@(t,y) TKKine3(t,y,CC,Ei(I)),tspan,Y0);
    Y = deval(sol,Time(I,:));

    for K = 1:NumResp
        for J = 1:NumSample(I)
            A(K) = A(K)+((YExp(K,J)-Y(K,J)))^2;
        end % for J
    end % for K

end % for I

%F = 0.0;
for I = 1:NumResp
    F = F + A(I);
end % for

Func = F;
return
```

APPENDIX VIII: Model Predictions and Residuals from Kinetic Parameter Estimation

A) Model predictions and residuals from the kinetic parameter estimation of the bioconversion of L-arabinose and Li-HPA to L-glucoheptulose using lysate as biocatalyst.

Where:

- HPA-E and HPA-P are the experimental and predicted Li-HPA concentrations, respectively.
- ARA-E and ARA-P are the experimental and predicted L-arabinose concentrations, respectively.
- GLU-E and GLU-P are the experimental and predicted L-glucoheptulose concentrations, respectively.
- Residuals (R1, R2, and R3) are the difference between predicted and experimental values.

	Time (min)	HPA-E	HPA-P	R1	ARA-E	ARA-P	R2	GLU-E	GLU-P	R3
Curve 1	0	85.744	85.744	0.000	31.635	31.635	0.000	0.000	0.000	0.000
	120	84.156	83.972	0.184	30.047	29.863	0.184	1.588	1.772	-0.184
	240	82.843	82.301	0.541	28.734	28.192	0.541	2.902	3.443	-0.541
	360	81.731	80.726	1.005	27.622	26.616	1.005	4.013	5.019	-1.005
	480	80.569	79.239	1.330	26.460	25.130	1.330	5.175	6.506	-1.330
	600	79.351	77.835	1.516	25.242	23.726	1.516	6.393	7.909	-1.516
	720	78.582	76.510	2.073	24.473	22.401	2.073	7.162	9.234	-2.073
	840	77.603	75.258	2.345	23.494	21.149	2.345	8.141	10.486	-2.345
	960	77.304	74.075	3.228	23.194	19.966	3.228	8.441	11.669	-3.228
	1080	77.066	72.958	4.108	22.957	18.849	4.108	8.678	12.786	-4.108
	1200	75.054	71.902	3.152	20.945	17.793	3.152	10.690	13.842	-3.152
	1320	74.635	70.904	3.730	20.525	16.795	3.730	11.110	14.840	-3.730
	1440	74.226	69.961	4.265	20.117	15.852	4.265	11.518	15.783	-4.265
Curve 2	0	29.086	29.086	0.000	85.825	85.825	0.000	0.000	0.000	0.000
	120	25.438	24.103	1.334	82.176	80.842	1.334	3.649	4.983	-1.334
	240	21.526	20.106	1.420	78.264	76.844	1.420	7.561	8.981	-1.420
	360	18.296	16.842	1.453	75.034	73.581	1.453	10.791	12.244	-1.453
	480	14.831	14.147	0.684	71.570	70.885	0.684	14.255	14.939	-0.684
	600	12.471	11.904	0.567	69.210	68.642	0.567	16.615	17.183	-0.567
	720	10.179	10.027	0.152	66.918	66.765	0.152	18.907	19.059	-0.152

	840	7.670	8.451	-0.782	64.408	65.190	-0.782	21.417	20.635	0.782
	960	6.327	7.126	-0.798	63.066	63.864	-0.798	22.759	21.960	0.798
	1080	5.318	6.009	-0.691	62.057	62.748	-0.691	23.768	23.077	0.691
	1200	4.866	5.068	-0.201	61.605	61.806	-0.201	24.220	24.019	0.201
	1320	4.859	4.273	0.586	61.598	61.012	0.586	24.227	24.813	-0.586
	1440	4.825	3.603	1.223	61.564	60.341	1.223	24.261	25.483	-1.223
Curve 3	0	51.973	51.973	0.000	106.539	106.539	0.000	0.000	0.000	0.000
	120	43.240	43.419	-0.179	97.806	97.985	-0.179	8.734	8.555	0.179
	240	34.370	36.655	-2.285	88.936	91.221	-2.285	17.604	15.318	2.285
	360	27.074	31.160	-4.086	81.639	85.726	-4.086	24.900	20.814	4.086
	480	20.712	26.615	-5.903	75.278	81.181	-5.903	31.261	25.358	5.903
	600	15.883	22.810	-6.927	70.449	77.376	-6.927	36.090	29.163	6.927
	720	11.127	19.597	-8.470	65.693	74.163	-8.470	40.847	32.377	8.470
	840	10.036	16.865	-6.829	64.602	71.431	-6.829	41.937	35.108	6.829
	960	9.859	14.533	-4.674	64.425	69.099	-4.674	42.114	37.441	4.674
	1080	9.656	12.534	-2.878	64.222	67.100	-2.878	42.317	39.439	2.878
	1200	9.536	10.817	-1.281	64.102	65.383	-1.281	42.437	41.156	1.281
	1320	8.529	9.339	-0.810	63.095	63.905	-0.810	43.445	42.634	0.810
	1440	8.292	8.066	0.226	62.857	62.632	0.226	43.682	43.908	-0.226
Curve 4	0	88.613	88.613	0.000	279.614	279.614	0.000	0.000	0.000	0.000
	120	64.885	66.521	-1.636	255.886	257.522	-1.636	23.728	22.092	1.636
	240	49.245	52.747	-3.501	240.246	243.748	-3.501	39.368	35.866	3.501
	360	39.364	42.926	-3.562	230.364	233.927	-3.562	49.249	45.687	3.562
	480	31.903	35.483	-3.580	222.904	226.484	-3.580	56.710	53.130	3.580
	600	25.953	29.641	-3.688	216.954	220.642	-3.688	62.660	58.972	3.688
	720	23.506	24.947	-1.441	214.507	215.948	-1.441	65.107	63.665	1.441
	840	22.405	21.116	1.288	213.406	212.117	1.288	66.208	67.497	-1.288
	960	20.137	17.952	2.186	211.138	208.953	2.186	68.476	70.661	-2.186
	1080	19.349	15.314	4.036	210.350	206.315	4.036	69.263	73.299	-4.036
	1200	18.998	13.099	5.898	209.998	204.100	5.898	69.615	75.514	-5.898
	1320	18.104	11.230	6.874	209.105	202.231	6.874	70.509	77.382	-6.874
	1440	17.779	9.646	8.133	208.780	200.647	8.133	70.834	78.967	-8.133
Curve 5	0	29.021	29.021	0.000	64.502	64.502	0.000	0.000	0.000	0.000
	120	26.274	25.056	1.218	61.755	60.537	1.218	2.747	3.965	-1.218
	240	23.368	21.682	1.685	58.849	57.163	1.685	5.654	7.339	-1.685
	360	20.745	18.787	1.957	56.225	54.268	1.957	8.277	10.234	-1.957
	480	18.533	16.288	2.245	54.013	51.769	2.245	10.489	12.734	-2.245
	600	16.461	14.121	2.340	51.942	49.602	2.340	12.560	14.900	-2.340
	720	14.453	12.238	2.215	49.934	47.719	2.215	14.568	16.783	-2.215
	840	12.521	10.599	1.922	48.002	46.080	1.922	16.501	18.422	-1.922
	960	11.476	9.172	2.305	46.957	44.652	2.305	17.545	19.850	-2.305
	1080	10.215	7.928	2.287	45.696	43.409	2.287	18.806	21.093	-2.287
	1200	7.903	6.845	1.057	43.384	42.326	1.057	21.119	22.176	-1.057
	1320	6.990	5.904	1.086	42.471	41.385	1.086	22.032	23.118	-1.086
	1440	6.410	5.086	1.324	41.891	40.567	1.324	22.612	23.936	-1.324

B) Model predictions and residuals from the kinetic parameter estimation of the bioconversion of L-arabinose and Li-HPA to L-glucoheptulose using pure TK as biocatalyst.

Where:

- HPA-E and HPA-P are the experimental and predicted Li-HPA concentrations, respectively.
- ARA-E and ARA-P are the experimental and predicted L-arabinose concentrations, respectively.
- GLU-E and GLU-P are the experimental and predicted L-glucoheptulose concentrations, respectively.
- Residuals (R1, R2, and R3) are the difference between predicted and experimental values.

	Time (min)	HPA-E	HPA-P	R1	ARA-E	ARA-P	R2	GLU-E	GLU-P	R3
Curve 1	0	144.738	144.738	0.000	131.166	131.166	0.000	0.000	0.000	0.000
	120	120.730	122.847	-2.117	107.158	109.275	-2.117	24.008	21.891	2.117
	240	104.170	103.636	0.534	90.598	90.064	0.534	40.568	41.102	-0.534
	360	90.206	87.146	3.060	76.634	73.574	3.060	54.532	57.592	-3.060
	480	77.961	73.303	4.658	64.389	59.731	4.658	66.777	71.435	-4.658
	600	65.780	61.915	3.865	52.208	48.343	3.865	78.958	82.823	-3.865
	720	57.651	52.704	4.947	44.079	39.132	4.947	87.086	92.034	-4.947
	840	47.000	45.339	1.661	33.428	31.767	1.661	97.738	99.399	-1.661
	960	40.762	39.483	1.280	27.190	25.911	1.280	103.975	105.255	-1.280
	1080	35.995	34.836	1.159	22.423	21.264	1.159	108.743	109.902	-1.159
	1200	29.632	31.144	-1.512	16.060	17.572	-1.512	115.106	113.594	1.512
	1320	25.549	28.193	-2.644	11.977	14.621	-2.644	119.189	116.545	2.644
	1440	24.174	25.819	-1.645	10.602	12.247	-1.645	120.563	118.919	1.645
Curve 2	0	123.901	123.901	0.000	91.591	91.591	0.000	0.000	0.000	0.000
	120	104.444	107.016	-2.573	72.134	74.707	-2.573	19.457	16.884	2.573
	240	91.957	92.608	-0.652	59.647	60.299	-0.652	31.944	31.292	0.652
	360	81.319	80.556	0.763	49.009	48.246	0.763	42.582	43.345	-0.763
	480	72.284	70.657	1.627	39.974	38.347	1.627	51.617	53.244	-1.627
	600	63.342	62.654	0.688	31.032	30.344	0.688	60.559	61.247	-0.688
	720	55.768	56.259	-0.491	23.458	23.949	-0.491	68.133	67.642	0.491
	840	48.860	51.190	-2.331	16.550	18.881	-2.331	75.041	72.710	2.331
	960	42.712	47.194	-4.481	10.402	14.884	-4.481	81.189	76.707	4.481
	1080	37.255	44.052	-6.797	4.945	11.742	-6.797	86.646	79.849	6.797
	1200	33.880	41.583	-7.703	4.945	9.273	-4.328	86.646	82.318	4.328
	1320	31.609	39.642	-8.034	4.945	7.332	-2.387	86.646	84.258	2.387
	1440	29.309	38.115	-8.806	4.945	5.806	-0.860	86.646	85.785	0.860
Curve 3	0	96.989	96.989	0.000	129.836	129.836	0.000	0.000	0.000	0.000
	120	82.000	81.190	0.810	114.847	114.037	0.810	14.989	15.798	-0.810
	240	67.658	67.016	0.641	100.505	99.864	0.641	29.331	29.972	-0.641
	360	56.069	54.549	1.520	88.916	87.396	1.520	40.920	42.440	-1.520
	480	46.584	43.816	2.768	79.431	76.663	2.768	50.405	53.173	-2.768

	600	37.123	34.778	2.345	69.970	67.625	2.345	59.866	62.211	-2.345
	720	29.247	27.328	1.918	62.094	60.176	1.918	67.742	69.660	-1.918
	840	21.292	21.306	-0.014	54.139	54.153	-0.014	75.697	75.683	0.014
	960	16.619	16.514	0.105	49.467	49.362	0.105	80.369	80.474	-0.105
	1080	10.380	12.748	-2.368	43.227	45.595	-2.368	86.608	84.240	2.368
	1200	8.001	9.813	-1.812	40.848	42.660	-1.812	88.988	87.176	1.812
	1320	7.410	7.541	-0.131	40.258	40.388	-0.131	89.578	89.448	0.131
	1440	5.282	5.790	-0.508	38.129	38.637	-0.508	91.707	91.199	0.508
Curve 4	0	96.898	96.898	0.000	166.538	166.538	0.000	0.000	0.000	0.000
	120	80.394	78.134	2.260	150.034	147.774	2.260	16.504	18.765	-2.260
	240	61.828	61.386	0.442	131.468	131.025	0.442	35.070	35.513	-0.442
	360	48.766	46.898	1.868	118.406	116.538	1.868	48.132	50.000	-1.868
	480	35.111	34.825	0.287	104.751	104.465	0.287	61.787	62.074	-0.287
	600	22.144	25.169	-3.025	91.784	94.809	-3.025	74.754	71.730	3.025
	720	14.566	17.763	-3.197	84.206	87.402	-3.197	82.333	79.136	3.197
	840	9.451	12.294	-2.843	79.091	81.934	-2.843	87.448	84.604	2.843
	960	7.862	8.379	-0.518	77.502	78.019	-0.518	89.037	88.519	0.518
	1080	5.976	5.644	0.333	75.616	75.283	0.333	90.922	91.255	-0.333
	1200	5.606	3.769	1.838	75.246	73.409	1.838	91.292	93.130	-1.838
	1320	5.146	2.507	2.639	74.786	72.147	2.639	91.752	94.391	-2.639
	1440	3.591	1.661	1.930	73.231	71.301	1.930	93.307	95.237	-1.930
Curve 5	0	52.471	52.471	0.000	92.426	92.426	0.000	0.000	0.000	0.000
	120	40.701	40.054	0.647	80.656	80.009	0.647	11.770	12.417	-0.647
	240	31.635	29.711	1.924	71.590	69.666	1.924	20.836	22.761	-1.924
	360	23.410	21.415	1.995	63.365	61.370	1.995	29.061	31.056	-1.995
	480	15.276	15.028	0.248	55.231	54.983	0.248	37.195	37.443	-0.248
	600	9.354	10.305	-0.951	49.309	50.260	-0.951	43.117	42.166	0.951
	720	6.057	6.925	-0.868	46.012	46.880	-0.868	46.414	45.546	0.868
	840	3.989	4.589	-0.601	43.944	44.544	-0.601	48.482	47.882	0.601
	960	3.733	3.000	0.733	43.688	42.955	0.733	48.738	49.471	-0.733
	1080	3.703	1.943	1.760	43.658	41.898	1.760	48.768	50.528	-1.760
	1200	3.156	1.254	1.902	43.111	41.209	1.902	49.315	51.217	-1.902
	1320	2.729	0.805	1.924	42.684	40.761	1.924	49.742	51.666	-1.924
	1440	2.309	0.517	1.792	42.264	40.472	1.792	50.162	51.954	-1.792
Curve 6	0	32.760	32.760	0.000	85.327	85.327	0.000	0.000	0.000	0.000
	120	26.564	25.645	0.919	79.130	78.212	0.919	6.196	7.115	-0.919
	240	22.452	19.622	2.829	75.019	72.189	2.829	10.308	13.137	-2.829
	360	17.560	14.672	2.888	70.127	67.239	2.888	15.200	18.087	-2.888
	480	14.420	10.731	3.689	66.987	63.297	3.689	18.340	22.029	-3.689
	600	10.480	7.691	2.789	63.047	60.258	2.789	22.279	25.068	-2.789
	720	7.675	5.418	2.256	60.241	57.985	2.256	25.085	27.341	-2.256
	840	5.358	3.764	1.594	57.925	56.330	1.594	27.402	28.996	-1.594
	960	3.956	2.585	1.371	56.523	55.152	1.371	28.803	30.175	-1.371
	1080	3.819	1.759	2.060	56.386	54.326	2.060	28.941	31.001	-2.060
	1200	3.251	1.190	2.061	55.818	53.757	2.061	29.508	31.570	-2.061
	1320	3.174	0.801	2.373	55.741	53.368	2.373	29.585	31.959	-2.373
	1440	2.967	0.538	2.429	55.533	53.105	2.429	29.793	32.222	-2.429
Curve	0	90.198	90.198	0.000	33.833	33.833	0.000	0.000	0.000	0.000

7	120	87.078	86.831	0.246	30.713	30.466	0.246	3.120	3.367	-0.246
	240	85.062	83.759	1.303	28.697	27.394	1.303	5.136	6.440	-1.303
	360	81.042	80.962	0.080	24.677	24.597	0.080	9.156	9.236	-0.080
	480	77.374	78.423	-1.049	21.009	22.058	-1.049	12.824	11.775	1.049
	600	74.789	76.123	-1.334	18.424	19.758	-1.334	15.409	14.076	1.334
	720	71.825	74.044	-2.219	15.460	17.679	-2.219	18.373	16.155	2.219
	840	70.081	72.168	-2.087	13.716	15.803	-2.087	20.117	18.030	2.087
	960	67.820	70.479	-2.659	11.455	14.114	-2.659	22.379	19.719	2.659
	1080	67.570	68.961	-1.391	11.205	12.596	-1.391	22.629	21.238	1.391
	1200	66.315	67.598	-1.282	9.950	11.232	-1.282	23.883	22.601	1.282
	1320	64.714	66.375	-1.662	8.349	10.010	-1.662	25.484	23.823	1.662
	1440	64.163	65.281	-1.119	7.798	8.916	-1.119	26.036	24.917	1.119
Curve 8	0	32.629	32.629	0.000	59.356	59.356	0.000	0.000	0.000	0.000
	120	27.724	26.860	0.864	54.451	53.588	0.864	4.905	5.769	-0.864
	240	24.040	21.848	2.192	50.767	48.575	2.192	8.589	10.781	-2.192
	360	21.098	17.558	3.539	47.825	44.286	3.539	11.531	15.070	-3.539
	480	18.494	13.947	4.547	45.221	40.674	4.547	14.135	18.682	-4.547
	600	15.683	10.954	4.729	42.411	37.682	4.729	16.946	21.675	-4.729
	720	12.816	8.514	4.302	39.544	35.241	4.302	19.812	24.115	-4.302
	840	10.896	6.555	4.341	37.623	33.282	4.341	21.733	26.074	-4.341
	960	9.093	5.004	4.089	35.820	31.731	4.089	23.536	27.625	-4.089
	1080	7.443	3.792	3.651	34.170	30.520	3.651	25.186	28.837	-3.651
	1200	5.648	2.857	2.792	32.376	29.584	2.792	26.981	29.772	-2.792
	1320	5.237	2.141	3.096	31.965	28.869	3.096	27.391	30.488	-3.096
	1440	4.762	1.599	3.163	31.490	28.326	3.163	27.867	31.030	-3.163

C) Model predictions and residuals from the kinetic parameter estimation of the bioconversion of D-galacturonic acid and Li-HPA to (2*S*,3*S*,4*S*,5*R*)-6-aminoheptane-1,2,3,4,5,7-hexaol using pure TK as biocatalyst.

Where:

- HPA-E and HPA-P are the experimental and predicted Li-HPA concentrations, respectively.
- DGA-E and DGA-P are the experimental and predicted L-arabinose concentrations, respectively.
- OOA-E and OOA-P are the experimental and predicted L-glucoheptulose concentrations, respectively.
- Residuals (R1, R2, and R3) are the difference between predicted and experimental values.

	Time (min)	HPA-E	HPA-P	R1	DGA-E	DGA-P	R2	OOA-E	OOA-P	R3
Curve 1	0	90.000	90.000	0.000	33.650	33.650	0.000	0.000	0.000	0.000
	60	88.257	88.560	-0.303	31.907	32.210	-0.303	1.743	1.440	0.303
	120	86.918	87.172	-0.253	30.568	30.822	-0.253	3.082	2.828	0.253
	180	85.660	85.834	-0.174	29.311	29.484	-0.174	4.340	4.166	0.174

	240	84.346	84.546	-0.200	27.997	28.197	-0.200	5.654	5.454	0.200
	300	83.123	83.307	-0.185	26.773	26.957	-0.185	6.877	6.693	0.185
	360	81.634	82.116	-0.481	25.285	25.766	-0.481	8.366	7.884	0.481
	420	80.443	80.970	-0.527	24.094	24.621	-0.527	9.557	9.030	0.527
	480	79.442	79.870	-0.428	23.093	23.520	-0.428	10.558	10.130	0.428
	540	78.135	78.814	-0.678	21.786	22.464	-0.678	11.865	11.186	0.678
	600	77.393	77.800	-0.408	21.043	21.450	-0.408	12.607	12.200	0.408
	660	76.233	76.828	-0.595	19.883	20.478	-0.595	13.767	13.172	0.595
	720	75.266	75.896	-0.630	18.916	19.546	-0.630	14.734	14.104	0.630
Curve 2	0	47.000	47.000	0.000	47.986	47.986	0.000	0.000	0.000	0.000
	60	42.958	43.287	-0.329	43.944	44.273	-0.329	4.042	3.713	0.329
	120	39.767	39.926	-0.159	40.753	40.912	-0.159	7.233	7.074	0.159
	180	36.755	36.903	-0.147	37.741	37.889	-0.147	10.245	10.097	0.147
	240	33.853	34.196	-0.343	34.839	35.182	-0.343	13.147	12.804	0.343
	300	31.734	31.779	-0.045	32.720	32.765	-0.045	15.266	15.221	0.045
	360	29.624	29.623	0.000	30.609	30.609	0.000	17.376	17.377	0.000
	420	27.816	27.699	0.117	28.802	28.685	0.117	19.184	19.301	-0.117
	480	26.170	25.979	0.191	27.156	26.965	0.191	20.830	21.021	-0.191
	540	24.691	24.439	0.252	25.676	25.425	0.252	22.309	22.561	-0.252
	600	23.302	23.055	0.247	24.288	24.041	0.247	23.698	23.945	-0.247
	660	21.561	21.808	-0.248	22.546	22.794	-0.248	25.439	25.192	0.248
	720	20.594	20.681	-0.087	21.580	21.667	-0.087	26.406	26.319	0.087
Curve 3	0	40.000	40.000	0.000	50.087	50.087	0.000	0.000	0.000	0.000
	60	35.254	35.596	-0.341	45.341	45.682	-0.341	4.746	4.404	0.341
	120	31.515	31.794	-0.279	41.601	41.881	-0.279	8.485	8.206	0.279
	180	28.484	28.539	-0.055	38.570	38.625	-0.055	11.516	11.461	0.055
	240	25.412	25.759	-0.347	35.499	35.845	-0.347	14.588	14.241	0.347
	300	23.274	23.381	-0.107	33.361	33.468	-0.107	16.726	16.619	0.107
	360	20.974	21.339	-0.366	31.060	31.426	-0.366	19.026	18.661	0.366
	420	19.434	19.575	-0.141	29.520	29.661	-0.141	20.566	20.425	0.141
	480	17.826	18.041	-0.215	27.912	28.127	-0.215	22.174	21.959	0.215
	540	16.505	16.698	-0.193	26.592	26.785	-0.193	23.495	23.302	0.193
	600	15.365	15.515	-0.150	25.451	25.601	-0.150	24.635	24.485	0.150
	660	14.504	14.465	0.039	24.590	24.552	0.039	25.496	25.535	-0.039
	720	13.404	13.529	-0.125	23.491	23.615	-0.125	26.596	26.471	0.125
Curve 4	0	80.000	80.000	0.000	37.186	37.186	0.000	0.000	0.000	0.000
	60	73.341	73.305	0.036	30.527	30.491	0.036	6.659	6.695	-0.036
	120	68.084	67.686	0.398	25.270	24.872	0.398	11.916	12.314	-0.398
	180	62.913	63.030	-0.117	20.099	20.216	-0.117	17.087	16.970	0.117
	240	59.499	59.207	0.292	16.685	16.393	0.292	20.501	20.793	-0.292
	300	56.309	56.090	0.220	13.495	13.276	0.220	23.691	23.910	-0.220
	360	53.380	53.559	-0.179	10.566	10.745	-0.179	26.620	26.441	0.179
	420	51.317	51.510	-0.192	8.503	8.696	-0.192	28.683	28.490	0.192
	480	49.986	49.853	0.133	7.172	7.039	0.133	30.014	30.147	-0.133
	540	48.446	48.514	-0.068	5.632	5.700	-0.068	31.554	31.486	0.068
	600	47.361	47.433	-0.072	4.547	4.619	-0.072	32.639	32.567	0.072
	660	46.646	46.558	0.088	3.832	3.744	0.088	33.354	33.442	-0.088
	720	45.892	45.850	0.042	3.078	3.036	0.042	34.108	34.150	-0.042

Curve 5	0	50.000	50.000	0.000	25.113	25.113	0.000	0.000	0.000	0.000
	60	43.410	43.289	0.122	18.523	18.401	0.122	6.590	6.711	-0.122
	120	38.410	38.420	-0.010	13.523	13.533	-0.010	11.590	11.580	0.010
	180	35.040	34.918	0.122	10.153	10.031	0.122	14.960	15.082	-0.122
	240	32.193	32.387	-0.194	7.306	7.500	-0.194	17.807	17.613	0.194
	300	30.154	30.541	-0.387	5.267	5.654	-0.387	19.846	19.459	0.387
	360	29.013	29.180	-0.166	4.126	4.292	-0.166	20.987	20.820	0.166
	420	28.041	28.166	-0.125	3.153	3.279	-0.125	21.959	21.834	0.125
	480	27.447	27.405	0.042	2.559	2.517	0.042	22.553	22.595	-0.042
	540	26.538	26.827	-0.289	1.651	1.940	-0.289	23.462	23.173	0.289
	600	26.054	26.387	-0.333	1.167	1.500	-0.333	23.946	23.613	0.333
	660	25.981	26.049	-0.068	1.094	1.162	-0.068	24.019	23.951	0.068
	720	25.760	25.789	-0.029	0.873	0.902	-0.029	24.240	24.211	0.029
Curve 6	0	70.000	70.000	0.000	30.016	30.016	0.000	0.000	0.000	0.000
	60	64.160	63.921	0.239	24.176	23.937	0.239	5.840	6.079	-0.239
	120	59.230	58.984	0.247	19.246	19.000	0.247	10.770	11.016	-0.247
	180	55.491	55.023	0.468	15.507	15.039	0.468	14.509	14.977	-0.468
	240	52.051	51.872	0.179	12.067	11.888	0.179	17.949	18.128	-0.179
	300	49.461	49.379	0.082	9.477	9.395	0.082	20.539	20.621	-0.082
	360	47.825	47.410	0.415	7.841	7.426	0.415	22.175	22.590	-0.415
	420	46.007	45.857	0.150	6.023	5.873	0.150	23.993	24.143	-0.150
	480	45.060	44.632	0.428	5.076	4.648	0.428	24.940	25.368	-0.428
	540	43.574	43.665	-0.092	3.590	3.682	-0.092	26.426	26.335	0.092
	600	43.035	42.902	0.133	3.051	2.918	0.133	26.965	27.098	-0.133
	660	41.995	42.298	-0.303	2.011	2.315	-0.303	28.005	27.702	0.303
	720	41.552	41.821	-0.269	1.568	1.837	-0.269	28.448	28.179	0.269
Curve 7	0	60.000	60.000	0.000	31.505	31.505	0.000	0.000	0.000	0.000
	60	50.257	49.746	0.511	21.762	21.250	0.511	9.743	10.254	-0.511
	120	42.997	42.831	0.166	14.502	14.336	0.166	17.003	17.169	-0.166
	180	37.941	38.251	-0.310	9.446	9.756	-0.310	22.059	21.749	0.310
	240	35.038	35.208	-0.170	6.542	6.712	-0.170	24.962	24.792	0.170
	300	32.842	33.160	-0.318	4.347	4.665	-0.318	27.158	26.840	0.318
	360	31.281	31.765	-0.484	2.786	3.270	-0.484	28.719	28.235	0.484
	420	30.677	30.803	-0.126	2.182	2.308	-0.126	29.323	29.197	0.126
	480	29.962	30.131	-0.169	1.467	1.635	-0.169	30.038	29.869	0.169
	540	29.768	29.659	0.110	1.273	1.164	0.110	30.232	30.341	-0.110
	600	29.517	29.325	0.192	1.022	0.830	0.192	30.483	30.675	-0.192
	660	29.207	29.088	0.118	0.711	0.593	0.118	30.793	30.912	-0.118
	720	29.046	28.919	0.127	0.551	0.424	0.127	30.954	31.081	-0.127
Curve 8	0	90.000	90.000	0.000	35.264	35.264	0.000	0.000	0.000	0.000
	60	81.923	81.736	0.187	27.188	27.001	0.187	8.077	8.264	-0.187
	120	74.874	75.213	-0.339	20.138	20.478	-0.339	15.126	14.787	0.339
	180	70.632	70.158	0.473	15.896	15.423	0.473	19.368	19.842	-0.473
	240	66.780	66.295	0.485	12.044	11.560	0.485	23.220	23.705	-0.485
	300	63.762	63.372	0.390	9.026	8.636	0.390	26.238	26.628	-0.390
	360	61.232	61.173	0.058	6.496	6.438	0.058	28.768	28.827	-0.058
	420	59.813	59.528	0.285	5.078	4.793	0.285	30.187	30.472	-0.285
	480	58.755	58.301	0.455	4.020	3.565	0.455	31.245	31.699	-0.455

	540	57.825	57.386	0.439	3.089	2.650	0.439	32.175	32.614	-0.439
	600	56.831	56.705	0.126	2.096	1.969	0.126	33.169	33.295	-0.126
	660	56.324	56.199	0.125	1.589	1.463	0.125	33.676	33.801	-0.125
	720	55.297	55.823	-0.526	0.561	1.087	-0.526	34.703	34.177	0.526
Curve 9	0	40.000	40.000	0.000	40.564	40.564	0.000	0.000	0.000	0.000
	60	24.856	24.022	0.833	25.420	24.587	0.833	15.144	15.978	-0.833
	120	16.926	16.676	0.250	17.490	17.241	0.250	23.074	23.324	-0.250
	180	13.032	12.750	0.282	13.596	13.314	0.282	26.968	27.250	-0.282
	240	10.462	10.330	0.131	11.026	10.895	0.131	29.538	29.670	-0.131
	300	8.675	8.690	-0.016	9.239	9.255	-0.016	31.325	31.310	0.016
	360	7.497	7.502	-0.005	8.061	8.066	-0.005	32.503	32.498	0.005
	420	6.551	6.600	-0.050	7.115	7.165	-0.050	33.449	33.400	0.050
	480	5.860	5.891	-0.032	6.424	6.456	-0.032	34.140	34.109	0.032
	540	5.308	5.319	-0.012	5.872	5.884	-0.012	34.692	34.681	0.012
	600	4.795	4.847	-0.052	5.359	5.411	-0.052	35.205	35.153	0.052
	660	4.441	4.450	-0.009	5.006	5.015	-0.009	35.559	35.550	0.009
	720	3.878	4.112	-0.234	4.442	4.677	-0.234	36.122	35.888	0.234